STUDIES ON SELECTED BIOMOLECULES & THEIR ROLES IN CELL PROLIFERATION, CYTOTOXICITY AND DISEASE

SUKHDEEP KUMAR

A Thesis submitted for the partial fulfillment

of the degree of

Doctor of Philosophy

Indian Institute of Science Education and Research Mohali

Department of Biological Sciences

Mohali-140306

June 2015

CERTIFICATE

The work presented in this thesis has been carried out by me under the supervision of Professor Purnananda Guptasarma and Dr. Tapan K Mukherjee at the Indian Institute of Science Education and Research Mohali.

This work has not been submitted in part or full for a degree, a diploma, or a fellowship to any other university or institute.

Whenever contributions of others are involved, every effort is made to indicate this clearly, with due acknowledgement of collaborative research and discussions. This thesis is a bonafide record of original work done by me and all sources listed within have been detailed in the bibliography.

Date: 22.02.2016

Place: Mohali **Sukhdeep Kumar**

In our capacity as supervisors of the candidate's thesis work we certify that above statements made by candidate are true to best of our knowledge.

Prof. P. Guptasarma **Dr. Tapan K Mukherjee**

Supervisor **Supervisor**

Dedicated

To

Parents

ACKNOWLEDGEMENTS

I owe my deepest gratitude to my mentors, Professor Purnananda Guptasarma and Dr. Tapan K Mukherjee.

To Professor Purnananda Guptasarma, I express my deepest gratitude for providing me his competent guidance not only in field of science but life also. Sir, your motivation, support and scientific discussions always stimulated me wander deeper into the world of proteins in context of their physiological roles in living systems. You are a true friend, philosopher and guide; in short, you are the best teacher one can have.

To Dr. Tapan K Mukherjee, I express my sincere gratitude for providing me opportunity to see life in action at microscopic scale and role small molecules play in its regulation. I heartily thank you for providing me the guidance and training in cell biology.

I am thankful to the Director IISER Mohali, Professor N.Satyamurthy, and biology faculty of Indian Institute of Science Education and Research for making available to me the excellent facilities of the Institute.

I extend my heartfelt thanks to all my seniors and lab mates like Dr. Neeraj, Dr. Uzma, Dr. Satyaprakash, Dr. Arpna, Dr. Javed , Dr Prerna, Kanika, Nitin, Pallavi, Prince, Bhisham and Prachi for their kind support and always keeping conducive lab environment.

I am thankful to my friends Matsyndernath, Karan, Ashutosh for being wonderful

company and extending their help whenever required. They are friends in need and friend indeed.

My sincere appreciation goes to all IISER faculty members, staff, library, and instrumentation etc. whose help and support was always there when needed.

I acknowledge my wife Minakshi for understanding me and motivating me.

Finally, I acknowledge with gratitude and love the support of all my family members especially parents for their love, understanding and encouragement.

The financial support by CSIR and CPSDE is duly acknowledged

Sukhdeep Kumar

Synopsis:

The complex interplay of cellular constituents and environment is essential for normal cell physiology. In an organism these processes are very tightly regulated, resulting in a state of homeostasis. Certain intrinsic and extrinsic stimuli may lead to disturbance in homeostasis, resulting in altered physiology and pathology. Below, some common players are introduced: (I) Calcium is one of the major divalent ions present in the serum in a high concentration range (1-2 mM), with the largest number of known physiological, metabolic, biochemical and structural roles, causing it to be the metal with the highest potential degree of relevance to any disease involving metal binding. The role of calcium in induction or promotion of amyloidosis is poorly understood. (II) Arsenic trioxide is a ubiquitous metalloid that has emerged as global problem of water contamination. Chronic exposure to arsenic results in metabolic disturbances and carcinogenesis. Epidemiological studies suggest that males are more susceptible to arsenic poisoning than females but the mechanism remains unclear. (III) Estrogens are steroid hormones secreted primarily from the ovaries and testes of females and males respectively, and play a crucial role in the normal physiology of both human genders. However, physiological levels of estrogens are significantly higher in females of reproductive age because of high-level generation of aromatase, the enzyme responsible for conversion of testosterone to estrogens. There is an increasing body of evidence indicating a role for estrogens in carcinogenesis. Estrogens are positively correlated with human breast cancers. Estrogens may induce carcinogenesis by receptor mediated signaling, free radical generation and induction of aneuploidy. (IV) The ubiquitin-proteasome system (UPS) is essential for estrogen signaling. Inhibition of proteasome with proteasome inhibitor MG132 also inhibits estrogen signaling. The UPS maintains the normal cell protein homeostasis by targeting nearly 90% of proteins found in the cell for degradation at various points of time depending upon cellular physiology. (V) E3 ubiquitin ligases are an important link in protein turnover in normal and diseased states. (VI) CHIP1 is an E3 ubiquitin ligase, which function as a tumor suppressor protein by targeting the proteins like P53, ER-α and HIF-1α to proteasome. (VII) 17α-ethinyl-estradiol (17α-EE) is a semisynthetic alkylated estradiol used as estrogenic component in oral contraceptives and hormone replacement therapy (HRT). 17α-EE has been positively correlated to probability of developing breast cancer in women undergoing long term HRT.

Overall, this thesis aims to understand the role of estrogens, arsenic trioxide and calcium in cell proliferation, cytotoxicity and disease; using the MCF-7 and N2A cell lines as in-vitro models. The variation in use of systems and approaches, and differences in issues addressed owe to work having been carried out under two supervisors.

The thesis is divided into three chapters or sections, details of which are mentioned below:

(I) Chapter/section I titled **"Novel calcium and 17β-estradiol (E2) binding activity of β2-microglobulin"** describes the expression of human β2-microglobulin in *E.coli* cells of the BL21 Star (DE3) pLysS strain and its subsequent purification, refolding, and discovery of binding interactions with calcium and 17β-estradiol (E2) and cytotoxicity of β2m oligomers, Human β2-microglobulin (β2m), also known as the MHC-I light chain, is a small protein constituent of all Class-I major histocompatibility (MHC-I) complexes. We have discovered that β2M at physiological concentrations binds to physiological concentrations of calcium, leading to formation of microaggregates that form amorphous pre-amyloid aggregates. Resonance Rayleigh scattering (RRS) experiments confirms the dose dependent microaggregation of β2M by calcium. Fourier transform infrared spectroscopy (FTIR) experiments suggest that incubation of β2M with calcium induce increase in β-sheet content in β2M. We further investigated the Stoichiometry of β2M-Ca interaction using isothermal calorimetry (ITC) and found four calcium-binding sites in β2M. Similarly, for the first time we have demonstrated that β2M interacts with estradiol using difference absorption spectroscopy (DAS) and surface plasmon resonance (SPR). E2 inhibits the β2M oligomers mediated cytotoxicity to N2a neuroblastoma cells.

(II) Chapter/section II titled **"Role of 17β-estradiol in arsenic trioxide induced cell proliferation and migration in MCF-7 breast cancer cells"** Effect of Arsenic trioxide on MCF-7 cell proliferation and migration was studied using concentrations ranging from 100 pM-20 μM. Arsenic trioxide at low concentration (100 pM-100 nM) induced cell proliferation in MCF-7 cells and was cytotoxic at high concentration (10 μM -20 μM). Previous research had shown similar effects of low dose arsenic on MCF-10A cells. The effects of arsenic trioxide on scratch wound healing assays were

similar to cell proliferation assays. Dose response to arsenic trioxide was further investigated in MCF-7 monolayer scratch wound healing using arsenic trioxide concentrations ranging between 100 pM-20 μM. It was found that arsenic trioxide at l0 nM concentration induced maximum wound healing. Previous research had shown that low dose arsenic induces generation of reactive oxygen species (ROS) that promotes cell proliferation through activation of cell growth and cell division pathways. We investigated the effect of ROS scavenger N-acetyl-L-cysteine (NAC) on low dose arsenic induced wound healing in MCF-7 monolayer. NAC inhibited low dose arsenic induced wound healing confirming the role of ROS as an effector of low dose arsenic induced wound healing in MCF-7 monolayer. Similarly efficacy of E2 in scratch wound healing in MCF-7 was determined at concentrations ranging between 100 pM-10 μM. It was found that E2 at 100 nM induced maximum wound healing. We further investigated the cumulative effect of ATO and E2. ATO at low dose failed to induce wound healing in MCF-7 monolayer in presence of E2. Through difference absorption spectroscopy we demonstrate for first time the binding interaction between ATO and E2. These results suggest that arsenic is physically sequestered by E2, which may be the one of the mechanisms resulting in decreased efficacy in MCF-7 monolayer wound healing.

(III) Chapter/Section III titled **"Role of CHIP1 in 17-α-ethinyl estradiol induced MCF-7 cell proliferation and survival**". 17α-EE is a semisynthetic alkylated estradiol used as estrogenic component in oral contraceptives. MCF-7 cell line is one of the most widely used cell lines, with characteristics of differentiated mammary epithelial cells and expression of cytosolic estrogen receptors (ERs). The C-terminal of HSc70 interacting protein 1 (CHIP1) is a chaperone dependent E3 ubiquitin ligase belonging to tertracopeptide repeats family (TPR) of proteins. The CHIP gene is located on chromosome 16p13.3 encoding a 35 kDa protein. The primary structure consists of three distinct domains: N-terminal TPR domain, an internal charged domain and a C-terminal U-box domain. CHIP1 has been demonstrated to regulate a broad spectrum of biological processes. CHIP1 predominantly acts as a tumor suppressor protein and it regulates the cellular levels of a large number of target proteins like P53, ER-α and HIF-1α etc. But the regulation of cellular levels of CHIP1 is poorly understood. We have found that 17αEE modulates the cellular levels of CHIP1, PARP1, p-Akt s473 and HSP90 in a time-dependent manner. 17αEE induced

time-dependent down regulation of CHIP1 was inhibited by the ER-α antagonist ICI 164384. Knockdown of CHIP1 induced cell proliferation. The nuclear levels of CHIP1 are also modulated by 17αEE in a time-dependent manner. We also discovered that CHIP1 interacts with Poly (ADP-Ribose) Polymerase 1 (PARP1) using co- immunoprecipitation. PARP1 is a nuclear tumor suppressor protein involved in the repair of the DNA single strand breaks by base excision repair (BER).

Abbreviations

%	Percent
mg	Milligram
M	Molar
ml	Milliliter
min	Minute
pM	Picomolar
nM	Nanomolar
μM	Micomolar
mM	Millimolar
kDa	Kilo dalton
CD	Circular dichorism
FTIR	Fourier transform infrared spectroscopy
ITC	Isothermal calorimetry
SPR	Surface plasmon resonance
PCR	Polymerase chain reaction
QT-PCR	Quantitative polymerase chain reaction
DAS	Difference absorption spectroscopy
β2m	β2-microglobulin
MHC1	Major histocompatibility complex1
EE	17-α-ethinyl estradiol
E2	17-β-estradiol
NAC	N-Acetylcysteine
CO_2	Carbon dioxide
FBS	Fetal bovine serum
$CaCl_2$	Calcium chloride
ATO	Arsenic trioxide
MCF-7	Michigan cancer foundation-7
CHIP1	C- terminal of HSc70 interacting protein
PARP1	Poly (ADP-ribose) polymerase 1
AKT-1	RAC-alpha serine/threonine-protein kinase
HSP90	Heat shock protein 90
MTT	3-(4,5-dimethylthiazol-2-yl)-2,5-diphenyl*tetrazolium* bromide
Co-IP	Co-immunoprecipitation

List of Publications:

S. No	Title	Journal
1	Calcium Binding to Beta-2-Microglobulin at Physiological pH Drives the Occurrence of Conformational Changes Which Cause the Protein to Precipitate into Amorphous Forms That Subsequently Transform into Amyloid Aggregates	PLoS ONE 9(4): e95725 April 2014
2	Role of estrogen receptors in pro-oxidative and anti-oxidative actions of estrogens: a perspective	Biochimica et Biophysica Acta 1800(10): 1127-35 · April 2010
3	Role of RAGE in idiopathic pulmonary fibrosis: Promising prospects	Respiratory Physiology & Neurobiology 165(2) · December 2008

Contents

Section A

Novel calcium and 17β-estradiol (E2) binding activity of β2-microglobulin

A.1.1 Introduction

Proteins are biological macromolecules consisting of covalently linked amino acid residues, arranged in a linear chain that folds into a globular form. The term protein is derived from the Greek adjective “proteios”, meaning ‘of first rank or position’, Essentially, proteins justify their name as they act as structural and functional workhorses of the cell, and their role covers structure, catalysis, transport, communication and regulation. Thus, an understanding of protein structure and associated function is of prime importance to understand the working of the living world. Living organisms use 20 standard amino acids to synthesize proteins. Various permutations and combinations of amino acid residues can give rise to diverse sequences, each constituting a unique protein. However, these permutations and combinations do not appear to occur at random, but have been selected through evolutionary pressure to adopt particular three-dimensional structures through folding, and perform specific functions. The shape into which a protein naturally folds under physiological conditions is termed as its native conformation.

After a series of elegant studies on refolding studies on bovine ribonuclease A, Christian Anfinsen postulated that folding of a protein into its native conformation is somehow controlled by the sequence of amino acids in that protein. Anfinsen also postulated the ‘thermodynamics hypothesis’ of protein folding, describing the native state to be in equilibrium with unfolded states, and the native conformation as the global minimum in Gibbs free energy attainable by a polypeptide chain (1). The primary structure of a protein determines not only the sequence of amino acid residues but also the local interactions between amino acid residues, solvent molecules and ions. Ostensibly, at least in some cases, these local interactions lead to the formation of nucleation centers for the protein to fold into secondary structures, or groups of secondary structures, such as super secondary structural elements. The secondary structures ultimately collapse into the robust three-dimensional structure known as the “native state” or structure.

Proteins synthesis and degradation in an organism is a highly coordinated process, with strict quality control that ensures that only functionally-active proteins are retained, while misfolded and chemically damaged proteins are subject to rapid degradation using chaperone-mediated autophagy or proteasome-mediated degradation. Under normal physiological conditions, this process is sufficient to avoid the accumulation of misfolded proteins. But under certain pathological conditions, misfolded proteins can accumulate and

aggregate. Some proteins have the inherent propensity to undergo structural changes from a soluble globular form into insoluble fibrous forms termed as “amyloids” (since they bind Congo Red and give rise to the characteristic apple-green birefringence shown by starch, under plain polarized light).

The insoluble amyloid fibrils are mostly observed as extracellular deposits, although they have also been reported in intracellular locations (2). Biophysical studies on amyloid fibrils have revealed a characteristic cross beta sheet arrangement of polypeptide chains in such fibrils. Amyloids fibrils appear to violate the Anfinsen principle by demonstrating a significant degree of polymorphism, involving variable packaging of protofilaments under different conditions (3).

A.1.2 Amyloidosis

Amyloidosis is a broad term applied to diseases caused by protein molecules undergoing conformational changes, or proteolytic truncation, resulting in soluble oligomeric species and insoluble fibrillar species forming from well-folded proteins in soluble form. The resulting insoluble fibrillar species are resistant to proteolytic degradation, and bind to the Congo red dye, yielding apple-green birefringence under plane polarized light. Insoluble fibrous species get deposited in the affected tissue and hinder the normal physiology of the tissue resulting in impaired tissue function and inflammation. Most proteins encoded by the human proteome can fold into their correct native three-dimensional structures, except for a few that are more prone to forming amyloids, which proteins are commonly found to be associated with amyloidosis-linked pathologies. Listed below in Table A.1 are human proteins associated with amyloidosis (4).

A.1.3 Proteins associated with systemic and localized amyloidosis

Amyloidogenic protein	Precursor protein	S/L	A/H	Organs affected
AL	Immunoglobulin light chain	S, L	A	All organs except CNS
AH	Immunoglobulin heavy chain	S, L	A	All organs except CNS
Aβ2m	β2-microglobulin, wild type	L	A	Musculoskeletal system

	β2-microglobulin, variant	S	L	ANS
ATTR	Transthyretin, wild type	S, L	A	Tenosynovium, Mainly in male heart
	Transthyretin, variants	S	H	PNS, ANS, heart, eye, leptomen
AA	(Apo) serum amyloid A	S	A	All organs except CNS
AApoAI	Apolipoprotein A I, variants	S	H	Heart, liver, kidney, PNS, testis, larynx, skin
AApoAII	Apolipoprotein A II, variants	S	H	Kidney
AApoAIV	Apolipoprotein A IV, variants	S	A	Kidney medulla and systemic
AGel	Gelsolin, variants	S	H	PNS, cornea
ALys	Lysozyme, variants	S	H	Kidney
ALect2	Leukocyte chemotactic factor-2	S	A	Kidney, primarily
AFib	Fibrinogen α, variants	S	H	Kidney, primarily
ACys	Cystatin C, variants	S	H	PNS, skin
ABri	ABriPP, variants	S	H	CNS
Adan	ADanPP, variants	L	H	CNS
Aβ	Aβ protein precursor, wild type	L	A	CNS
	Aβ protein precursor, variant	L	H	CNS
APrP	Prion protein, wild type	L	A	CJD, fatal insomnia
	Prion protein variants	L	H	CJD, GSS syndrome, fatal insomnia

ACal	(Pro) calcitonin	L	A	C-cell thyroid tumors
AIAPP	Islet amyloid polypeptide	L	A	Islets of langerhans, insulinomas
AANF	Atrial natriuretic factor	L	A	Cardiac atria
APro	Prolactin	L	A	Pituitary
AIns	Insulin	L	A	Iatrogenic, local injection
ASPC	Lung surfactant protein	L	A	Lung
AGal7	Galectin 7	L	A	Skin
ACor	Corneodesmin	L	A	Cornified epithelia, hair follicles
AMed	Lactadherin	L	A	Senile aortic, media
Aker	Kerato-epithelin	L	A	Cornea
ALac	Lactoferrin	L	A	Cornea
AOaap	Odontogenic ameloblast-associated protein	L	A	Odontogenic tumors
ASem1	Semenogelin 1	L	A	Vasicula seminalis

Legends to table L: Localized, S: Systemic, H: Hereditary, A: Acquired, CNS: Central nervous system, PNS: Peripheral nervous system.

A.1.4 Mechanism of amyloid-associated toxicity/pathogenesis:

The mechanisms underlying amyloid-associated pathology are poorly understood. Initially amyloid plaques consisting of amyloid fibrils were considered to be the main culprit in amyloid-associated pathogenesis. However, there is a growing number of reports that it is actually the proto fibrillar oligomeric species and amyloid fiber fragments of amyloid-associated proteins which are cytotoxic, while mature amyloid fibrils act as inert supramolecular assemblies of proto fibrils, which are not excessively associated with cytotoxicity (5). Soluble oligomeric species affect the normal physiology of affected tissue by

disrupting membrane integrity, membrane permeability, altering cell signaling cascade, oxidative stress and result in cell death by apoptosis. (6) Biophysical studies involving conductance experiments on phospholipid bilayers incubated with oligomeric β2m demonstrate an increase in conductance, which is inhibited by Congo red, suggesting oligomeric β2m forms pores or ion channels in synthetic membranes further emphasize that oligomeric β2m may demonstrate DRA associated pathophysiology in part through formation of pores in target cells (7).

A.1.5 β2-microglobulin and Dialysis Related Amyloidosis

Human β2-microglobulin (β2m), also known as the MHC-I light chain, is a small protein constituent of all Class-I major histocompatibility (MHC-I) complexes displayed on the surfaces of all nucleated human cells (9). The mature β2m chain consists of 99 amino acid residues which are found folded into a beta barrel structure consisting of two antiparallel beta sheets consisting of four and three strands, respectively, stabilized by a single inter-sheet disulfide bond formed between Cys 25 and Cys 80 (10). β2m complexed with HLA chain is depicted in figure A.1.A and free β2m is depicted in figure A.1.B. The structures of the protein obtained through X-ray crystallography and ^{1}H NMR studies demonstrate striking structural differences between β2m bound to the HLA chain in MHC1, and free β2m. These structural differences have been proposed to responsible for the propensity of free β2m to aggregate (11). β2m chaperones the folding of the much larger MHC-I heavy chain polypeptide in the MHC-I complex, which is known as the human leukocyte antigen, or HLA, chain. The binding and display of peptides to T-cell receptors by the HLA chain is also critically dependent on the correctness of its assembly with β2m (12). When the complex is disassembled

During natural turnover, the non-covalently associated β2m molecule is thought to be simply ‘shed’ into extracellular fluids by the displaying cell whereas the membrane-tethered HLA chain is internalized. The ‘shed’ β2m molecule is then carried to the kidney where it is degraded. This results in an equilibrium β2m concentration of ~1-3 μg/ml in the serum of healthy humans. In patients suffering from renal dysfunction, the degradation of β2m in the kidney becomes compromised (13), leading to the elevation of β2m concentrations in the serum. Under such conditions, β2m levels can be as high as 25-60 times the concentrations of β2m seen in healthy humans (14).

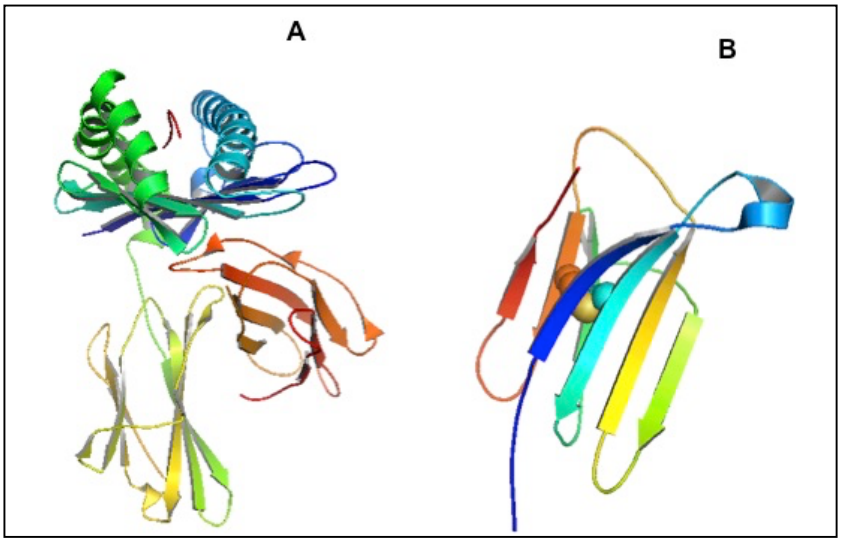

Figure A.1 Panel: A. Ribbon diagram of Major histocompatibility Complex1 (β2m is depicted in orange/red). **Panel: B:** β2m ribbon diagram (PDB ID: 2YXF) (8).

An apparent consequence of these elevated levels is that β2m tends to aggregate and deposit as insoluble amyloid precipitates within the joints of patients receiving hemodialysis-based treatment. This leads to Dialysis Related Amyloidosis (DRA), a condition that includes carpal tunnel syndrome, amyloid arthropathy, and pathological bone disruption (11), (14). There is much interest, therefore, in the aggregation and deposition of this small seven β-stranded (anti-parallel β-sandwich) protein. The proposed mechanism of DRA is shown in figure A.2. The trouble with DRA, however, is that the cause-effect relationship between elevated β2m concentrations and β2m deposition is not at all clear. As a protein, β2m is exceptionally soluble in aqueous solutions at physiological pH and ionic strength. Under these conditions, the protein displays no evidence whatsoever of its possessing any tendency to undergo aggregation; in fact, β2m can even be concentrated up to levels as high as several tens of milligrams per milliliter (i.e., millimolar concentrations) with no consequent aggregation. The protein can even be incubated for several months at such high concentrations, at 37 °C, in buffers of neutral pH, with no observable precipitation (11, 16-18).

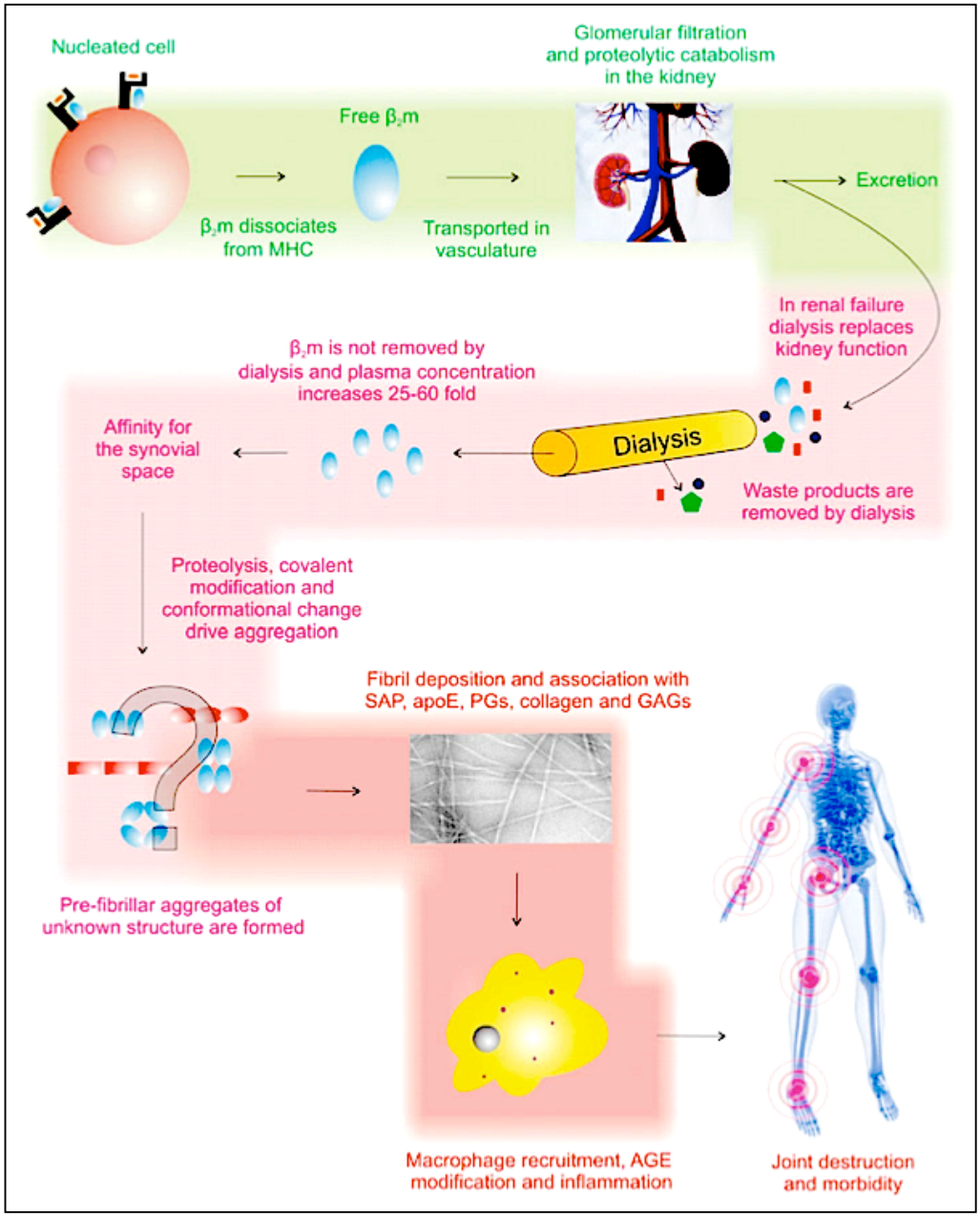

Figure A.2: Proposed mechanism and series of events leading to DRA: During kidney function impairment plasma levels of β2m rise abnormally following dialysis. β2m has intrinsic affinity for synovial space where it undergoes conformational changes resulting in aggregation and formation of amyloid fiber deposits (11)

Notably, such concentrations are orders of magnitude higher than both (a) the elevated levels seen in DRA patients, and (b) the levels seen in healthy individuals. Attempts have been made to create a mouse model for DRA using transgenic mice that overexpress human β2m to such high levels that serum concentrations exceed those seen in DRA patients by a factor of four. Such mice are neither found to be prone to develop DRA on their own, nor prone to develop DRA through the introduction of pre-existing β2m amyloid fibrils as seeds (19). It is not even as if differences in conformation between soluble β2m and HLA-bound β2m reveal very significant clues to its precipitation, because the molecule's solution structure and HLA-bound structures are both very similar, with only minor changes in beta-strand composition and arrangement distinguishing the two (reviewed in reference). Perhaps most intriguing of all is the fact that β2m displays the highest structural stability in solutions of physiological pH, of all pH values tested (20). The precipitation and deposition of β2m under physiological conditions at pH 7.4 thus continues to perplex those studying the molecule's behavior, and many papers discussing how deposition occurs *in vivo* have failed to arrive at any definitive conclusions.

In the absence of clear insights into how physiological deposition occurs, the bulk of studies on β2m have focused instead on non-physiological conditions eliciting aggregation and precipitation. Thus, it is now well known that β2m amyloids form quite easily under acidic conditions, requiring only weeks of incubation.

Fibrils with different morphologies, lengths and twists tend to be observed under different acidic conditions, e.g., (i) long and straight fibrils are obtained in the pH range of 1.5-4.0 in buffers of ionic strength ≤ 50mM, (ii) worm-like fibrils are obtained in the pH range of 2.5-4.0 in buffers of ionic strength ≥ 100mM,while (iii) rod-like fibrils are obtained in the pH range of 3.0-4.0 in buffers of ionic strength ≥ 50mM (11). In addition to acidic pH, certain physical factors such as sonication (21), as well as chemicals such as glycosaminoglycan and proteoglycans (22-24), sodium dodecyl sulfate (25), collagen (26), lysophosphatidic acid (27), non-esterified fatty acids (28), and heparin (29), have been reported to lower the stability of β2m's native state at neutral pH, and also aid in the extension of amyloid fibrils. Therefore, much is now known about how β2m aggregates under non- physiological conditions, as well about how the morphologies of its aggregated amyloid forms vary widely. A definitive understanding of physiological deposition, however, remains elusive.

A.1.6 Metal ion binding by β2m

Notably, some studies have focused on β2m oligomer formation at physiological pH and ionic strength in the presence of metal ions (30-34). Miranker and colleagues tested the interaction of β2m with divalent ions such as Cu^{2+}, Ca^{2+} and Zn^{2+} (31). The group reported that only the Cu^{2+} ion binds specifically to β2m, with a maximum stoichiometry of 4:1 (as observed using LC-coupled ESI mass spectrometry). The group also demonstrated the presence of two bound Cu^{2+} ions in soaked crystals of β2m (28). Working separately, Vachet and colleagues examined the binding of copper to β2m in considerably greater detail (32,33). They reported that monomeric β2m binds Cu^{2+} via the N-terminal amine, the amide of Gln2, the imidazole ring of His31, and the carboxylate of Asp59. However, they also reported that in dimeric and tetrameric β2m, Asp59 is no longer involved in the binding of Cu^{2+}, although the remaining elements continue to maintain a site with weaker binding.

Vachet and colleagues feel that Cu^{2+} binding by Asp59 in monomeric β2m requires a large conformational reorganization in the molecule (relative to its HLA chain-bound conformation), and they propose that this conformational reorganization is important for establishing certain dimer-stabilizing salt bridges between Asp59 and Lys19. The group has also shown that when β2m is unfolded, up to four copper ions can bind, respectively, to the N-terminal amine, and to three histidine residues, His31, His51, and His81. The group feels that a cis-trans isomerization necessarily occurs at Pro32 and also that there is large-scale repositioning of residues in the protein, involving a sequential series of conformational changes. What remains puzzling, however, is the fact that this group holds that copper is ultimately expelled from oligomeric β2m, with the tetramer being the smallest oligomer that manages to expel copper. This contention, at first sight, appears to be at variance with the observation of Miranker and colleagues that monomeric β2m itself is able to bind to up to four copper ions (34), this being an observation based entirely on mass spectrometric experiments for which there is still no structural rationale; unless, of course, one proposes that four copper atoms bind only to the unfolded form of β2m, as suggested by Vachet and colleagues, and also that there is sequential binding accompanying progressive structural reorganization, or unfolding, leading to observations of binding of up to 4 copper atoms by both groups (33).

In summary, metal binding by β2m (in particular, copper binding) has been observed and commented upon in the past, and also held to be important for oligomer formation that could

ultimately lead to significant aggregation. The relevance of Cu^{2+} to DRA is also not commonly questioned, even though copper is only present in vanishingly low concentrations in the human body. The relevant argument appears to be that concentrations of copper increase during dialysis, due to the presence of copper in the equipment used for dialysis. Thus, it has been suggested by Miranker and colleagues that levels of copper probably rise during dialysis and induce oligomerization, aggregation and precipitation of β2m (34). However, it is not yet established unequivocally whether copper is physiologically involved in the formation of oligomers by β2m, or in the deposition of β2m as amyloid fibrils (35). The extent to which the role of copper in DRA is accepted by the medical fraternity is also not entirely clear from the literature.

A.1.7 Objectives behind study of β2m interaction with Calcium

In present study we have revisited the entire subject of metal binding by β2m. However, at the outset we wish to clarify that we are far more interested in the binding of β2m to calcium than to any other metal. There are several reasons for this. (i) Of all the divalent metal ions present in the human body, calcium is probably the one present in the serum in the highest concentration range (1-2 mM), with the largest number of known physiological, metabolic, biochemical and structural roles, causing it to be the metal with the highest potential degree of relevance to any disease involving metal binding; (ii) It is conceivable that Miranker and colleagues did not explore the binding of calcium sufficiently, owing to their preoccupation with the binding of copper. They reported that calcium and zinc binding to β2m occur non-specifically. We feel that significant calcium binding by β2m could potentially be observed if this aspect were to be re-explored, perhaps with changes in concentrations of proteins and ions, or with the exploration of biological buffers. Further, it could also be exciting to examine where such ‘non-specific’, or even ‘specific’ binding of calcium occurs in β2m; (iii) It is conceivable that different metal ions bind to β2m in somewhat different ways, such that the affinity or specificity of binding of one metal would not necessarily be entirely correlated with effects on protein conformation (if any), or on the propensity of the protein to aggregate and precipitate (if any) due to any other metal. In other words, we felt that calcium could potentially reproducibly cause not just oligomerization, but also significant aggregation and precipitation under physiologically relevant conditions of metal and protein concentration, regardless of whether copper is observed to do the same. This alone could make it worth our while to try and test this out; (iv) There is a little-noticed piece of work in the literature which indicates some sort of a cause-effect relationship between β2m and calcium, in respect of the

behavior of calvariae. The protein, β2m, is thought to be mitogenic for both osteoblasts and osteoclasts. It has been reported that the addition of β2m to calvariae leads to a net efflux of calcium and osteoclast stimulation (36). Although the report did not further investigate the mechanism by which this occurs, there are two possible explanations for such an observation. On the one hand, it is possible that β2m binds to some cell surface proteins and induces the efflux of calcium. On the other hand, it is also possible that there is a net ongoing influx-efflux of calcium that is affected by the presence of β2m as a titrant of calcium outside the cell. Certainly, the presence of an extracellular calcium binder could lead to a net efflux of calcium from cells. Indeed, a separate report suggests that there is a negative correlation between β2m levels in the serum and the concentrations of free calcium in the serum (37). We feel, therefore, that a strong case exists for examination of the direct binding (and sequestering) of calcium by β2m. Since there is not a singly report in the literature to suggest either that such binding occurs quantitatively either in vitro or in vivo, or indeed that any such binding has effects upon β2m conformation or aggregation behavior [discounting, of course, the remark made by Miranker and colleagues, in passing, that β2m binds to calcium non- specifically], we decided to examine whether indeed β2m binds to calcium under physiological conditions.

First, we examined the structure and sequence of β2m in the light of the possible presence of metal binding sites other than those reported by Vachet and colleagues, or Miranker and colleagues. Figure A.3 panel A shows, the sequence of β2m while Figure A.3 panel B, shows a ribbon diagram representation of its beta sheet structure with potential calcium binding motifs. From the figure, and in the light of what is known now about calcium-binding motifs, it is immediately evident that there are several potential alternative metal-binding motifs in β2m. It has been reported that DXD motifs in numerous enzymes participate in metal binding in association with sugar binding, through involvement of the second aspartate residue in the motif (38-40), and it has also been reported that in certain instances DXD motifs can even bind directly to metal atoms through both the aspartate side chains (41).

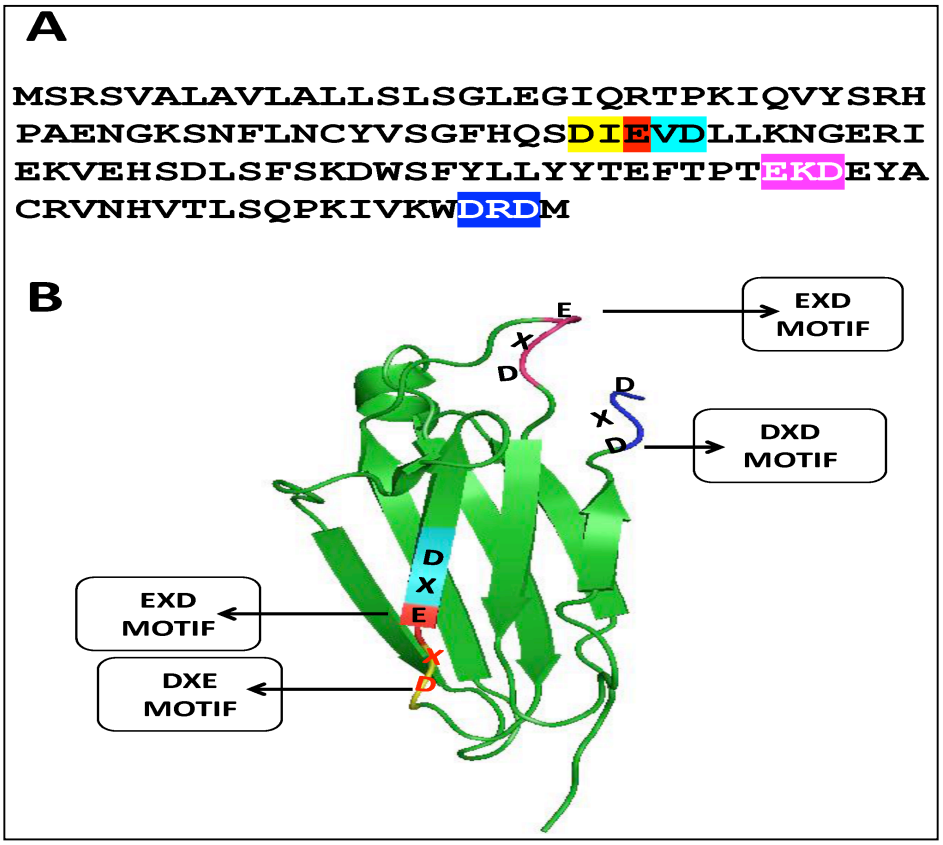

Figure A.3: **Potential additional/alternative sites for metal-binding and, in particular, calcium-binding in the sequence** (**A.3.A**) and structure (**A.3.B**) of the HLA-interacting protein, β2m.

Further, in certain primase enzymes from thermophiles, and also in topoisomerases of various kinds, it has been reported that a DXDXD motif directly binds to calcium (42). Allowing for substitutions of D by E, there are either three or four sites containing the sequences DXD, DXE, EXD, DXDXD / DXDXE / DXEXD in the β2m sequence. A protein with known roles in calcium efflux from cells and in the development of osteoclasts and osteoblasts in the bone (with the status of a bone growth factor) would be quite unlikely to possess four potential metal/calcium binding sites in its sequence, unless such sites were indeed involved in the binding of calcium. Thus, it would seem as if the issue of calcium binding needed to be examined in greater detail. Here, we show for the first time ever that calcium does indeed bind quantitatively to β2m, causing conformational changes as a consequence and also bringing about the aggregation and precipitation of β2m into amorphous aggregates that subsequently turn into amyloid fibrils. We also show that this behavior is displayed by the binding of other divalent ions too, including copper. Indeed, we show that the precipitation induced by copper is by far the highest, for all divalent metal ions tested, using comparable metal ion concentrations. However, we also show (and argue) that calcium binding remains the most relevant of all metal binding to β2m because none of the other ions are present in the serum at concentrations comparable to those of calcium. The second part of section I explores the interactions between β2m and 17-β-Estradiol (E2). Using biophysical techniques like difference absorption spectroscopy, fluorescence spectroscopy and surface plasmon resonance we have explored binding interaction between β2m and E2. The third part of the section I, focuses on the cytotoxicity associated with oligomeric β2m and female steroid hormone E2. As background information, formation of oligomers has been demonstrated to be the essential step in amyloidosis (43). Oligomeric protein species is now established to be the precursors of amyloid plaques (44). Monomeric β2m spontaneously forms oligomers in solution and these oligomers are cytotoxic to mouse neuroblastoma cell line Neuro2a (N2A) *in vitro*. In the present work we demonstrate that SDS resistant β2m oligomers are formed during sonication. The oligomers follow logarithmic regression in distribution from monomer to higher order oligomers. Here we also demonstrate for the first time, that β2m oligomers are cytotoxic and that E2 and N-Acetylcysteine (NAC) abrogate the cytotoxicity of β2m oligomers. We also demonstrate that labeling the oligomeric β2m with any dye that covalently modifies amines leads to loss of cytotoxic activity. As an aside, we also demonstrate for the first time a physical interaction between β2m and E2 proving that β2m binds to E2.

A.2.1 Materials:

All chemicals were purchased from Sigma Chemical Co., New England Biolabs, US biologicals and were of highest purity available. Ni-NTA agarose was purchased from Qiagen. PD-10 desalting columns were purchased from GE Healthcare Biosciences. 17β-estradiol, N-acetylcysteine (NAC), MTT cell proliferation assay kit; were purchased from sigma. Animal cell culture media components were purchased from Himedia, India or Difco, USA.

A.2.2 Bacterial strains and vectors used:

Escherichia coli strains and cloning/expression vectors were purchased from Novagen. The usage of *E. coli* strains and vectors for present study is depicted in the following table:

Expressed Proteins	**Vector used**	***E. coli* strain (s) used**	
		Cloning host	**Expression host**
β-2 microglobulin	pET 23A	XL-1 BLUE	BL21-Plys
MUT-β-2 microglobulin	pET 23A	XL-1 BLUE	BL21-Plys

E. coli strains bearing the respective plasmid were maintained as glycerol stock and stored at -80 °C. For expression *E.coli* strains were grown in Luria Bertani (LB) supplemented with suitable antibiotics. Bacterial cultures for β-2 microglobulin was grown at 37 °C with shaking at 200 rpm till OD_{600} of 0.6 followed by overnight induction with 1mM IPTG at 18 °C.

A.2.3 Cell Line

Mouse neuroblatoma cell line Neuro2A (N2a) of ATCC origin, was kindly provided by Dr. Samarjit's group at IISER Mohali.

A.2.4 Chemicals and Kits

All reagents used in this study were of analytical grade or higher. Restriction/modification enzymes and molecular biological reagents were obtained from New England Biolabs, USA or Promega Life Sciences, USA. Protein molecular weight markers were purchased from

Fermentas. Plasmid isolation kits, Gel extraction kits, PCR purification kits, Plasmid miniprep kits, Ni-NTA Agarose/Superflow used in this study were obtained from Qiagen, Germany. All other fine chemicals were from Sigma Aldrich, USA.

A.2.5 Antibiotics

The antibiotics used in this study were procured from Sigma Aldrich, USA and their 1000X stocks compositions are mentioned below.

Antibiotic	Stock concentration
Ampicillin	100mg/ml in water
Tetracycline	12.5mg/ml in 70% ethanol
Chloroamphenicol	35mg/ml in methanol

Antibiotic stock solutions were filter sterilized through 0.22 μM filters (Millipore) and stored in aliquots at -20 °C.

A.2.6 Antibodies

Anti β-2m antibody was purchased from Santa-cruz

A.2.7 Luria Broth (LB)

Luria bertini media was prepared by dissolving following constituents in 900 ml deionized water.

Components	Weight for 1 L (g)
Tryptone	10
Sodium chloride	10
Yeast Extract	5

pH was adjusted to 7.4 with 1N NaOH and final volume was brought to 1 L with water. Media was sterilized by autoclaving on liquid cycle for 20 minutes at 15 psi.

LB agar: LB agar was prepared by adding 1.5 % agar in LB medium.

A.2.8 Primers for SOE

The primers for SOE work were designed using Gene runner software.

Primer1 (P1): β2m NdeI fwd
5'- AAGCATAGCATATGATCCAGCGTACTC- 3'

Primer2 (P2): β2m C25S fwd
5'-TTTCCTGAATTCCTATGTGTCTGG- 3'

Primer3 (P3): β2m C25S rev
5'-CCAGACACATAGGAATTCAGGAAA- 3'

Primer4 (P4): β2m C81S fwd
5'-GATGAGTATGCCTCCCGTGTGAAC-3'

Primer5 (P5): β2m C81S rev
5'-GTTCACACGGGAGGCATACTCATC-3'

Primer6 (P6): β2m XhoI (his tag) rev
5'-AATACTAACTCGAGCATGTCTCTATCCCAC-3'

A.2.9 Buffers and solutions for recombinant DNA work

All the buffers and solutions for recombinant DNA work were prepared in deionized water (18 Ω).

A. 6X DNA gel loading buffer

10 ml of 6X DNA gel loading buffer was prepared by dissolving the following components in deionized water

Components	Amount
Bromophenol Blue	25 mg
Xylene Cyanol	25 mg
Glycerol	3 ml

B. 50X TAE Buffer

Components	Amount
Tris.Cl	242 g
Glacial acetic acid	57.1 ml
0.5M EDTA (pH 8.0)	100 ml

pH was adjusted to 8.3 and buffer was sterilized the by autoclaving on liquid cycle for 20 minutes at 15 psi.

A.2.10 Buffers and solutions for protein purification

(I) Denaturing purification of 6X His-tagged proteins

The denaturing purification of over expressed proteins was carried out according to denaturing protein purification protocol provided in "The Qiaexpressionist^{TM}: A handbook for high-level expression and purification of 6xHis-tagged proteins. Composition and pH of buffers used in denaturing protein purification is mentioned in following tables:

Lysis Buffer B	
Urea	8 M
NaH_2PO_4	100 mM
Tris.Cl	10 mM
pH was adjusted to 8.0 with NaOH	

Wash Buffer C	
Urea	8 M
NaH_2PO_4	100 mM
Tris.Cl	10 mM
pH was adjusted to 6.3 with HCl	

Elution Buffer D	
Urea	8 M
NaH_2PO_4	100 mM
Tris.Cl	10 mM
pH was adjusted to 5.9 with HCl	

Elution Buffer E	
Urea	8 M
NaH_2PO_4	100 mM
Tris.Cl	10 mM
pH was adjusted to 4.5 with HCl	

All the buffers for denaturing protein purification were prepared in double deionized water and filtered through 0.22 μm filter.

A.3 Methods

A.3.1 Polymerase chain reaction (PCR)

Standard PCR amplification was carried out with 1-2 ng plasmid DNA as template, in a final reaction volume of 20 μl, containing 500 μM concentration of each dNTP (dATP, dTTP, dCTP and dGTP), 1.25 μM of each primer, 2-14 mM $MgSO_4$, 1X Thermopol buffer and 0.2 units of Phusion polymerase (New England Biolabs. For Splicing by Overlap Extension PCR, (SOE-PCR), forward and reverse primers (having overlap regions of 20-25 base pairs) at 1.25 μM concentration alone were used as templates along with the other standard PCR components as described above. All PCR reactions were performed in Eppendorf mastercycler thermal cycler. PCR was usually carried out for 25-30 cycles with initial denaturation at 95 °C for 5 min, subsequent denaturations at 95 °C for 1 min, annealing at 56-65 °C for 2 min (the annealing temperatures varied with each template-primer set) and extension at 72 °C for 1-3 min, depending upon the size of the fragment to be amplified. DNA ladders were electrophoresed along with PCR products on agarose gels for size analysis of the amplified fragments.

A.3.2 Restriction endonuclease digestion of DNA

DNA samples were digested with restriction endonucleases in their specific reaction buffers. Both restriction enzymes and the buffers were purchased from MBI Fermentas. Double enzyme digestions were carried out for 15-30 minutes. Figure A.4 describes the schematic for SOE based mutagenesis in β2m

A.3.3 Agarose gel electrophoresis

DNA fragments were fractionated on 0.8, 1.0, 1.5 or 2 % agarose gels depending on their sizes. 6X gel loading buffer was added to DNA samples at a final concentration of 1X prior to loading onto the gel. Electrophoresis was carried out in 1X TAE buffer at ~ 8V/cm. Ethidium bromide (0.5 μg/ml) was supplemented in the agarose gel for visualizing DNA on an UV transilluminator. DNA ladders resolved at 100 bp and 1 kb were used as markers for calculating the size of DNA fragments from their relative mobility.

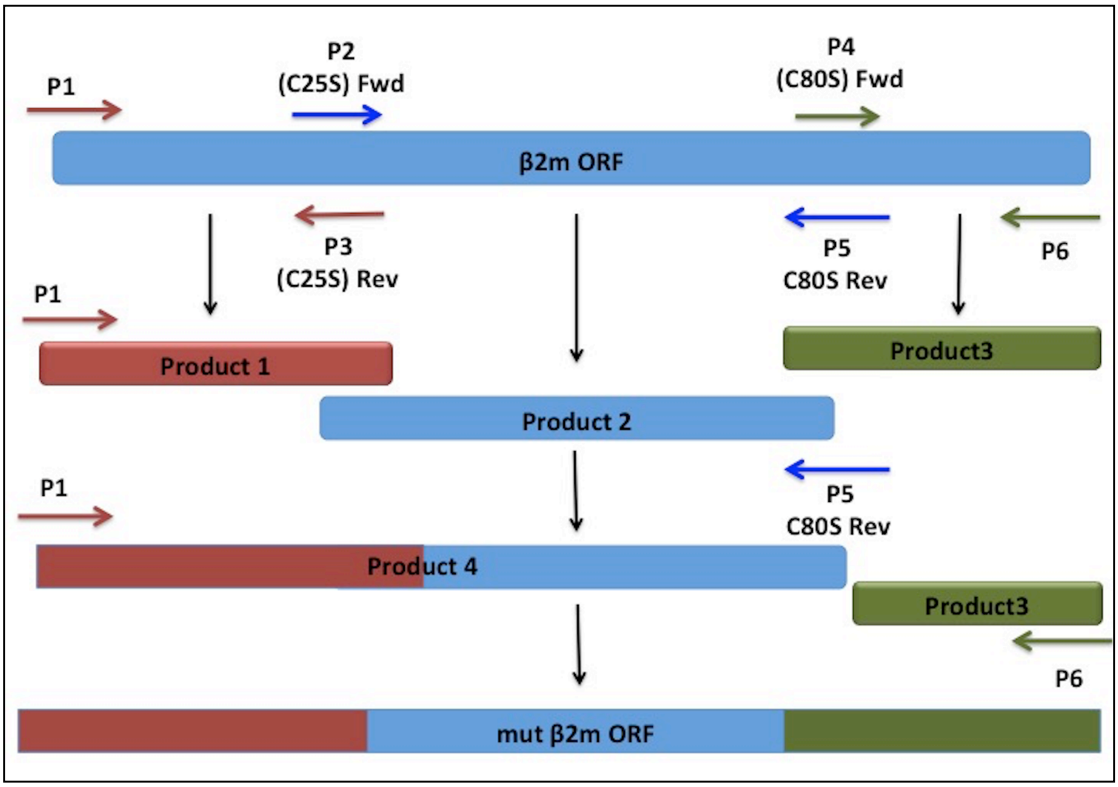

Figure A.4: Schematic for SOE based mutagenesis in β2m: β2m open reading frame (ORF) was isolated from plasmid bearing human β2m clone using primer pairs P1 and P6. The β2m ORF was subjected to standard PCR using primer pairs P1-P3, P2-P5, P4-P6; yielding products 1,2 and 3 respectively. The Product 1 and Product 2 were mixed and subjected to PCR using primer pair P1-P5 yielding product 4. Finally product 4 and product 3 were mixed and subjected to PCR using primer pair P1-P6 to synthesise mutated β2m ORF.

A.3.4 Purification of DNA fragment(s) from agarose gels

After electrophoresis, DNA was visualized using a UV transilluminator. Agarose blocks containing the desired DNA fragment(s) were excised out and weighed. DNA was extracted using a gel extraction kit (Qiagen, Germany) as described below:

(1) Solubilization and binding buffer (Buffer QG,) was added at 3 volumes per volume of the agarose gel slice.

(2) Incubation was done at 50 °C till complete dissolution of the agarose gel was achieved.

(3) The dissolved agarose solution containing the DNA was then poured onto a QIAquick spin column (provided by the manufacturer) to allow the adsorption of DNA onto the silica gel matrix.

(4) The impurities were washed away with an ethanol-containing buffer (PE, supplied by the manufacturer)

(5) DNA was finally eluted in autoclaved distilled water, and quantitated.

A.3.5 Ligation

Digested and purified plasmids and inserts were set up for cohesive-end ligation using Quick Ligation Kit (New England Biolabs, USA). An insert**:** vector ratio of 3**:**1 was used and the ligation reactions were incubated at 25 °C for 30 minutes.

A.3.6 Preparation and Transformation of *E. coli* competent cells

1. A single colony of *E. coli* was inoculated in LB media and grown to saturation at 37 °C.
2. The culture was re-inoculated into 200ml fresh LB medium and grown to early log phase (A_{600} of 0.4-0.5)
3. The cells were chilled on ice for 15 min, centrifuged at 1600x g for 7 minutes at 4 °C in prechilled centrifuge tubes. Cells were kept on ice at all subsequent steps.
4. The supernatant was discarded and cells were resuspended in 20 ml of ice-cold calcium chloride, after which they were again centrifuged at 1100x g for 5 min at 4 °C.
5. The supernatant was again discarded and step 4 was repeated.
6. The cell pellet obtained in step 5 was resuspended in 20 ml of ice-cold calcium chloride and kept on ice for 30 min.

7. The cells were again centrifuged at 1100x g for 5 min at 4 °C and supernatant was carefully discarded after which the cells were resuspended in 4 ml of ice-cold calcium chloride.
8. Finally aliquots of 100 µl were made from the suspension obtained above and these were used immediately or stored at –80 °C till further use.

A.3.7 Transformation

For transformation by heat shock method, ligation mix (10 µl containing ~ 20 ng DNA) or sequenced positive clone DNA (2-5 ng) was added to an aliquot of competent cells and given heat shock at 42 °C for 90 seconds in water bath (Amersham Pharmacia). 1 ml LB was added to the transformed cells and incubated at 37 °C for 1 hr. 50-100 µl aliquots were plated on LB agar plates supplemented with desired antibiotics.

A.3.8 Isolation of plasmid DNA

Plasmid bearing the desired construct was isolated using Qiagen quick mini prep kit according to manufacturers protocol

1. A vial containing 5 ml of LB supplemented with appropriate antibiotics was inoculated with *E. coli* stock bearing the plasmid and incubated overnight at 37 °C.
2. Cells were collected by centrifugation at 3000 rpm and resuspended in 0.1 ml of ice-cold GTE solution by vigorous vortexing.
3. The tube was centrifuged at 13000 rpm for 10 min at room temperature and the supernatant was transferred to a fresh tube followed by addition of 0.8 ml of 95% ethanol to precipitate the DNA.
4. The solution was again centrifuged at 13000 rpm for 10 min to pellet down the plasmid DNA.
5. The supernatant was discarded and plasmid pellet was washed with 1 ml of 70% ethanol and spun again as in step 6.
6. The supernatant was discarded and the plasmid pellet was air-dried or vacuum dried and dissolved in 25 µl TE. The plasmid DNA was then stored at -20 °C.

A.3.9 Screening for positive transformants

The presence of the insert was confirmed by electrophoresing the plasmids on 0.8-1.2% agarose gels alongside a control plasmid lacking the insert. This was further confirmed by

restriction digestion using the endonucleases used for cloning, or by PCR using the gene-specific/vector-specific primers, followed by electrophoresis on gels of appropriate percentage.

A.3.10 β2m expression

A clone of human β2m and mutant β2m with a C-terminal 6xHis tag were sub-cloned in the pET 23A vector (between a 5' -NdeI site and a 3' -XhoI site) were overexpressed in, and purified from, *E.coli* cells of the BL21 Star (DE3) pLysS strain. Transformed cells were grown overnight at 37 °C with 100 mg/ml ampicillin and 35 mg/ml chloramphenicol. An overnight culture was sub-cultured into 500 ml of LB broth in a 1.0-liter flask containing the same antibiotics and cells were grown at 37 °C in a rotary shaker until the culture reached an OD_{600} of 0.6. Protein expression was then obtained through induction by 1 mM IPTG, with induced cultures being grown overnight. Cells were pelleted through centrifugation at 5000 rpm for 10 minutes and treated as given below.

A.3.1.11 β2m purification under denaturing conditions

Both wild type and mutant β2m were purified in denaturing conditions. Pelleted cells containing overexpressed β2m protein were re-suspended in 100 mM NaH_2PO_4, 10 mM Tris-Cl, 8 M urea, pH 8 (50 ml per ml of culture), and sonicated to effect cell lysis. The supernatant was separated from cell debris through centrifugation at 16,000 rpm for 20 minutes at 4 °C. Purification was achieved by loading the supernatant onto a Ni-NTA affinity column (1 ml resin, Qiagen) pre-equilibrated with the sonication buffer. Non-specifically bound proteins were removed by washing with 40 ml of wash buffer (100 mM NaH_2PO_4, 10mM Tris-Cl, 8 M urea, pH 6.5). The bound 6xHis tagged protein was eluted using standard elution buffer (100 mM NaH_2PO_4, 10 mM Tris-Cl, 8 M urea, pH 4.5).

A.3.12 Glycine SDS-PAGE

Expression and purification of β2m was checked by using 15% separating gel and 5% stacking gel. Denaturing SDS electrophoresis was run according to method derscribed by Laemmli (40). Protein samples were mixed with 5X sample buffer containing 8 molar urea and boiled for 5 minutes. Samples were centrifuged at 13,000g for 5 minutes prior to loading onto the gel. Protein samples were loaded onto gels along with protein molecular weight marker and run in Laemmli gel running buffer at constant voltage of 150V in a BioRad Mini Protean electrophoresis apparatus. The gels were stained for 1 hour with staining solution

followed by destaining for 2-3 hours.

A.3.13 ImageJ analysis of β2m oligomers

Purified β2m was boiled with non-reducing loading buffer and loaded onto 15% non reducing SDS-PAGE. After staining and destaining the gel was imaged using Bio-Rad Gel imager. The gel image was analyzed using ImageJ software to quantify the relative distribution of oligomers.

A.3.14 Intact mass analysis by mass spectroscopy

Various β2m elutions from Ni-NTA purification were prepared for intact mass spectroscopy. Samples were reduced and alkylated. Processed samples were isolated using Zip-Tip c-18 tips (Millipore) containing C18 resin attached to the tip, occupying about 0.5µl volume. The Zip-Tip was washed with 0.1% TFA in 1:1 acetonitrile:water followed by equilibration twice with 0.1% TFA in water. The sample was repeatedly passed through the Zip-Tip by pipetting the sample in-and-out to allow binding of sample to resin. Post binding, the Zip-Tip was washed three times with a solution of 0.1% TFA, 5% methanol in water. The sample was eluted from the Zip-Tip in 1.8 µl of alpha-cyano-4-hydroxycinnamic acid in 0.1% TFA, 50% acetonitrile, directly onto the MALDI-TOF sample plate. Sample plate was allowed to dry for 2 hours followed by MALDI-TOF analysis for intact mass distribution using Applied Biosystems Voyager System 4402.

A.3.15 Western Blotting

The identity of purified protein was confirmed with Western blotting technique. The purified protein was subjected to non-reducing SDS-PAGE. The gel was run until the dye front reached the end of the gel. The gel was soaked for 10 minutes in transfer buffer to remove SDS, and to fix the protein in the gel. After soaking, the gel was subjected to Western blotting using Bio-Rad semi-dry transfer apparatus at 18V for 18 minutes. Followed by transfer, the PVDF membrane was blocked with 5% non-fat skimmed milk in PBST (1X PBS, 0.01% tween-20) for 1 hour with constant shaking. The PVDF membrane was washed thrice with PBST for 10 minutes each time. The washed membrane was incubated overnight with the anti-β2m antibody at 1:5000 dilutions. After incubation with the anti-β2m antibody, the membrane was washed thrice with PBST for 10 minutes each, followed by incubation with the secondary antibody for 1 hour with shaking. Secondary antibody was removed and the membrane was washed thrice with PBST for 10 minutes each. TBST was soaked off the

membrane with tissue paper, and the membrane was soaked in ECL substrate for 5 minutes in the dark. The membrane was exposed for 2 minutes to detect bands of interest in GE LAS densitometer scanner.

A.3.16 β2m refolding and reconstitution

The eluted β2m was reconstituted by extensive dialysis against deionized water to remove urea, followed immediately by dialysis against either Tris-buffered saline (TBS), or phosphate-buffered saline (PBS) of progressively decreasing pH values of 8, 7.8, 7.6 and 7.4, to obtain protein in physiological buffers of pH 7.4. The TBS used had the following composition and characteristics: 25 mM Tris, 150 mM NaCl, 2 mM KCl, pH 7.4. Similarly, the PBS used had the following composition and characteristics: 137 mM NaCl, 2.7 mM KCl, 10 mM Na_2HPO_4, 1.8 mM KH_2PO_4. It may be noted that this series of dialysis steps is critical. If eluted protein is directly dialyzed against TBS or PBS without first being dialyzed against water to remove urea, there is extensive protein precipitation observed; however, no precipitation whatsoever is observed when dialysis is initially carried out against deionized water (with a pH of ~6.0) and followed by progressively dialysis against TBS or PBS, initially using mildly alkaline pH before gradually reducing the pH to 7.4. It may be noted that for isothermal titration calorimetry (ITC) experiments, TBS or PBS were not used; instead, eluted β2m was extensively dialyzed against deionized water with several changes of deionized water, and this protein was used. TBS or PBS buffers were not used for ITC experiments because of problems with the heat of dilution observed in mixing buffered solutions of protein with buffered solutions containing metal ions. The dialyzed protein was concentrated using Amicon centrifugal concentrators with 3000 Dalton cutoffs.

A.3.17 Experiments with calcium addition:

A.3.17.1 Resonance Rayleigh Scattering (RRS)

A Cary Eclipse spectrofluorimeter (Varian) was used to measure RRS spectra and intensities using a cuvette with a path length of 1 cm. The RRS spectrum was collected by synchronously scanning excitation and emission monochromators between 200 to 700 nm, using a wavelength difference ($\Delta\lambda$) of 0 nm, and monochromator bandpass values of 5 nm each. The concentration of β2m protein used was 0.83 μM and the following concentrations of calcium chloride were used to monitor the RRS signal: 0.083, 0.166, 0.249, 0.332, 0.415, 0.497, 0.579 and 0.66 mM respectively.

A.3.17.2 Horizontal Attenuated Total Reflectance (HATR) Fourier Transform infrared (FT-IR) spectroscopy

FTIR spectra of β2m (20 μM) were measured in TBS, using a Tensor 27 spectrometer equipped with the sealable, temperature-controlled Bio-ATR-II protein sample accessory and CONFOCHECK software. For this, a 25 μl volume of β2m solution was placed in a conical chamber associated with the HATR crystal, and the control spectrum for the protein was collected. Following this calcium chroride was added (final concentration 125 mM) and spectra were collected either immediately, or after the passage of 10 minutes and 2 hours, respectively, to monitor spectral changes indicative of structural changes, if any, in the protein. Any microscopic aggregates would have settled onto the crystal's surface and contributed to the spectrum during the experiment. In any HATR crystal, the absorption signal only owes to the layers of molecules immediately proximal to the crystal's surface (and within the distance accessed by the evanescent wave associated with the FTIR beam undergoing total internal reflection in the crystal). Thus, spectra collected at later time points could owe to a combination of molecules in solution and any depositing aggregates, although no visible deposition was seen, owing to the low calcium concentration used.

A.3.17.3 Isothermal Titration Calorimetry (ITC)

ITC experiments were done using an ITC 200 instrument (GE-Microcal). Purified β2m was extensively dialyzed against MilliQ deionized water with ten changes. The dialyzed protein was filtered through a 0.22 μm filter. Calcium chloride was also dissolved in the same miliQ water used in final change during dialysis, to reduce effects due to heat of dilution due to ITC. Calcium chloride (14 mM) solution was injected into the sample cell (different injection volumes as mentioned below) containing 200 ml of β2m solution (125 mM). The titration was done at 25 °C with an initial 0.4 ml injection followed by 19 injections of 2 ml each, with 180-second intervals between each injection. The data were plotted as a function of molar ratio and binding isotherms were fitted using Origin 7.0 software provided with the instrument.

A.3.17.4 Transmission Electron Microscopy (TEM)

20 μM β2m in TBS containing 4 mM $CaCl_2$ in TBS was incubated to create precipitates. The precipitates were spread out on grids, and negatively stained with phosphotungstic acid (PTA) and imaged using standard protocols on a JEOL JEM- 2100 microscope.

A.3.17.5 Thioflavin T fluorescence

Fluorescence spectra of thioflavinT (ThT) dye controls as well as dye bound to protein aggregates were collected on a Horiba Fluoromax-4 spectrofluorimeter, with the excitation monochromator set at 440 nm and emission collected between 450 and 550 nm, using with bandpasses of 2.5 nm, and 5 nm, respectively. Samples were prepared in deionized water. The protein sample containing 20 μM β2m, 4 mM $CaCl_2$ and 12.5 mM ThT was incubated for three weeks at 37 °C with shaking.

A.3.17.6 Visual examination of precipitation

Precipitation with other metals: The ability of metal ions to precipitate β2m was assessed visually by monitoring the amount of precipitate obtained, at various intervals of time. Tubes containing precipitates were photographed. Stock solution of $CaCl_2$, $NiSO_4$, $CuSO_4$, $ZnCl_2$, $FeCl_3$, $MgCl_2$, were prepared in Tris buffered saline (pH7.4) and filtered through 0.2 μm filter and added to final concentration of 5 mM, in 20 μM β2m present in Tris buffered saline (pH 7.4).

A.3.17.7 Effects of using different concentrations of calcium

Various concentrations of calcium (0.5 to 5.0 mM) were incubated with 20 μM solutions of β2m protein, in different tubes. Photographs were taken to visually monitor the extent of precipitation.

A.3.17.8 Disassembly of aggregates with EDTA

Tubes containing precipitated protein (containing 5 mM calcium chloride) were incubated with 5 mM or 10 mM EDTA for 24 hours to monitor dissolution. Photographs were collected with appropriate controls. Similarly calcium precipitated β2m was incubated with 10 mM EDTA and RRS spectra was collected after every thirty minutes.

A.3.18 Experiments with 17-β-estradiol addition

A.3.18.1 Difference absorption spectroscopy

Difference absorption spectroscopy was performed to detect interactions between β2m and 17-β-estradiol. Difference absorption spectra were taken on a Cary 50 UV-Visible spectrophotometer, using a tandem absorption cuvette containing two compartments of path length ~ 0.45 cm separated by a thin 0.1 cm-thick quartz wall. 10 μM β2m in PBS was taken in one compartment, and 100 μM 17-β-estradiol in PBS was taken in other compartment and the baseline was collected. Then the cuvette was inverted to let the contents of both

compartments mix, and inverted again to allow the mixed solution to fall back in roughly equal volumes in each of the two compartments. The absorbance scan was then performed, against the older collected baseline, between 200 and 600 nm.

A.3.18.2 Fluorescence spectroscopy

Fluorescence spectroscopy was carried out on a Cary Varian Eclipse Fluorimeter. For fluorescence emission spectra, excitation wavelength was set at 280 nm and emission spectrum was collected from 300-400 nm. The band passes used were 5/5 nm for excitation and emission monochromators. Emission spectrum was collected for 10 μM β2m in PBS was taken in one compartment and 100 μM 17-β-estradiol separately, and after mixing.

A.3.18.3 Surface Plasmon Resonance Measurements

Surface Plasmon Resonance measurements were done to confirm binding of β2M and 17-β-estradiol. Surface plasmon resonance (SPR) measurements were performed on a Bia-core 3000 (GE Healthcare Life Sciences) instrument at 25 °C using a CM5 sensor chip with immobilized anti-β2M antibodies. The chip surface was equilibrated with PBS (pH 7.4). 20 μl of β2M in PBS (7.4) was injected at a flow rate of 5 μl/min. Subsequently; 20 μl of 17-β-estradiol was injected at a flow rate of 1 μl/min. The experiment was repeated for different concentrations of 17-β-Estradiol.

A.3.19 Experimental design to study oligomeric β2m induced cytotoxicity

A.3.19.1 In-*vitro* culture of the N2A cell line

Mouse neuroblastoma cell line N2A cells were grown in minimum essential medium (DMEM) supplemented with 10% FBS, 2 mM L-glutamine, 1U/ml antibiotic-antimycotic and 1.5 g/L sodium bicarbonate. The cells were induced to differentiate by incubating with minimum essential medium (DMEM) supplemented with 2% FBS, 2 mM L-glutamine, 1U/ml antibiotic-antimycotic and 1.5 g/L sodium bicarbonate. For experimentation, the culture medium was replaced by phenol red free DMEM supplemented with 1U/ml antibiotic-antimycotic and 1.5 g/L sodium bicarbonate.

A.3.19.2 FITC labeling of β2m

β2m was dialyzed against 100 ml of carbonate buffer (500 mM, pH 9.5) overnight at 4 °C. Dialyzed β2m was mixed with 122 μl of 10 mg/ml FITC solution in water, and the final

volume was adjusted to 1ml with water and incubated overnight at room temperature. After incubation of β2m with FITC, the reaction mixture was mixed with 9 ml of binding buffer (100 mM NaH_2PO_4, 10 mM Tris-Cl, 8 M urea, pH 8) and loaded onto Ni-NTA column pre-equilibrated with binding buffer. The column was washed with 5 column volumes of washing buffer (100 mM NaH_2PO_4, 10 mM Tris-Cl, 8 M urea, pH 6.5) to retain bound labeled protein and remove unreacted FITC. FITC labeled β2m was then eluted with 5 ml of elution buffer (100 mM NaH_2PO_4, 10 mM Tris-Cl, 8 M urea, pH 4.3). Eluted protein was concentrated to 2.5 ml using Millipore's Amicon Ultra-15 centrifugal concentrator with 3 KDa molecular weight cut-off. Concentrated protein was applied to a PD-10 desalting column pre-equilibrated with phosphate buffered saline (pH 7.4) and eluted with 3.5 ml of PBS. Resulting protein was concentrated using Millipore's Amicon Ultra-15 centrifugal concentrator with 3 kDa molecular weight cut-off. Labeled protein was diluted 100-fold and absorbance was recorded at 280 and 493 nm simultaneously. Protein and FITC concentrations were calculated according to following formulas:

Protein concentration = (A280- (0.31*A493))*dilution factor/ ε protein

FITC concentration = (A493*dilution factor) / ε FITC

Degree of substitution = [FITC]/[protein]

Where ε protein is 20065 cm^{-1} M^{-1} for β2m and ε FITC is 68,000 cm^{-1} M^{-1}

A.3.19.3 MTT Assay to check cell viability

MTT assay was used to determine the cytotoxic effects of oligomeric β2m. N2A cells were plated in 6-well plates and incubated in a humidified CO_2 incubator. Cells were induced to differentiate for 24 hours in differentiation media. Cells were washed with serum-free media twice to remove any traces of serum and treated with 10 μM β2m, and 10 nM 17-β-estradiol, and incubated for 24 hours in serum-free DMEM containing 1U/ml antibiotic-antimycotic. Media was removed following incubation and cells were gently washed with sterile PBS and incubated for 3 h with 1 ml of 5 mg/ml of MTT, dissolved in serum free medium (MEM). After incubation cells were washed with sterile PBS and 1ml MTT solvent (0.1 N HCl propanol) was added to each well. Cell plates were covered with aluminum foil and placed on a rotary shaker for 10 minutes to completely dissolve the MTT product. Absorbance was measured with a Cary 50 spectrophotometer at 570 nm with background subtraction being

done at 650 nm. All treatments were given in triplicates and experiments were repeated thrice.

A.3.19.4 Cellular Effects of unlabelled and FITC-labeled β2m

N2A cells were seeded in 6-well plates and incubated in humidified CO_2 incubator at 37 °C. Cells were induced to differentiate for 24 hours in differentiation media. Cells were washed with serum-free media twice to remove any traces of serum and treated with 10 μM β2m, and 10 nM 17-β-estradiol, and incubated for 24 hours in serum-free DMEM containing 1U/ml antibiotic-antimycotic. Cells were treated with 10 μM β2m, 10 μM β2m-FITC, 10 nM 17-β-estradiol and observed under Nikon-Ti microscope.

A.3.19.5 High-resolution microscopy

N2A cells were plated on coverslips in 6-well plates and incubated in a humidified CO_2 incubator at 37 °C. After reaching 50-60% confluence, the cells were incubated in differentiation medium for 24 hours. Cells were washed with serum-free media twice to remove any traces of serum and treated with 10 μM β2m (FITC labeled and unlabeled), and 10 nM 17-β-estradiol, and incubated for 24 hours in serum free DMEM. For imaging, media was removed and cells were washed with PBS. Cells were fixed with 4% paraformaldehyde on ice for 5 minutes followed by three washes with ice cold PBS for five minutes each and mounted with a drop mounting media. Slides were allowed to dry overnight in dark. Cells were imaged using Delta Vision deconvolution microscope (GE Healthcare) with a solid-state illumination and coolsnap HQ2 1.4 megapixel monochrome CCD camera (Photometrics). Samples were illuminated with 100 % transmission at the FITC wavelength of the solid-state illumination (475/28 nm). The imaging was conducted using a Plane Apochromatic 100X/1.4 NA Oil DIC objective (Olympus).

Results and Discussion

Overexpression and Purification of β2m

The expression of recombinant β2m was obtained (Panel A in Figure A.5) and the identity of β2m was confirmed using SDS-PAGE analyses with molecular weight markers (panel B in Figure A.5). Following refolding, the protein was found to exist as a mixed population of monomers and various multimers, as evident in non-reducing SDS-PAGE, with the monomeric form being the dominant species and numerous multimeric forms (panel B in Figure A.5). The microenvironment of the *E.coli* cytoplasm, or indeed of any bacterium, is well known to be reducing, due to the excess of reduced glutathione. Hence, the bulk of cysteine residues in overexpressed β2m are expected to remain in a reduced state while the protein is still in the cytoplasm. Upon bacterial cell lysis by sonication in a lysis buffer of pH 8, in the presence of 8 M urea, the reduced cysteine residues of β2m are allowed to undergo aerial oxidation, leading to formation of β2m oligomers. The β2m oligomers observed after sonication appear to be stabilized by intermolecular disulfide bonds.

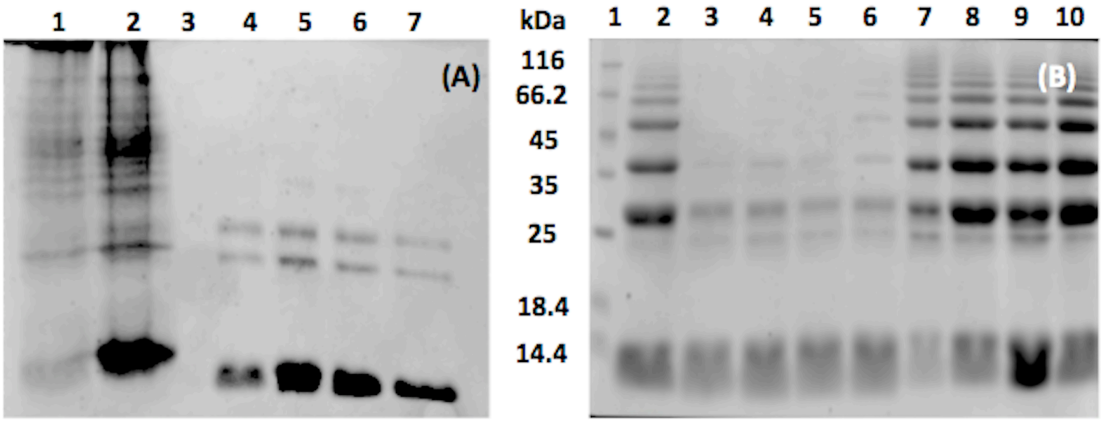

Figure A.5: A.5.A: Expression of C-terminal 6xHis tagged β2m. Lane 1 shows total cell lysate for un-induced culture showing leaky expression. Lane 2 shows total cell lysate for induced culture. Lanes 4, 5, 6, 7 show Ni-NTA purified β2m. **A.5.B:** Non -reducing SDS-PAGE of various β2m elutions after 24-hour storage at 4 °C. Lane 1 shows protein molecular weight marker. Lanes 2-10 shows various β2m elutions.

β2m forms SDS resistant oligomers that are susceptible to reduction by β-mercaptoethanol

β2m purified by denaturing purification was subjected to both reducing and non-reducing SDS-PAGE. The β2m upon boiling with reducing loading buffer containing β-mercaptoethanol is resolved mainly in form of a single band corresponding to monomeric β2m, whereas β2m boiled in non-reducing gel loading buffer, resolves a ladder like distribution of protein. Figure A.6 shows the reducing and non-reducing SDS-PAGE of β2m

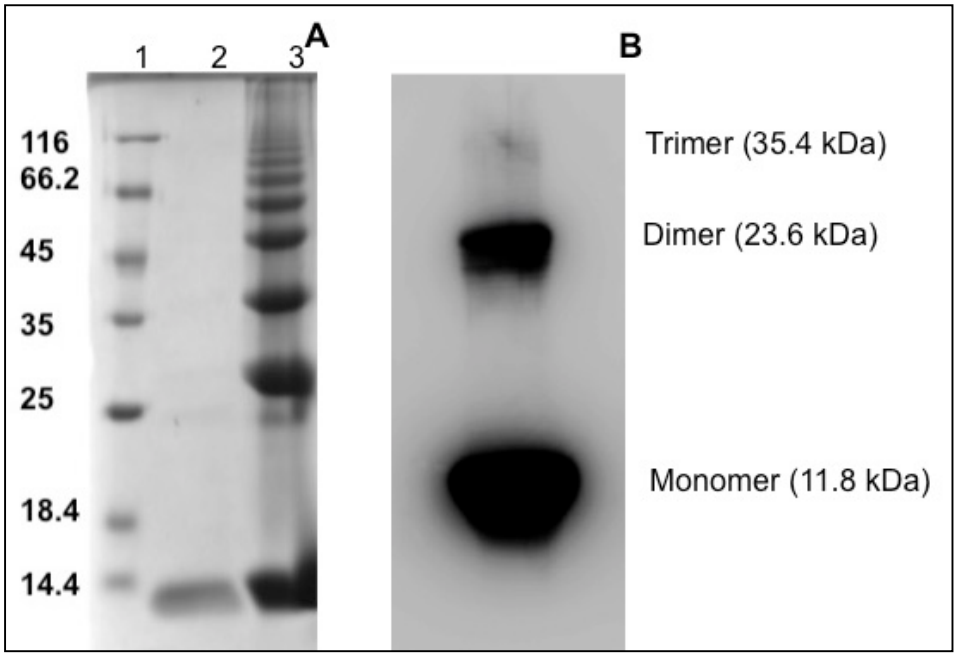

Figure A.6: A.6.A: Reducing and non-reducing SDS-PAGE of β2m: **Lane 1:** Protein molecular weight markers (14.4-116 kDa), **Lane 2:** β2m boiled in loading buffer containing β-mercaptoethanol, **Lane 3:** β2m boiled in non-reducing loading buffer. **A.6.B:** Western blotting of purified β2m resolved on SDS-PAGE under non-reducing conditions.

Intact mass analysis of purified β2m using MALDI-TOF mass spectroscopy

The possible role of SDS in producing oligomeric artifact was ruled out through MALDI-TOF mass spectroscopy. MALDI-TOF spectra of β2m in absence of SDS, demonstrate peaks corresponding to β2m monomer and oligomers. Figure A.7 represents the MALDI-TOF spectra of β2m purified through denaturing purification.

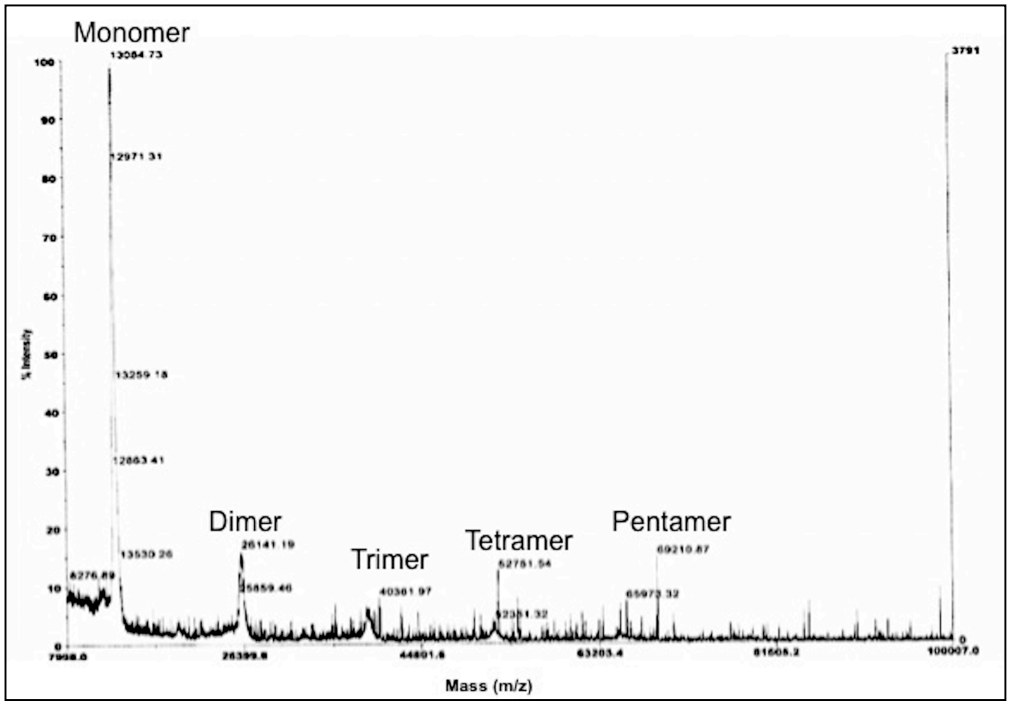

Figure A.7: MALDI-TOF MS of Ni-NTA purified β2m: Ni-NTA purified β2m was isolated from elution fractions and subjected to MALDI-TOF after C18 resin based ZIP-Tip

MALDI-TOF data confirms the presence of oligomeric β2m covalently bonded through intermolecular disulfides, as multimers observed in non-reducing SDS-PAGE were also observed using mass spectrometry.

ImageJ analysis of band intensities of β2m oligomers

The Ni-NTA purified β2m was boiled in non-reducing SDS-PAGE loading buffer and resolved by subjecting to SDS-PAGE in a 15% polyacrylamide gel. Upon completion of run the gel was stained in staining solution for 1 hour and subsequently destained in destaining solution. The destained gel was imaged using trans illuminator. The image of gel was subjected to ImageJ analysis to quantify the intensity of β2m bands corresponding to monomer and higher order oligomers. Figure A.8 represents the relative intensities of oligomeric β2m to that of monomeric β2m.

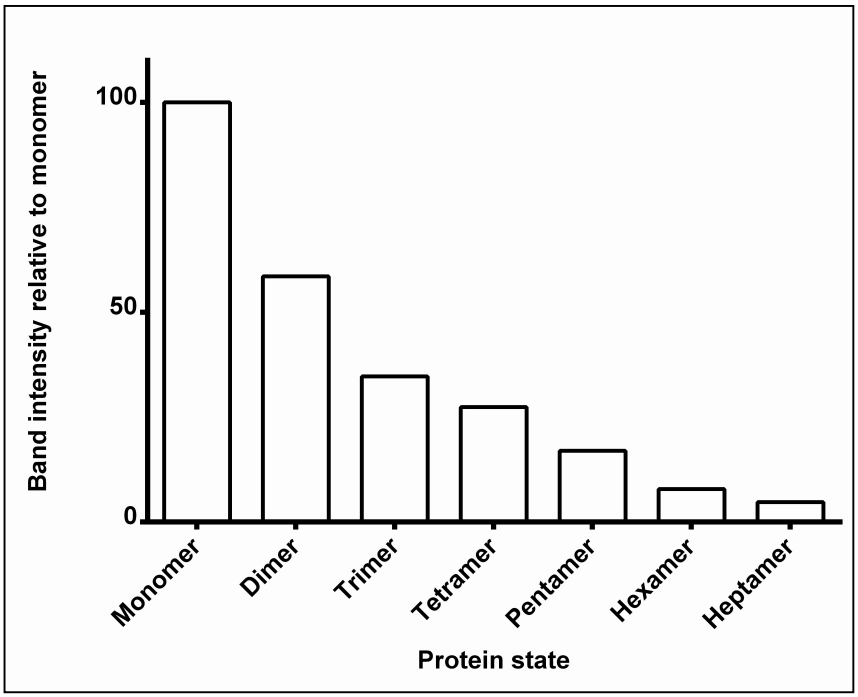

Figure A.8: Relative band intensities of monomeric and oligomeric population in Ni-NTA purified β2m determined using ImageJ: The Ni-NTA purified β2m was boiled in non-reducing SDS-PAGE loading buffer and resolved by subjecting to SDS-PAGE in a 15% polyacrylamide gel. After staining and destaining procedure, gel was imaged and image of gel was processed using ImageJ to quantitate the intensity of monomeric and oligomeric β2m bands. Band intensity data was normalized to intensity of β2m monomer

Synthesis of Cys25, 80 to Ser25, 80 mutated β2m using splicing by overlap polymerase chain reaction (SOE-PCR)

The role of disulfide linkage in β2m oligomerization was further verified by synthesizing mutant β2m, in which cysteine residues at position 25 and 80 were substituted by serine using SOE-PCR. Figure A.9.A, depicts the amplification of β2m template from pET 23a vector bearing wild type β2m sequence corresponding to mature β2m. β2m template was also generated using cDNA isolated from MCF-7 breast cancer cells. Figure A.9.B, depicts the products of SOE PCR for synthesis of mutant β2m

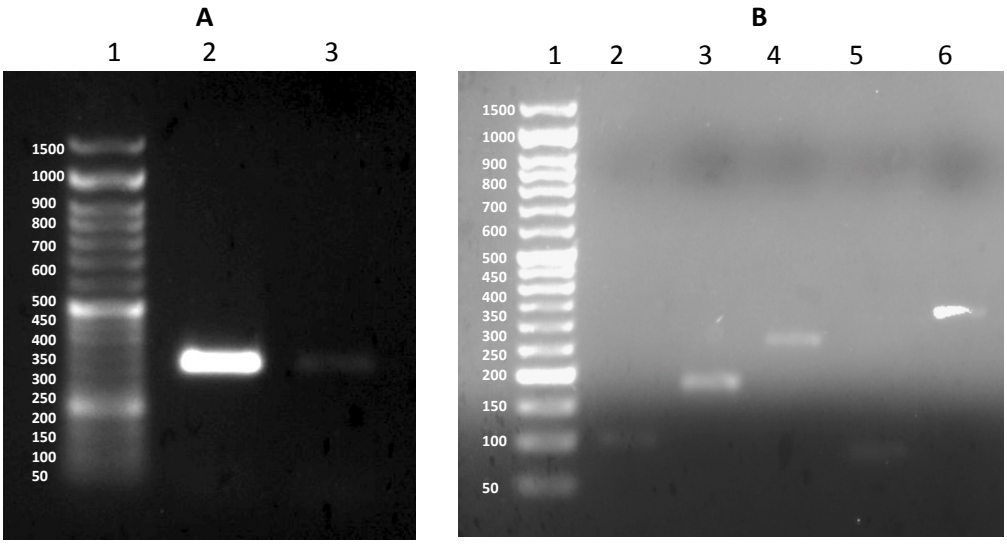

Figure A.9: A.9.A: Amplification of β2m ORF: Lane 1 50 base pair DNA molecular weight ladder, Lane 2 β2m ORF amplified from plasmid bearing β2m ORF, Lane 3 β2m ORF amplified from cDNA obtained from MCF-7 cells. **A.9.B: Splicing by overlap polymerase chain reaction (SOE-PCR) to synthesize mutant β2m (Cys25, 80 to Ser25, 80)**: **Lane 1:** 50 base pair DNA molecular weight ladder, **Lane 2:** PCR product of primer pair P1-P3, **Lane 3:** PCR product of primer pair P2-P5, **Lane 4:** PCR product of primer pair P1-P5, **Lane 5:** PCR product of primer pair P4-P6, **Lane 6:** PCR product of primer pair P1-P6.

Expression and purification of mutant β2m:

Mutant β2m was expressed and purified similarly to wild type β2m expression and purification. The mutant β2m does not form SDS resistant oligomers, further confirming that β2m oligomer formed during expression and purification from *E.coli*, are domain swapped oligomers formed through inter-chain disulfide linkages. Figure A.10 represents the wild type and mutant β2m resolved by non-reducing 15% SDS-PAGE.

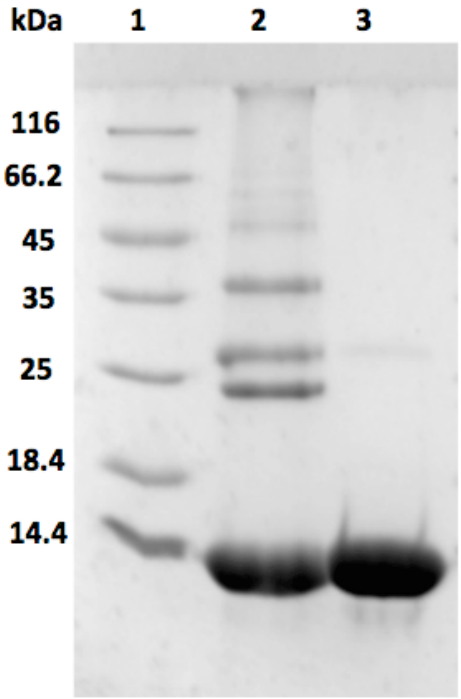

Figure A.10: Non-reducing SDS-PAGE of wild type and mutant β2m: Equal amounts of wild type and mutant β2m were boiled in SDS-PAGE loading buffer devoid of any β-mercaptoethanol and loaded onto 15% SDS-PAGE. **Lane 1:** protein molecular weight marker, **Lane 2:** wild type β2m purified through denaturing Ni-NTA purification, **Lane 3:** mutant β2m

Calcium and β2m interact and bind at physiological concentrations

Resonance Rayleigh scattering (RRS)

RRS indicates that micro- aggregation of β2m occurs at serum-like concentrations of protein and calcium, with reversal seen upon chelation of calcium by EDTA. A well-accepted method for examining microscopic protein aggregation is to examine whether scattering levels in Rayleigh scattering measurements (see materials and methods) peak in the vicinity of, 400 nm during collection of RRS spectra, between 200 and 600 nm on a spectrofluorimeter using synchronous scanning of the excitation and emission monochromators, and a delta lambda setting of 0 nm (45). RRS scans essentially plot changes in levels of Rayleigh scattering observed as a function of the wavelength of incident light. In the present instance, we monitored calcium-induced aggregation of β2m at a physiological pH of 7.4, and a physiological temperature of 37 °C, using a β2m concentration of 0.8 μM which is comparable to that seen in healthy humans (1–3 mM), and various increasing concentrations of the calcium ion [up to 0.9 μM] well below those observed in the serum of healthy humans (1–2 μM). Our objective was to examine whether calcium can elicit an increase in the RRS signal in some dose-dependent manner indicative of microscopic aggregation. The inset in Figure A.11.A clearly shows that RRS spectra obtained at different concentrations of calcium display an increase in Rayleigh scattering in the range of 400 to 500 nm with increasing concentrations of calcium. Representative spectra for four different calcium ion concentrations are shown in the inset, while the main graph in Figure A.11.A, plots changes in the peak RRS signal for different concentrations. The observed increase was non–linear and displayed a clear dose-dependence. Scattering levels increased manifold at ionic concentrations of a few mill molar calcium. This increased scattering is evidence of the presence of micro-aggregated protein and hints at the possibility of β2m aggregation occurring in the serum, since comparable concentrations of β2m were used with lower-than-normal concentration of calcium. While the RRS data is shown for the use of phosphate buffered saline (PBS), entirely similar results were obtained with tris-buffered saline (TBS). Therefore, unless otherwise mentioned (where water alone was used, e.g., in isothermal titration calorimetry experiments), for most experiments described below only TBS was used to create physiological conditions. Interestingly, there is also a time-dependent reduction in scattering observed upon addition of EDTA in the resonance Rayleigh scattering data, as shown in Figure A11.B

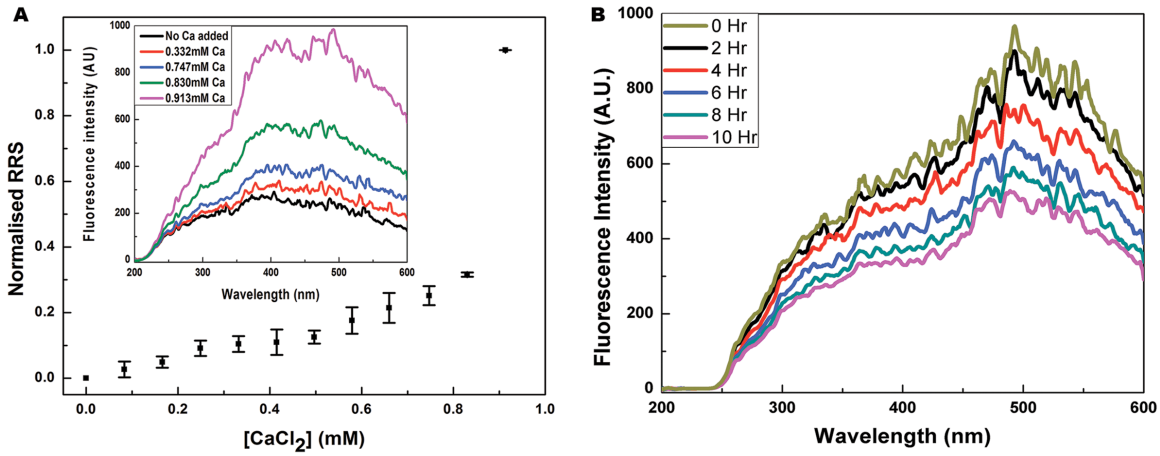

Figure A.11: Resonance Rayleigh scattering data for calcium-induced aggregation of β2m. A.11.A shows normalized RRS intensities plotted against increasing calcium chloride concentration. The concentration of β2m protein was 0.83 μM, and calcium chloride concentrations were 0.083, 0.166, 0.249, 0.332, 0.415, 0.497, 0.579, 0.66, 0.747, 0.83 and 0.913 mM. The inset shows representative RRS spectral scans at calcium chloride concentrations of 0, 0.332, 0.747, 0.830 and 0.913 mM to illustrate how RRS spectra appear. Peak intensities from such spectra were used for the main plot. **A.11.B** shows reduction in RRS signal upon incubation with 10 mM EDTA, at time points of 0, 2, 4, 6, 8, and 10 hours.

Increasing calcium increases visible turbidity in β2m

Figure A.12.A shows that visible precipitation of β2m is observed within a few tens of minutes of addition of calcium when the concentration of the β2m protein is raised from 4 μM to 20 μM, and that of the calcium ion is raised from below 0.66 mM to 5.0 mM, or above. The identity of the aggregates formed and precipitated was confirmed to be β2m by centrifuging and collecting the aggregated protein and analyzing it on SDS-PAGE by boiling the aggregate with SDS-PAGE loading buffer, to visualize the β2m protein band (data not shown). Figure A.12.B shows the increase in visible sedimentation of protein obtained as calcium ion concentrations are raised from 0 mM to 8 mM, in 1 mM increments.

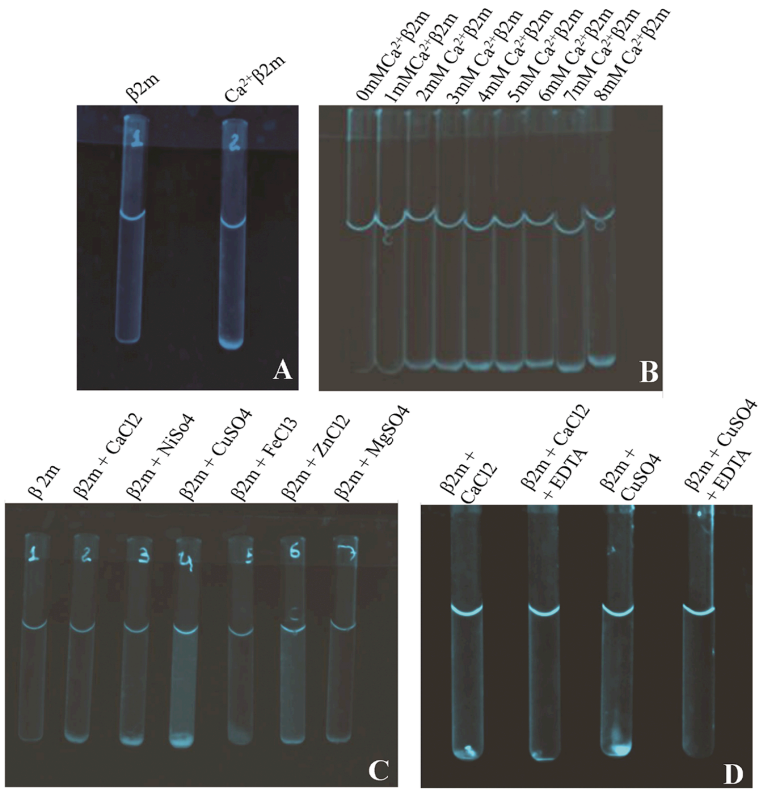

Figure A.12: Visual evidence of the role of calcium and other metal ions in causing the aggregation and precipitation of β2m, and the role of EDTA in reversing such aggregation if added immediately after the formation of amorphous aggregates. **A.12.A**: shows solutions of β2m (control) and calcium-precipitated β2m, respectively, in tubes 1 and 2. For these experiments, a β2m solution (20 μM) was allowed to stand in the tubes for over one hour in the absence (tube 1) and presence (tube 2) of 5 mM calcium chloride, followed by mild centrifugation to sediment the precipitated β2m visible at the bottom of the tube. **A.12.B:** shows precipitation of β2m in 20 μM solutions by the following different concentrations of calcium chloride: 0, 1, 2, 3, 4, 5, 6, 7 and 8 mM $CaCl_2$, respectively, in tubes numbered 1 through 9, further (visually) establishing the dose-dependence. **A.12.C:** shows the comparative visible precipitation of β2m in 20 μM solutions by 5 mM concentrations of $CaCl_2$, $NiSO_4$, $CuSO_4$, $FeCl_3$, $ZnCl_2$, and $MgSO_4$, in experiments similar to those shown in previous panels, with the control sample shown in tube 1. **A.12.D:** shows the formation, deposition and clearance of aggregates of β2m in 20 μM solutions by 5 mM calcium and copper, respectively, in tubes 1 and 3, and the clearance of the same through 24 hours of incubation with EDTA (10 mM), in tubes 2 and 4, respectively.

Aggregation and precipitation are also seen with other metal ions

Figure A.12.C shows evidence of precipitation by a host of different metal ions under entirely similar conditions of buffer pH and concentration and metal ion concentrations (5 mM). It was observed that the greatest amount of precipitation could be obtained with copper. Importantly, the precipitation seen with calcium is comparable to that seen with most other metals. Of course, the important thing is that of all metals for which these experiments are described, only calcium exists in the serum at concentrations (1–2 mM) comparable to those used here (5 mM).

Visible reversal of turbidity upon addition of EDTA

The visible aggregates that had been formed disappeared within 24 hours of addition of the divalent ion-chelating agent, EDTA, as shown in Figure A.12.D. This reversal occurred regardless of whether centrifugation had been done (and aggregates re-suspended, prior to calcium addition), or aggregates were still in suspension prior to sedimentation. This observation essentially establishes that the visible aggregation and precipitation of β2m owes to the presence of calcium. It also suggests that there is binding of calcium by β2m, since EDTA could potentially interfere with such binding equilibria by bleeding calcium away and sequestering it. We also examined the relative clearing of aggregates by EDTA for aggregation induced by copper and by calcium, both visually and by RRS measurements.

Transmission electron micrographs show amorphous

The morphology of the aggregates was analyzed by transmission electron microscopy (TEM), using standard methods of staining. Figures A.13.A shows a representative view of the TEM field filled with scattered clusters of aggregates that are clearly amorphous. A few rare representative specimens of somewhat larger (more well delineated) aggregates present in the field are also shown in Figure A.13.B, hinting at the possibility of some reorganization of the amorphous aggregates into more ordered aggregates. However, there is no evidence of any amyloid-like macrostructure, or the presence of fibrils. Transmission electron micrographs show amyloid networks after 3–4 weeks of incubation. The amorphous aggregates described above were allowed to remain sedimented in the presence of calcium for 3–4 weeks with, or without, periodic shaking. Two representative micrographs of such incubated aggregates are shown, for aggregates subjected to shaking, in Figures A.13.C and A.13.D.

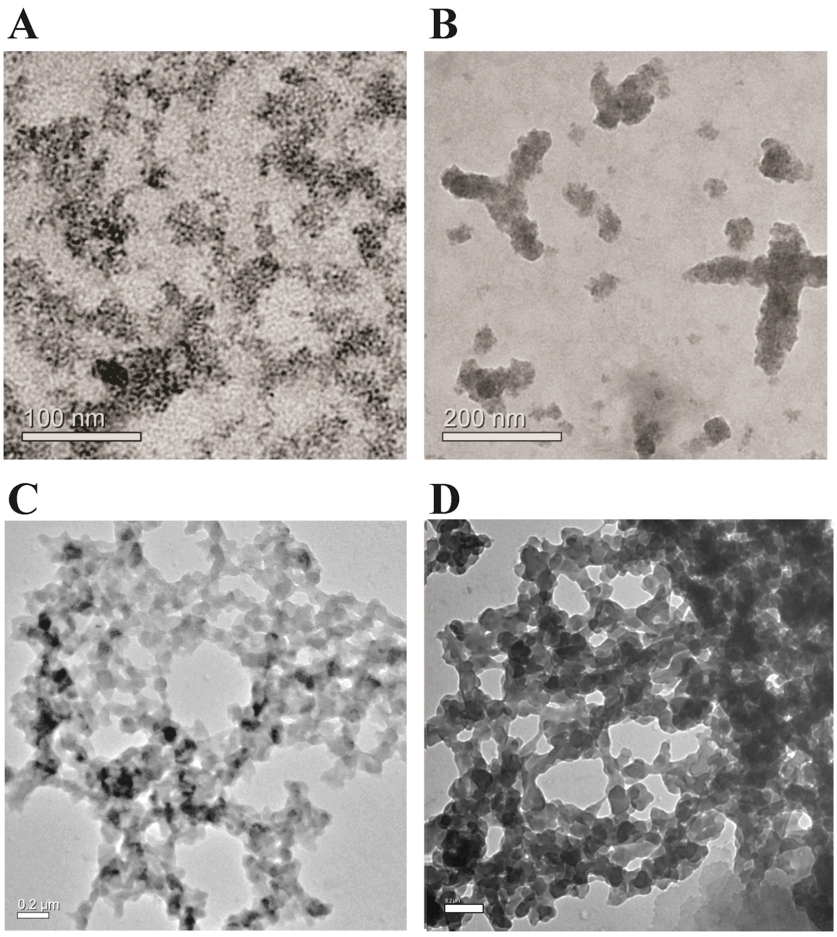

Figure A.13: Transmission electron micrographs of amorphous and mesh-like (amyloid-containing?) aggregates of β2m, from experiments such as those described in Figure B.7. **A.13.A** and **A.13.B**, respectively, show representative views of dispersed amorphous aggregates, and some rare self-organizing aggregates, seen when imaging is done immediately after the aggregation and precipitation of the protein. **A.13.C** and **A.13.D**, respectively, show representative views of the networked and branched aggregates that are formed by incubating the amorphous aggregates for three weeks with, or without, periodic shaking. The views in Panels C and D cannot be compared with any previously seen amyloid forms, but could represent a pre-fibrillar morphology. The scale bar in **A.13.D** which is not very clear is 0.2 μM.

The morphology of the aggregates appears to have changed considerably after incubation, with a definite 'branched' and 'networked' pattern of aggregates observed in addition to a somewhat unusual fibrillar character, especially in the parts of the structure that give it a 'meshwork' appearance, suggesting that these could be amyloid in nature. The unusual morphology is not of great concern, however, because the morphologies of amyloid aggregates do vary considerably from protein to protein (46) and also for aggregates of the same protein formed under different conditions (11, 47).

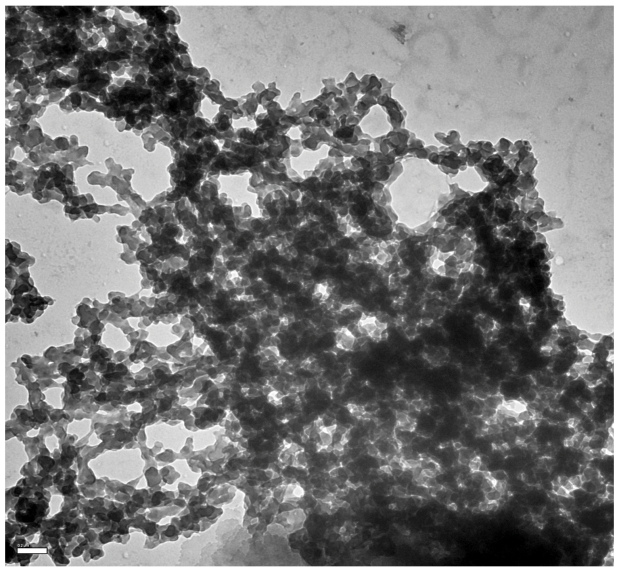

Figure A.14: A detailed and representative 'wide-field' view covering an area of nearly 3 μm X 3 μm is shown for a mesh- like (amyloid-containing?) aggregate of β2m formed without shaking of samples, through three weeks of incubation of amorphous aggregates deposited through calcium-induced precipitation. Within the aggregate, strands (fibrils) varying in diameter from 10 nm to 70–80 nm are seen to network in interconnected fashion.

In the case of β2m too, as already mentioned, amyloid aggregates have very different morphologies depending on how they were caused to form (23). Of course, the morphologies of the aggregates reported here are different from the ones formed at acidic pH, or under other conditions, and the modes and mechanisms of formation would also appear to be different. The transformation of the amorphous aggregates into such meshwork- like aggregates with time would be very interesting indeed, if these aggregates were to show any signs of being amyloid-like in nature; this is because this would suggest that amorphous aggregates can act as 'nurseries' for the formation of amyloid aggregates. Notably, this is a contention, which has previously put forward by other groups, including our own (46,47).

The hypothesis advanced by Prusiner and colleagues (48) is that either individual molecules, or assemblies of molecules, dissociate from amorphous aggregates and deposit into fibrils or proto-fibrillar structures that are being formed in the vicinity of the amorphous aggregate, through a process of diffusion and re-adsorption, Or that there is a transformation of chains into proto-fibrillar structures within the amorphous aggregates themselves, and that these then somehow reorganize into progressively more fibrillar morphologies. We have reported (46) that amyloids can form through the assembly of bead-like intermediate structures seen within clumped amorphous aggregates that line-up and transform into amyloid fibers, with some fibers possessing spherical bead-like ends (i.e., displaying evidence of having been generated from bead-like structures). We have also reported the formation of pore-like structures in amorphous aggregates (46) that seem to result from the 'head' region of a short amyloid fiber assembling with the 'tail' region of the same fiber. Notably, Lindquist and colleagues have also reported that a subpopulation of proto-fibrils may function as pathogenic amyloid pores (49). In fact, this group has also suggested in the same paper, and in other publications, that amyloid fibers are a product of the deposition of the real pathogenic (pre-fibrillar) species that are cytotoxic, resulting in a protection of cells from the toxicity of the pre-fibrillar forms. Pre-fibrillar species which do not need to have any clear fibril-like morphology can best be examined through the binding of amyloid-specific dyes. To summarize this section, we wish to emphasize that the unusual mesh-worked structures observed by us could be pre-fibrillar amyloid forms, with an amyloid-like cross beta sheet structure having already been attained at the level of the reorganization of the polypeptide backbone. The only way of establishing whether this is true would be to examine these aggregates using amyloid-specific dyes like Thioflavin T (ThT).

Strong Thioflavin T (ThT) fluorescence is seen with aggregates incubated for 3–4 weeks, while none is seen with the amorphous aggregates obtained initially

The presence of amyloid-like microstructure in the calcium-induced β2m aggregates incubated for 3–4 weeks (which have undergone transformation from amorphous microaggregates to amyloid-like networks of aggregates) was investigated through examination of the binding of the dye, ThT, to resuspended aggregates placed in the light path of a spectrofluorimetric cuvette, using the characteristic ThT fluorescence seen upon amyloid- binding as a diagnostic criterion. The fluorescence of ThT increases upon amyloid binding

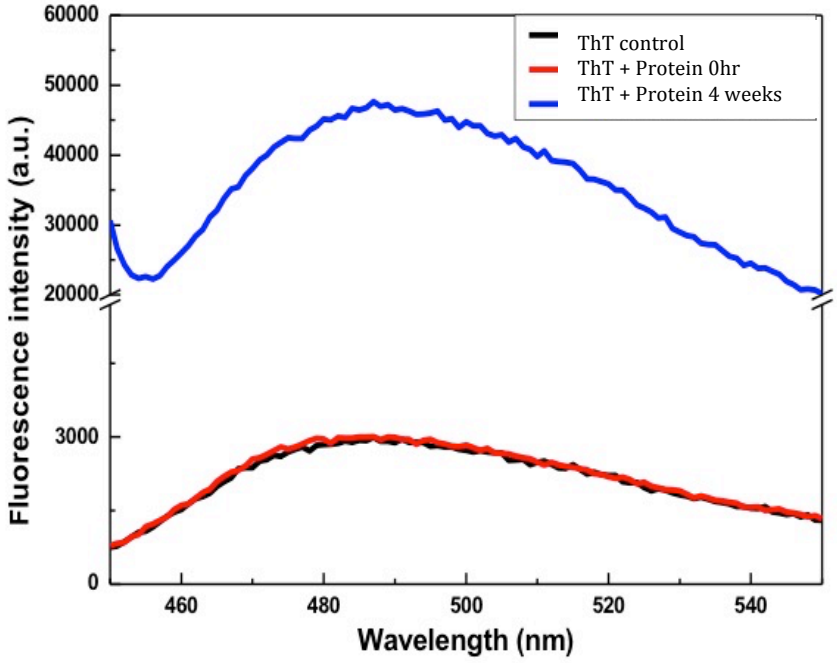

Figure A.15: Dye fluorescence spectrum collected with Thioflavin T (ThT) alone (black) and with ThT in the presence of β2m aggregates (red) for aggregates such as those imaged in Figure A.8. A profound increase in the emission of ThT is seen to peak at 482 nm (note the break in the y-axis) upon its binding to the cross beta-sheet structure in the aggregates. With amorphous aggregates, no such increase was seen and fluorescence was similar to that seen in control solutions of the dye.

This is a qualitative test, which depends on the quantitation of ThT fluorescence, i.e., the quantum of increase in the intensity of ThT fluorescence depends on the type of amyloid, the relative amounts of the dye and the amyloid, the nature and quality of the re-suspension etc. The fluorescence spectra recorded with ThT alone and with ThT added to the calcium-induced β2m aggregates and incubated for 4 weeks, are both shown in Figure A15. There is a clear increase in fluorescence of the dye in the presence of the aggregates, indicating the presence of amyloid-like microstructure. Notably, as Figure A.15 shows, no such increase was seen with amorphous aggregates, immediately after their formation and deposition in tubes, whereas ThT fluorescence is seen after the passage of a few weeks.

Isothermal titration calorimetry (ITC) indicates that β2m binds up to 4 calcium atoms

The β2m aggregation at higher calcium concentrations can be a consequence of two possibilities. On the one hand, there could be a non-specific 'bulk' effect of the presence of calcium in terms of changes in ionic strength which are sensed by the protein, perhaps through some non-specific binding or adsorption of the metal on to the protein's surface. Miranker and colleagues have suggested that there could be such non-specific binding of calcium to the protein (31). On the other hand, there could be some reasonably specific binding of the calcium to specific sites, or to metal-binding motifs present in β2m, leading to an overall conformational change in the structure and thereby leading to aggregation. By controlling the rate and amount of aggregation, i.e., by using lower protein concentrations, isothermal titration calorimetry could be used to determine whether there is indeed any binding of calcium. An ITC thermogram obtained through titration of calcium chloride (14 mM) into protein (125 μM) is shown in Figure A.16.A. The fitting of the thermogram is shown in Figure A.16.B and the parameters obtained for the 4 binding sites along with the assessment of the fitting are shown in Figure A.16.C. The thermogram suggests specific binding of calcium to β2m. The fitted data suggests sequential binding of the metal ion to the protein at up to 4 sites. Whether these sites are identical to the sites indicated by Vachet and colleagues for copper binding (i.e., the N-terminus and the protein's three histidines in the unfolded state), or whether they are the sites in the sequence that have been pointed out by us (see Figure 1 and the introduction section), of course, remains to be established. Binding constants and other parameters are provided in the box adjacent to the fitted curve. ITC thermograms give a measure of the overall heat change of the system upon binding of two interacting molecules. Here, many changes could be simultaneously taking place, e.g., binding of calcium to metal-binding motifs present on β2m, a resultant conformational change in the structure of the protein, formation of micro-aggregates or oligomers, and finally the aggregation of micro-aggregates into larger amorphous aggregates etc. To investigate this further, we performed FTIR spectroscopy of the protein incubated with calcium as a function of time, since slow sequential binding accompanying the development of turbidity could very well result from an observable time-dependent bulk change in the population's conformation.

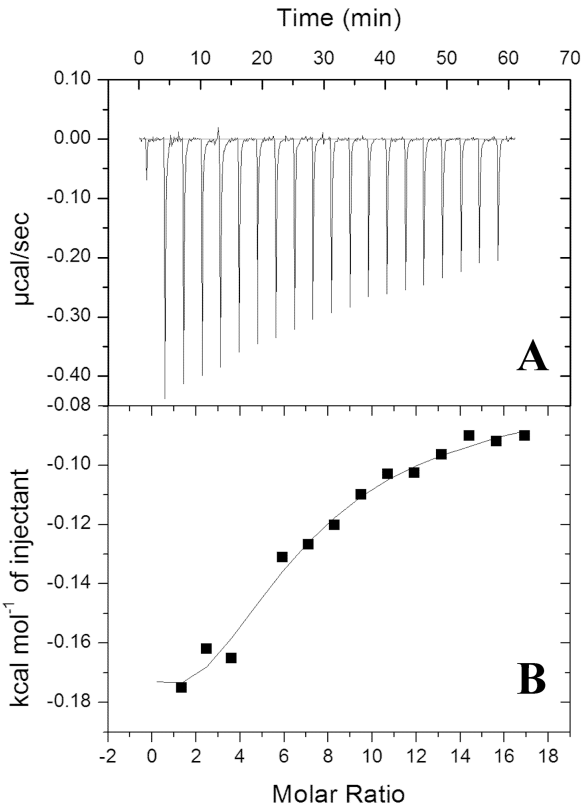

Data: Data1_NDH
Model: Sequential Binding Sites
Chi^2/DoF = 28.38

K1	**479**	**±5.1E2 M^{-1}**
ΔH1	**-3052**	**±3.28E3 cal/mol**
ΔS1	**2.03 cal/mol/deg**	
K2	**610**	**±84 M^{-1}**
ΔH2	**-546.1**	**±4.60E3 cal/mol**
ΔS2	**10.9 cal/mol/deg**	
K3	**-143**	**±1.5E2 M^{-1}**
ΔH3	**-8917**	**±8.85E3 cal/mol**
K4	**-2.07E3**	**±2.7E2 M^{-1}**
ΔH4	**7411**	**±6.51E3 cal/mol**

C

Figure A.16 Isothermal calorimetry to determine calcium binding sites on β2m. Panel A: An ITC thermogram obtained through titration of calcium chloride (14 mM) into protein (125 µM) **Panel B:** The fitting of the data. The data was best fitted in the sequential-binding model suggesting 4 binding sites. **Panel C:** The parameters of the fit.

Calcium binding induces increase in beta-sheet conformation in β2m

A representative set of Fourier-transform infrared spectra are shown in Figure A.17, to establish the effect of calcium binding on the conformation of β2m upon binding of calcium. For this, a solution of the protein was first placed in a conical chamber on the horizontal attenuated total reflectance (HATR) crystal of the FTIR spectrometer, and spectral data was collected for two absorption bands originating in the peptide bond, amide I (1700 to 1600 cm^{-1}) and amide II (1600–1500 cm^{-1}). Subsequently, calcium was added in a very 'small volume' aliquot to the protein, from a highly concentrated stock solution (to prevent any significant dilution effects on the protein, or its FTIR spectrum). Spectral data was collected for the amide I and amide II bands after different time intervals to allow for a 'phased' and sequential binding of calcium at different sites in a time-dependent manner. Thus, in Figure A.17, spectra were collected immediately before addition of calcium, immediately after addition of calcium, 10 minutes after addition and 2 hours after addition. A single composite band maximum, seen at, 1660 cm^{-1} in the amide I band envelope of native β2m, transforms into two band maxima. The original envelope with the band maximum at, 1660 cm^{-1} is constituted of a linear combination of contributions from the beta- sheet signal below 1640 cm^{-1} and the signal from the unstructured component (random coil), which dominates the longer wavenumbers closer to, 1680 cm^{-1}. Against the background of this spectrum, upon addition of calcium, a second band maximum is seen to 'break through' the band envelope and become prominent at 1629 cm^{-1}, presumably owing to increase in the beta sheet content of β2m at the expense of some unstructured (random coil) regions. The 1629 cm^{-1} peak is distinctly visible in the spectrum collected after 2 hours of incubation with calcium. The highlight of this experiment is that the data is collected 'in situ' on the HATR crystal maintained at a constant temperature, with nothing further being added to the solution, such that the data for solutions incubated for 0, 10, and 120 minutes are all collected on the exact same solution without anything being done to disturb the solution. The data thus owes to both protein in solution, and any settling aggregates coming into contact with the HATR crystal. Satisfyingly, the amide II spectrum, which displays two band maxima at 1550 and 1520 cm^{-1} also shows a shift in the 1550 cm^{-1} peak towards 1540 cm^{-1} upon calcium addition. The amide II band is also sensitive to changes in protein secondary structure, although deconvolution of the band into its component secondary structural contents is not yet technically feasible.

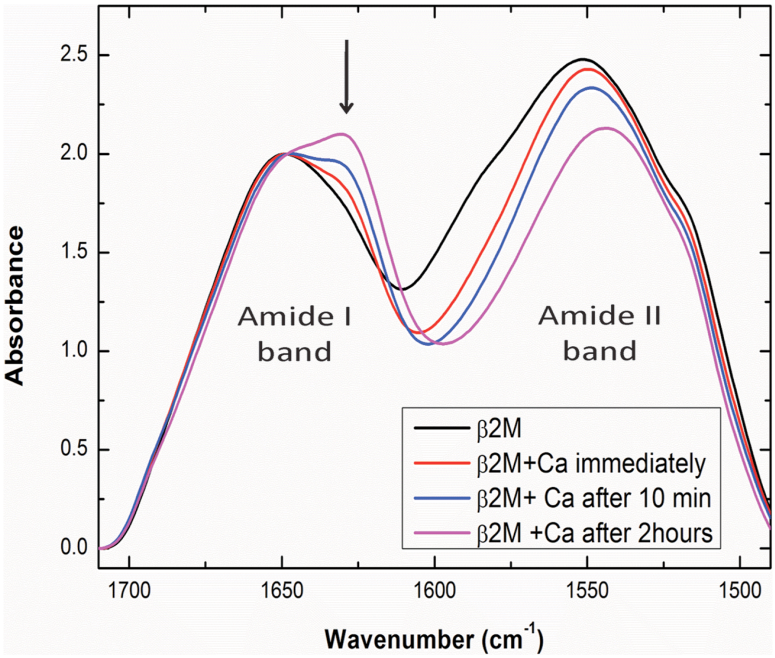

Figure A.17: Infra red (HATR-FTIR) spectra of β2m alone (black) and β2m in the presence of calcium, taken immediately after addition of calcium (red), or after the passage of 10 minutes (blue) or 2 hours (pink).

β2m interacts and binds with E2

β2m interaction with E2 was studied using difference absorption spectroscopy and surface Plasmon resonance measurement.

Difference absorption studies on β2m and E2

Difference absorption spectroscopy indicates β2m interaction with E2. β2m shows a shift in absorbance in aromatic and peptide region as depicted in figure A.18, These results indicate a potential role of β2m as a calcium and hormone binding protein. Interestingly the sex hormone-binding globulin (SHBG) is known protein involved in trafficking of androgen and estradiol in a calcium dependent dimerization state. Our findings of β2m binding with calcium and E2 are thus significant enough to warrant more studies with animal models to assess the physiological significance of β2m interaction with E2.

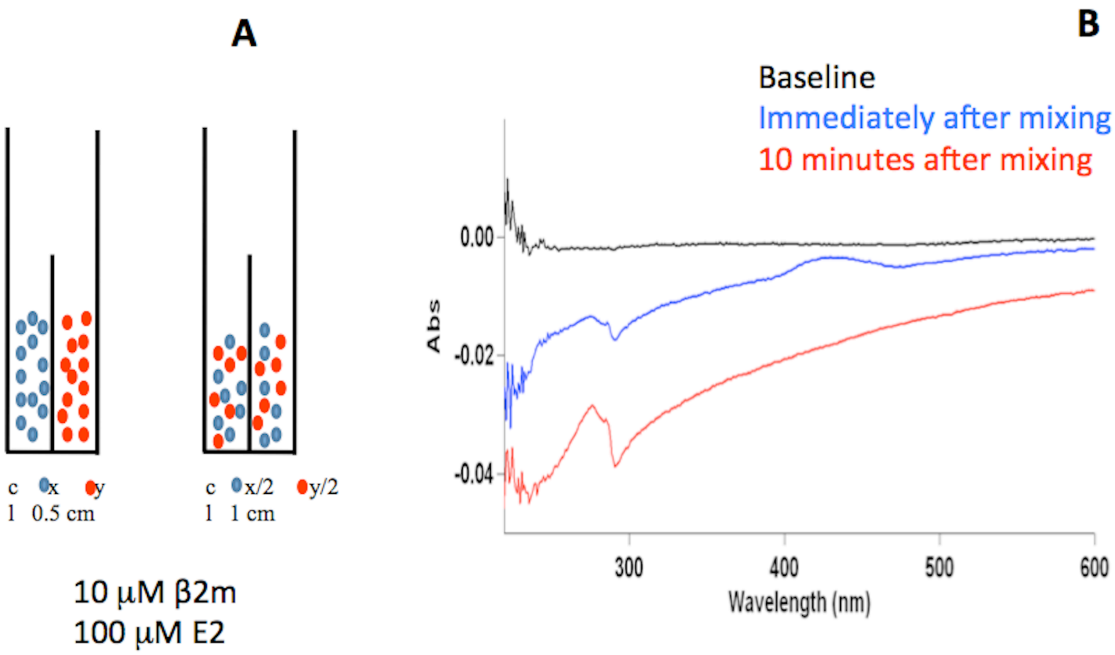

Figure A.18: Difference absorption spectroscopy to check β2m interactions with E2. **A.18.A:** Schematic representation of difference absorption experiment. **A.18.B:** Black line shows absorption scan collected in a tandem absorption cuvette after baseline correction without mixing β2m and 17-β-estradiol. Blue line display absorption scan collected immediately after mixing. Red line depicts absorption scan after 10 minutes of mixing

Surface plasmon resonance confirms the binding interaction between β2m and E2

Surface plasmon resonance studies further confirm binding interaction between β2m and E2, as depicted in Figure A.19, where a concentration dependent response (sensorgram) is observed for varying concentrations of the hormone. These initial results – which clearly indicate binding - have not yet been analyzed further, since the sloping nature of the sensorgrams suggests some further standardization involving buffer systems used for the experiment.

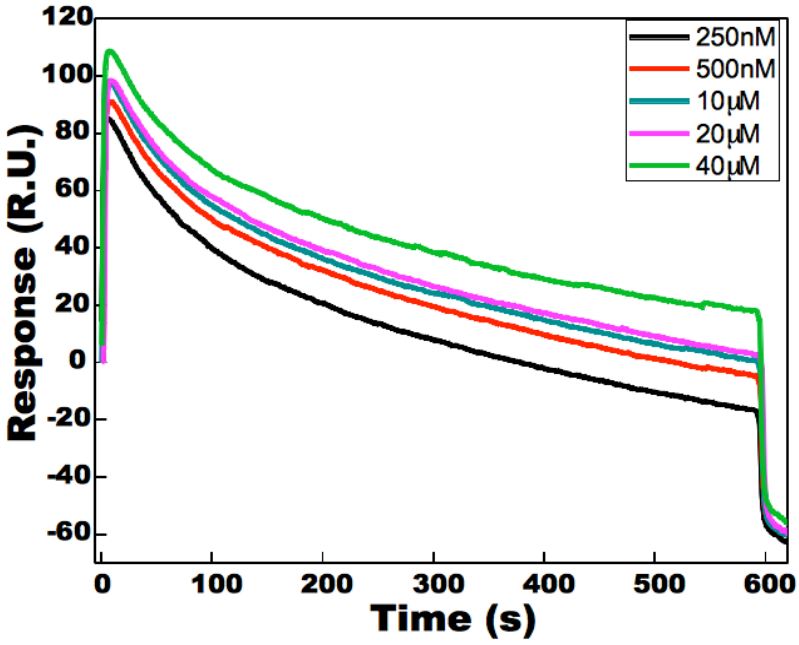

Figure A.19: Surface plasmon resonance measurements to confirm β2m interactions with E2. β2m concentration was kept constant 0.4 μM while E2 concentrations were 250 nM, 500 nM, 10 μM, 20 μM and 40 μM respectively.

β2m oligomers are cytotoxic

We find that neuronal neuro-2a (N2a) cells treated with β2m oligomers show a decrease in cell viability. Oligomeric proteins are considered to be equivalent to protofibrillar intermediates during the conversion of monomeric protein to amyloid fibrils. This partially explains the cytotoxicity associated with higher order oligomers of β2m. Mouse neuroblastoma cell line N2a incubated with β2m in serum free media shows a decrease in cell viability as determined by MTT assay shown in Figure A.20.A. However, treating cells simultaneously with Estradiol (E2) or N-acetylcystine (NAC) counters this observed cytotoxic effect of oligomeric β2m. Both E2 and NAC are well known antioxidants. Morphologically, N2a cells treated with β2m look apoptotic while N2a cells treated with β2m in presence of E2 look normal. Cells treated with β2m alone, have a vacuolated appearance, whereas N2a cells treated with β2m in presence of E2 appear normal. These results suggest that either E2 is preventing cytotoxicity by providing additional prosurvival signaling or it might be binding to β2m, as consequences of which β2m loses its cytotoxic potential

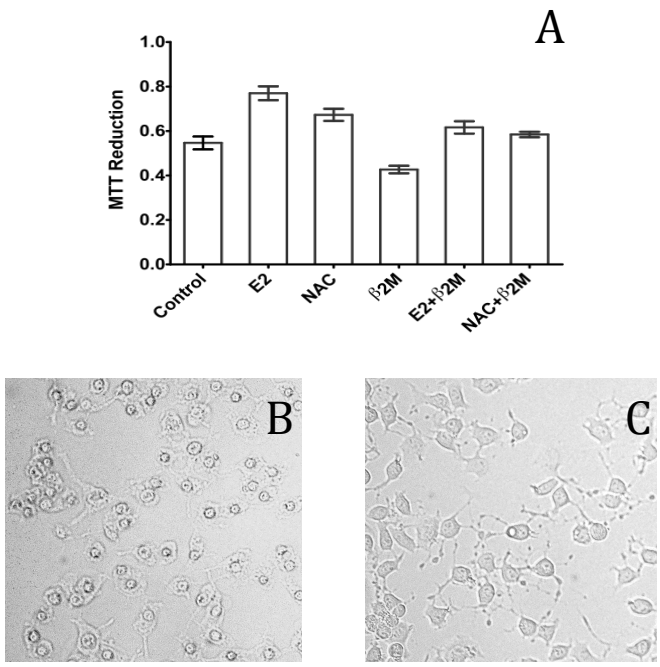

Figure A.20: Panel A: MTT assay to check the cell viability after treatment with E2 (10 nM), β2m (10 µM), N-acetylcystine (100 µM). **Panel B:** N2A cells treated with β2m after 3 hours incubation. Panel C: N2a cells treated with β2m and E2 after 3 hours incubation

FITC labeled β2m and cytotoxicity

We find that labeling by fluorescein isothiocyanate (FITC) neutralizes the cytotoxic activity of β2m. N2a cell line was treated with equal concentration of FITC labeled β2m and unlabeled β2m. Figure A.21.A clearly shows vaculation in cytoplasm treated with unlabeled β2m whereas cells treated with FITC-labeled β2m show normal and healthy morphology, as seen in figure A.21.B. FITC is a common protein labeling dye that covalently modifies the primary amine groups of a protein being labeled. FITC labeling also introduces a partial excess negative charge to the labeled protein and lowers its isoelectric point (to the extent that labeling occurs), thus further retarding the potential of labeled protein interacting with the cell membrane which is also negatively charged. This possibility provides further insights into the mode of action of oligomeric β2m with cells, in that it appears that the positively charged residues are important to the cytotoxic activity of oligomeric β2m. FITC labeling presumably destroys cytotoxic potential by firstly inducing negative charge on the protein and secondly by modifying the positively charged lysine residues. It's noteworthy that lysine residues have been found essential in cytotoxicity associated with oligomeric amyloid beta protein (50). This points toward a common mechanism underlying oligomeric protein induced cytotoxicity.

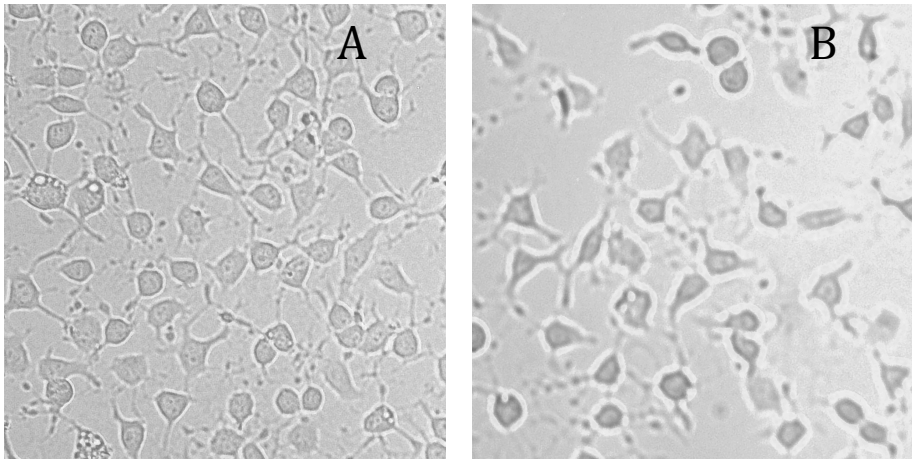

Figure A.21: Effects of FITC conjugation on oligomeric β2m cytotoxicity. **A.21.A:** N2A cells treated with FITC labeled β2m after 3 hours incubation. **A.21.B:** N2a cells treated with FITC labeled β2m and 17-β-estradiol after 3 hours incubation

β2m intracellular localization studies

Using high-resolution microscopy, it was found that β2m localizes to cell surfaces and is also being internalized by the N2a cells as shown in figure A.22. Although the lysine residues that are supposed to be responsible for cytotoxic activity of oligomeric β2m were modified during FITC conjugation of β2m; still, it is able to bind to cells and internalize without any deleterious effects on cells. This further supports our observation that FITC conjugation leads to neutralization of cytotoxic potential of oligomeric β2m and lysine residues are important in fold recognition that provides such kind of binding interaction with cell membrane or cell surface receptors leading to cell death in N2a cells.

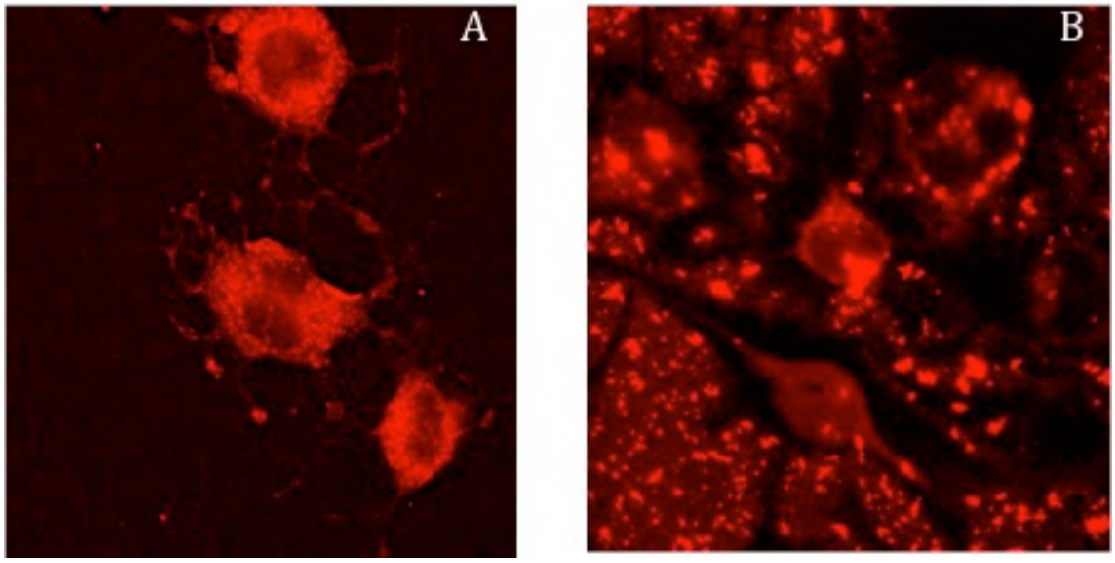

Figure A.22: High-resolution microscopy imaging of N2a cells treated with FITC conjugated β2m. A.22.A: N2A cell treated with β2m for 15 minutes. **A.22.B:** N2A cells treated with FITC conjugated β2m for 6 Hours.

Conclusions and future prospects:

In the present work, we have explored various physiological factors that might play a role in β2m deposition in the disease known as 'DRA'. In the first part of this chapter, we have demonstrated that β2m very likely has four calcium binding motifs in its sequence and that, under physiological conditions, calcium can bind with β2m and induce microaggregation of the protein. Isothermal calorimetry studies indicate the binding of 4 calcium ions to one β2m molecule. Under conditions of normal kidney function, this might be physiologically harmless, since the body sequesters excess free calcium which is released in kidney for reabsorption or excretion. However, in the case of impaired kidney function where β2m catabolism is severely compromised and plasma levels of the protein can rise up to 60-fold, the same microaggregation becomes significant. *In vitro* experiments carried out in this study demonstrate that calcium can induce structural changes leading to increase in beta sheet content in β2m and that, upon prolonged incubation with calcium, β2m forms amorphous aggregates that bind to the amyloid binding dye ThT with significant increase in ThT fluorescence.

In the second part of this study, we have demonstrated the binding of β2m with 17-β-estradiol. Difference absorption spectroscopy indicates that β2m binds with 17-β-estradiol and that binding results in the difference absorption spectrum changing with time. 17-β-estradiol binding also alters the native fluorescence characteristics of the protein, as is evident from fluorescence spectra of β2m in presence of 17-β-estradiol. β2m binding with 17-β-estradiol was further confirmed with surface Plasmon resonance measurements. These results point towards multifaceted role of β2m. Apart from being a subunit of MHC-1; it might also play a role in neutralizing, sequestering and transport of metal ions and steroid hormones along with other plasma proteins.

The third part of this study explores the cytotoxic effects of oligomeric β2m. At the plasma concentration equivalent to DRA, β2m oligomers are cytotoxic to the neuronal cell line N2a. Here we have used these cells as general model to demonstrate cytotoxicity associated with β2m oligomers. We also demonstrate that 17-β-estradiol and N-acetylcysteine can protect the N2a cells against β2m oligomers induced cytotoxicity. Also covalent modification of primary amines of β2m oligomers with FITC conjugation completely neutralizes their cytotoxic effects.

The present work demonstrates the affinity of β2m to calcium and 17-β-estradiol. Further work involving animal models can be carried out to further establish the physiological relevance of calcium and 17-β-estradiol binding by β2m. This will further establish the role of β2m as carrier protein for both metal ions and steroids.

References:

1. Anfinsen CB (1973) Principles that govern the folding of protein chains. Science. 181: 223-30.
2. Glenner GG (1980) Amyloid deposits and amyloidosis. N Engl J Med 302:1283-1292.
3. Depierreux M, Goldman M, Fayt I, Richard C, Quintin J, et al. (1988) Osteoarticular amyloidosis associated with haemodialysis: An immunoultrastructural study. J Clin Pathol 41:158–162.
4. Jean D. Sipe, Merrill D. Benson, Joel N. Buxbaum, Shu-ichi Ikeda, Giampaolo Merlini, et al. (2012) Amyloid fibril protein nomenclature: 2012 recommendations from the Nomenclature Committee of the International Society of Amyloidosis, Amyloid 19: 167–170.
5. Xue W-F, Hellewell AL, Gosal WS, Homans SW, Hewitt EW, et al. (2009) Fibril Fragmentation Enhances Amyloid Cytotoxicity. The Journal of Biological Chemistry 284: 34272-34282.
6. Marshall KE, Marchante R, Xue W-F, Serpell LC (2014) The relationship between amyloid structure and cytotoxicity. Prion 8: 192-196.
7. Milanesi L, Sheynis T, Xue W-F, Orlova EV, Hellewell AL, et al. (2012) Direct three-dimensional visualization of membrane disruption by amyloid fibrils. Proceedings of the National Academy of Sciences of the United States of America 109: 20455-20460.
8. Iwata K, Matsuura T, Sakurai K, Nakagawa A & Goto Y (2007) High-resolution crystal structure of beta2-microglobulin formed at pH 7.0. J Biochem 142: 413–419.
9. Porcelli SA, Modlin RL (1999) The CD1 system: antigen-presenting molecules for T cell recognition of lipids and glycolipids. Annu Rev Immunol 17: 297–329.
10. Saper MA, Bjorkman PJ, Wiley DC (1991) Refined structure of the human histocompatibility antigen HLA-A2 at 2.6 Å resolution. J Mol Biol 219: 277–319.
11. Radford SE, Gosal WS, Platt GW (2005) Towards an understanding of the structural molecular mechanism of β2-microglobulin amyloid formation in vitro. Biochim Biophys Acta 1753: 51–63.
12. Shiroishi M, Kuroki K, Rasubala L, Tsumoto K, Kumagai I, et al. (2006) Structural basis for recognition of the nonclassical MHC molecule HLA-G by the leukocyte Ig-

like receptor B2 (LILRB2/LIR2/ILT4/CD85d). Proceedings of the National Academy of Sciences of the United States of America 103: 16412-16417.

13. Miyata T, Jadoul M, Kurokawa K, Van Ypersele de Strihou C (1998) Beta-2 microglobulin in renal disease. J Am Soc Nephrol 9: 1723–1735.
14. Floege J, Ketteler M (2001) Beta2-microglobulin-derived amyloidosis: an update. Kidney Int 59: 164–171.
15. Drueke TB (1998) Dialysis-related amyloidosis. Nephrol Dial Transplant 13: 58–64.
16. McParland VJ, Kad NM, Kalverda AP, Brown A, Kirwin-Jones P, et al. (2000) Partially unfolded states of beta2-microglobulin and amyloid formation in vitro. Biochemistry 39: 8735–8746.
17. Myers SL, Jones S, Jahn TR, Morten IJ, Tennent GA, et al. (2006) A systematic study of the effect of physiological factors on beta2-microglobulin amyloid formation at neutral pH. Biochemistry 45: 2311–2321.
18. Verdone G, Corazza A, Viglino P, Pettirossi F, Giorgetti S, et al. (2002) The solution structure of human beta2-microglobulin reveals the prodromes of its amyloid transition. Protein Sci 11: 487–499.
19. Zhang P, Fu X, Sawashita J, Yao J, Zhang B, et al. (2010) Mouse model to study human A beta2M amyloidosis: generation of a transgenic mouse with excessive expression of human beta2-microglobulin. Amyloid 17: 50–62.
20. Eichner T, Radford SE (2011) Understanding the complex mechanisms of β2-microglobulin amyloid assembly FEBS J. 278: 3868–3883.
21. Ohhashi Y, Kihara M, Naiki H, Goto Y (2005) Ultrasonication-induced Amyloid Fibril Formation of 2-Microglobulin J Biol Chem. 280: 32843–32848.
22. Yamaguchi I, Suda H, Tsuzuike N, Seto K, Seki M, et al. (2003) Glycosaminoglycan and proteoglycan inhibit the depolymerization of beta2-microglobulin amyloid fibrils in vitro. Kidney Int 64: 1080–1088.
23. Yamamoto S, Yamaguchi I, Hasegawa K, Tsutsumi S, Goto Y, et al. (2004) Glycosaminoglycans enhance the trifluoroethanol-induced extension of beta2-microglobulin-related amyloid fibrils at a neutral pH. J Am Soc Nephrol 15: 126–133.
24. Borysik AJ, Morten IJ, Radford SE, Hewitt EW (2007) Specific glycosaminoglycans promote unseeded amyloid formation from beta2-microglobulin under physiological conditions. Kidney Int 72: 174–181.

25. Yamamoto S, Hasegawa K, Yamaguchi I, Tsutsumi S, Kardos J, et al. (2004) Low concentrations of sodium dodecyl sulfate induce the extension of β2-microglobulin related amyloid fibrils at neutral pH. Biochemistry 43: 11075–11082.
26. Relini A, Canale C, Stefano SD, Rolandi R, Giorgetti S, et al. (2006) Collagen plays an active role in the aggregation of β2-microglobulin under physiopathological conditions of dialysis-related amyloidosis. J Biol Chem 281: 16521–16529.
27. Ookoshi T, Hasegawa K, Ohhashi Y, Kimura H, Takahashi N (2008) Lysophospholipids induce the nucleation and extension of beta2-microglobulin related amyloid fibrils at a neutral pH. Nephrol Dial Transplant 23: 3247–3255.
28. Hasegawa K, Tsutsumi-Yasuhara S, Ookoshi T, Ohhashi Y, Kimura H, et al. (2008) Growth of beta2-microglobulin-related amyloid fibrils by non-esterified fatty acids at a neutral pH. Biochem J 416: 307–315.
29. Relini A, De Stefano S, Torrassa S, Cavalleri O, Rolandi R, et al. (2008) Heparin strongly enhances the formation of β2-microglobulin amyloid fibrils in the presence of type I collagen. J Biol Chem 283: 4912–4920.
30. Calabrese MF, Eakin CM, Wang JM, Miranker AD (2008) A regulatable switch mediates self-association in an immunoglobulin fold. Nat Struct Mol Biol 15: 965–971.
31. Morgan CJ, Gelfand M, Atreya C, Miranker AD (2001) Kidney dialysis-associated amyloidosis: a molecular role for copper in fiber formation. J Mol Biol 309: 339–345.
32. Srikanth R, Mendoza VL, Bridgewater JD, Zhang G, Vachet RW (2009) Copper binding to beta-2-microglobulin and its pre-amyloid oligomers. Biochemistry 48: 9871–9881.
33. Mendoza VL, Antwi K, Barón-Rodríguez MA, Blanco C, Vachet RW (2011) Structure of the preamyloid dimer of beta-2-microglobulin from covalent labeling and mass spectrometry. Biochemistry 49: 1522–1532.
34. Eakin CM, Miranker AD (2005) From chance to frequent encounters: origins of beta2-microglobulin fibrillogenesis. Biochim Biophys Acta 1753: 92–99.
35. Hodkinson JP, Radford SE, Ashcroft AE (2012) The role of conformational flexibility in β2-microglobulin amyloid fibril formation at neutral pH. Rapid Commun Mass Spectrom 26: 1783–1792.
36. Moe SM, Sprague SM (1992) Beta 2-microglobulin induces calcium efflux from cultured neonatal mouse calvariae. Am J Physiol 263: F540–545.

37. Quesada JM, Alonso J, Gonzalez J, Muñoz R, Jans I, et al. (1998) Serum beta-2 microglobulin is a marker of high bone remodelling in elderly women. Mech Ageing Dev 102: 293–298.
38. Boeggeman E, Qasba PK (2002) Studies on the metal binding sites in the catalytic domain of beta1,4-galactosyltransferase. Glycobiology 12: 395–407.
39. Zhang Y, Wang PG, Brew K (2001) Specificity and mechanism of metal ion activation in UDP-galactose: beta -galactoside-alpha -1,3-galactosyltransferase. J Biol Chem 276: 11567–11574.
40. Nielsen MM, Suits MD, Yang M, Barry CS, Martinez-Fleites Cet al (2011) Substrate and metal ion promiscuity in mannosylglycerate synthase. J Biol Chem 286: 15155–15164.
41. Li J, Rancour DM, Allende ML, Worth CA, Darling DS, et al. (2001) The DXD motif is required for GM2 synthase activity but is not critical for nucleotide binding. Glycobiology 11: 217–229.
42. Rigden DJ, Galperin MY (2004) The DxDxDG motif for calcium binding: multiple structural contexts and implications for evolution. J Mol Biol 343: 971–984.
43. Ruzafa D, Morel B, Varela L, Azuaga AI, Conejero-Lara F (2012) Characterization of Oligomers of Heterogeneous Size as Precursors of Amyloid Fibril Nucleation of an SH3 Domain: An Experimental Kinetics Study. PLoS ONE 7: e49690.
44. Zerovnik E (2011) Oligomerization preceding amyloid fibril formation: a process in common to intrinsically disordered and globular proteins. Network 22: 154-61.
45. Long X, Zhang C, Cheng J, Bi S (2008) A novel method for study of the aggregation of protein induced by metal ion aluminum (III) using resonance Rayleigh scattering technique. Spectrochim Acta A Mol Biomol Spectrosc 69: 71–77.
46. Shukla A, Raje M, Guptasarma P (2008) Coalescence of spherical beads of retro-HSP12.6 into linear and ring-shaped amyloid nanofibers. Biochem (Mosc). 73: 681–685.
47. Khan JM, Qadeer A, Chaturvedi SK, Ahmad E, Rehman SA (2012) SDS can be utilized as an amyloid inducer: a case study on diverse proteins. PLoS One 7: e29694.
48. Prusiner SB, Scott MR, Armond SJ, Cohen FE (1998) Prion protein biology. Cell 93: 337–345.
49. Treush S, Cyr DM, Lindquist S (2009) Amyloid deposits: Protection against toxic protein species? Cell Cycle 8: 1668–1674

50. Sinha S, Lopes DHJ, Bitan G (2012) A Key Role for Lysine Residues in Amyloid β-Protein Folding, Assembly, and Toxicity. ACS Chemical Neuroscience 3: 473-481

Section B

Role of 17β-estradiol in arsenic trioxide induced cell proliferation and migration in MCF-7 breast cancer cells

B.1 Introduction:

Arsenic is 20th most abundant element in earth's crust and is a metalloid. Arsenic occurs in rocks as a component of more than 245 minerals containing sulfides. Upon weathering of these rocks arsenic sulfides are release arsenic trioxide, which gets dissolved in surface and ground water bodies. Arsenic minerals have been identified as a significant environmental health hazard in general, worldwide and particularly in India (1,2), Argentina (3), Bangladesh (4), Chile (5), Mexico (6), Taiwan (7) and Vietnam (8) and USA (9). Arsenic contamination of ground water is very severe in West Bengal and Bangladesh, where arsenic concentration has been found to reach up to 1 mg/l, which is well above the safe arsenic limit of 10 µg/l set for drinking water recommended by the world health organization. Upon ingestion of arsenic-contaminated water and food, arsenic is absorbed by stomach and intestine that finally release absorbed arsenic into blood. Small amounts of arsenic are also absorbed through inhalation and dermal exposure to arsenic-laden dust and smoke (10).

Arsenic is found in inorganic as well as organic forms in nature. Arsenic minerals primarily consist of oxides, phosphates and sulfides. Although inorganic arsenic occurs in several oxidation states but oxidation states of (III) and (V) are commonly found in environmental arsenic contaminants and are frequently implicated in arsenic linked carcinogenesis (11). Arsenic acid and arsenous acid depicted in figure B.1 have Arsenic in pentavalent and trivalent states respectively. The oxidation states of arsenic are inter-convertible depending upon the redox conditions of surroundings.

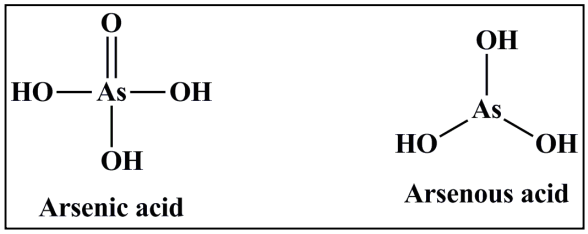

Figure B.1: Common inorganic arsenic contaminants of ground water: Arsenic acid with oxidation state of (V) and arsenous acid with oxidation state of (III).

Organic arsenicals like monomethyl arsonic acid (MMA) and dimethyl arsinic acid (DMA) are herbicide-derived pollutants. Interestingly both MMA and DMA are also produced as a result of methylation of inorganic arsenic species and excreted in urine (12).

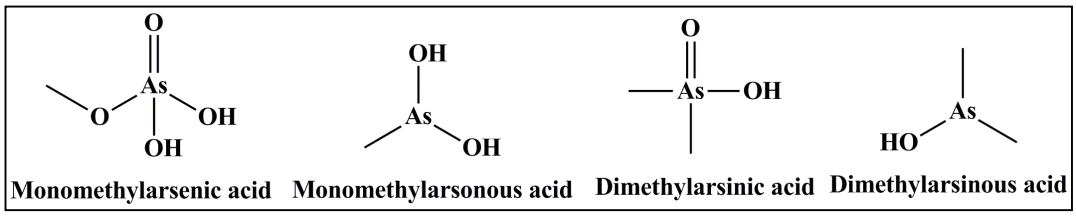

Figure B.2: Common organic arsenic contaminants: Arsenic occurs in oxidation state of (V) in monomethylarsenic acid and dimethylarsenic acid. Arsenic is present in oxidation state of (III) in Monomethylarsenous acid and dimethylarsinous acid

B.1.1 Sources of arsenic exposure

Human exposure to arsenic results from arsenic contaminated water, industrial processes and smoking.

B.1.1.1 Drinking water and food

Arsenic contaminated groundwater is a major source of exposure to inorganic arsenic (13). Arsenic in ground water exposes the human population to arsenic at many levels. It directly exposes the population to inorganic arsenic through drinking water and food prepared in contaminated water. Arsenic enters the food chain through food crops irrigated with arsenic contaminated water (14).

B.1.1.2 Industrial processes

Arsenic is released during the smelting process of ores of copper, cobalt, gold, lead, nickel and zinc. This exposes the smelting workers and peoples in nearby area to arsenic (15).

B.1.1.3 Smoking tobacco

Smoking tobacco also leads to arsenic exposure. Tobacco plants accumulate arsenic from soil to its plant parts including leaves (16). The extent of arsenic accumulation in tobacco plants cultivated in the areas affected by arsenic contamination and irrigated with arsenic contaminated water is still higher (17). Simultaneous exposure to arsenic and tobacco smoking also results in increased instances of lung cancer.

B.1.1.4 Wood industry

Arsenic has been historically used in preservation of wood. The use of furniture made from arsenic treated wood exposes humans to arsenic (18,19).

B.1.2 Metabolism of arsenic

Initially liver was considered to be the sole site of arsenic metabolism but new studies with mice models show that the other organs also have arsenic methylation capability with methylation occurring in decreasing order testes>liver>lung (20). Inorganic arsenic is metabolized in the liver by reduction and methylation forming MMA and DMA that are excreted by kidneys (21). Arsenic in trivalent form is subjected to methylation and pentavalent arsenic is first reduced to trivalent form before methylation. Pentavalent arsenic in inorganic and organic forms is reduced by arsenic reductase, reduced glutathione (GSH), a tripeptide and other thiol-containing proteins (20). Little is known about arsenic methyltransferases. Current arsenic methylation model proposes binding of arsenite to a dithiol carrier protein and subsequent methylation by S-adenosyl methionine (SAM). There is a great level of variation in rate and degree of methylation in the human population. Despite these variations; relative distribution of inorganic and organic arsenic metabolites in urine is constant. The relative distribution of arsenic in urine of persons exposed to arsenic consists of 10-30% inorganic arsenic, 10-20% MMA and 60-70% DMA (22). Arsenic was considered to be most toxic in inorganic forms than the organic forms. But subsequent research have demonstrated that the organic arsenic in trivalent form is more toxic than arsenite (23,24).

B.1.3 Health problems caused by arsenic exposure:

B.1.3.1 Acute arsenic toxicity

Arsenic acts as a protoplasmic poison by interfering with cellular enzymes, cell respiration and mitosis. Arsenic depending upon its oxidation state can exert its toxic effects differently. In trivalent oxidation state arsenic can interact with free thiol groups present in the transmembrane and cellular proteins resulting in altered conformational states that may culminate in altered protein-protein interaction and downstream signaling (25). In pentavalent state, arsenic may replace phosphate in many biochemical reactions acting as a metabolic poison (26). Consequently exposure to High levels (1-3 mg As/Kg) of inorganic arsenic results in anuria, bloody urine, convulsions, diarrhea, gastrointestinal discomfort, vomiting, coma and death.

B.1.3.2 Chronic arsenic toxicity:

Prolonged exposure to arsenic has been associated with many human diseases. While a high level of exposure to arsenic is fatal, a moderate level of arsenic exposure adversely affects multiple organ systems like cardiovascular and nervous system, kidney, liver, lungs and skin (27). Arsenic exposure has also been strongly correlated to skin and other types of cancers (28).

B.1.4 Mechanism of arsenic-induced carcinogenesis

There are ample pieces of evidence that chronic exposure to arsenic can result in carcinogenesis. Chronic exposure to arsenic has been positively correlated to bladder, lung and skin cancers. The molecular mechanism underlying low dose arsenic-induced carcinogenesis is poorly understood. Several models have been proposed to describe the mechanism of arsenic-induced carcinogenesis including cell proliferation, epigenetic changes, impaired DNA repair, genotoxicity, co-carcinogenesis and tweaking of signal transduction pathways (29).

B.1.4.1 Arsenic induced cell proliferation:

Arsenic has been shown to induce cell proliferation and carcinogenesis at low concentration. *In vitro* studies have shown low dose arsenic trioxide (0.01-1 μM) to induce cell proliferation in MCF10A breast epithelial cell line. Low dose arsenic trioxide treatment resulted in cell cycle progression from G1 to S/G2 phases with increased expression of cell cycle related proteins like cyclin D1 and cell division cycle 6 (CDC6) in non-tumorigenic MCF 10A cell line. The low dose arsenic-treated MCF-10A showed greater Low dose arsenic has been demonstrated to induce reactive oxygen species (ROS) and activated prosurvival protein AKT, and mitogen-activated protein kinases like ERK1/2 and p38 MAPK pathways in time-dependent manner. Low dose arsenic-induced ROS mediated cell proliferation is abrogated in the presence of N-acetylcysteine (NAC), which is an ROS inhibitor (30).

B.1.4.2 Arsenic induced epigenetic changes:

Inorganic arsenic can cause epigenetic changes that favor carcinogenesis by altering the methylation pattern of the genome, hyperacetylation of histones and altered microRNA expression. Hypomethylation of certain genomic regions related to cancer has been observed in cells exposed to low dose arsenic (31, 32).

B.1.4.3 Arsenic inhibition of DNA repair

Inorganic arsenic acts as a genotoxin. Arsenic exposure results in oxidative stress through the generation of ROS, which in turn leads to DNA damage in the form of single strand breaks. In vitro studies have demonstrated impairment of DNA repair ability of fibroblast cells in the

presence of inorganic arsenic (32). Arsenic also inhibits the base excision repair. Arsenic inhibits of DNA repair by down regulation of the proteins associated with nucleotide excision repair and base excision repair processes. Arsenic down regulates DNA Polymerase beta and apurinic/apyrimidine endonuclease and DNA ligase I and III (33). Epidemiological studies have also confirmed the arsenic exposure associated downregulation of DNA repair associated proteins (34,35).

B.1.4.4 Co-carcinogenesis:

Inorganic arsenic enhances the carcinogenic potential of other carcinogens like UV irritation and benzopyrene. Simultaneous exposure to arsenic and cigarette smoke carcinogens like benzopyrene, which is a polycyclic aromatic hydrocarbon present in cigarette smoke increases the risk of developing lung cancer (36). Intratracheal co-administration of arsenic and benzopyrene in mouse models showed a positive correlation in the development of respiratory tract carcinoma. Similarly, arsenic enhances the tumorigenesis in mice irradiated with UV light. As described earlier arsenic can interfere with DNA repair machinery and hence simultaneous exposure to DNA damaging UV radiation and DNA repair inhibition by arsenic may result in the greater propensity of developing skin cancer (37).

B.1.4.5 Arsenic induces oxidative stress

Arsenic is a very potent oxidative stressor in vitro and in vivo. The trivalent arsenic reacts with reduced glutathione leading to depletion of ROS scavenging potential of the cell. The excess ROS reacts with cellular lipids and proteins further contributing to pathophysiology. The arsenic exposed cells rapidly undergo oxidative stress. In one study it was demonstrated that human-hamster hybrid cells produce ROS within few minutes of arsenic exposure (38). Low dose arsenic induced ROS stimulates the proliferation of MCF-10A breast cancer line by activating MAPK pathways (30). Organic arsenical contribute to generation of ROS by inducing release of iron from ferritin even in presence of an antioxidant like ascorbic acid (39).

B.1.4.6 Arsenic as an endocrine disruptor:

Arsenic exposure acts as an endocrine disruptor by modulating E2 binding with estrogen receptor (ER). Arsenic competes with E2 for binding with ER, through cysteine residues in vicinity of hormone binding domain of ER. Studies involving binding assay arsenite blocked ER-Estradiol binding with Ki of 5 nM (40). Arsenic binding with ER results in aberrant ER mediated transcriptional activity (41). Arsenic further complicates the endocrine disruption

by down regulation of ER-α (40). In albino female rats the administration of arsenic significantly decrease estrogen levels and ER regulated gene products (42).

B.1.4.7 Rationale behind the present study:

17-β-estradiol (the primary natural estrogen present in the female blood) is a steroid hormone that is essential for normal physiological functions in humans. Despite the physiologically beneficial effects of 17-β-estradiol, it is also considered as a risk factor for breast cancer in women. Arsenic is a common environmental carcinogen found positively correlated to various kinds of cancers in humans. But the role-played by the interaction between 17-β-estradiol and arsenic trioxide in human carcinogenesis is poorly understood. There are few reports that establish Arsenic as an endocrine disruptor with estrogenic activity. In the present study, we have established that 17-β-estradiol and arsenic can physically interact with each other, and both induce cell proliferation in human and bacterial cells. In the presence of arsenic, the cell proliferation stimulation by 17-β-estradiol is abrogated.

B.2 Materials:

Minimum essential medium, fetal bovine serum, charcol-dextran treated fetal bovine serum, L-glutamine, sodium pyruvate, 17-β-estradiol and arsenic trioxide were obtained from Sigma Chemical (St. Louis, USA), Sterile cell culture flasks and plates were obtained from Corning. Antibiotic-antimycotic, FBS and insulin were purchased from HiMedia.

B.3 Methods

B.3.1 *In-vitro* culture of MCF-7 breast cancer cells

MCF-7 breast cancer cells were procured from ATCC and maintained in minimum essential medium (MEM) supplemented with 5% fetal bovine serum (FBS), 1mM sodium pyruvate, 1mM L-glutamine, 2.2 g/l sodium bicarbonate, 0.01 mg/ml insulin, 1X antibiotic-antimycotic, at 37 °C and incubated in a humidified incubator in an atmosphere of 5% CO_2.

B.3.2 MTT Assay to check cell viability

MCF-7 cells were seeded in 24-well plates at a cell density of 2×10^4 cells/well. The assay was optimized for the cell lines used in the experiments. Briefly, for the purposes of the experiments at the end of the incubation time, cells were incubated for 3 hours with 1 ml of 5 mg/ml of MTT, dissolved in serum free medium (MEM). 1 ml of MTT solvent (0.1N HCl-

propanol) was added to each well and cell plates were covered with aluminum foil and placed on rotary shaker for 10 minutes to completely dissolve the MTT product. Absorbance was taken with Cary 50 spectrophotometer at 570 nm with background subtraction at 650 nm. All treatments were given in triplicates and experiments were repeated thrice.

B.3.3 Wound healing assay

The effect of arsenic and estradiol on cell migration was tested by the following wound-healing or wound-closure assay. MCF-7 breast cancer cells were seeded at 5 x 10^5 cells/ml in 6-well plates, and incubated in a humidified CO_2 incubator at 37 °C. Incubations were carried out, with cell culture media being changed after every 24 hours, until it was evident that the cells had formed a monolayer. The cells were then washed with sterile phosphate-buffered saline (PBS) to remove serum, and incubated in phenol red free MEM supplemented with 2% charcoal-dextran-treated fetal bovine serum (FBS) and 1X antibiotic-antimycotic for 24 hours. A scratch wound was inflicted in each well, using a sterile 20 μl pipette tip and cells were washed twice with sterile 1x PBS to remove free floating cells. Treatment with ATO and E2 was given in phenol red free medium supplemented with 1X antibiotic-antimycotic. The region of interest (ROI) was marked on wells and images were collected using an inverted microscope (Nikon Ti-Eclipse) at 10x magnification, for each condition of treatment involving E2, ATO, or E2 and ATO. Following incubations, cells were washed with sterile PBS and images were collected from ROIs. Images were processed with the software Image J from NIH (http://rsb.info.nih.gov/ij/) to quantify and measure the degree of wound healing or wound-closure. Wound healing was calculated using the following formula:

$$\%\ wound\ healing = \frac{Initial\ area\ of\ wound - Final\ area\ of\ wound}{Initial\ area\ of\ wound}$$

B.3.4 Difference absorption spectroscopy

Difference absorption spectroscopy was carried out to detect interactions between ATO and E2. Difference absorption spectra were taken on Cary 50 UV-Visible spectrophotometer. This technique is commonly used by pharmacological researchers but not so commonly used in other biochemical research. Therefore, a brief description of the technique is also given here. Difference absorption spectroscopy is performed using a quartz cuvette made with thinner quartz walls, and containing a thin quartz wall running right down the middle of the cuvette (extending from the bottom of the cuvette until approximately three-fourths of its

height). This wall separates the cuvette with a path length of 1 cm into two compartments of equal path length of 0.5 cm each. Two different chemicals are placed in the two compartments, with the prerequisite that at least one of them absorbs either ultraviolet or visible light of any wavelength, and with the two solutions being of absolutely identical volumes. When the two chemicals are placed in the two compartments, and the absorption spectrum for light passing through both compartments is collected, this spectrum which involves light passing through each solution with a path length of 0.5 cm is 'zeroed' using the spectrometer's software and taken to be the 'blank' spectrum. The cuvette is then closed with a 'stopper', and inverted, or up-turned, such that the two solutions of equal volume are allowed to mix thoroughly. The mixed solution now contains each of the two reagents at half of the original concentration used, since equal volumes are mixed. This is followed by inverting the up-turned cuvette once again, such that it sits with its right side-up. As a consequence, the 'pre-mixed' solution falls back into both compartments. Even if the two volumes are no longer equal, as long as light passes through both solutions, it is ensured that the concentrations of each chemical is now effectively halved, and the path length is doubled from 0.5 cm to 1 cm, since both compartments contain both chemicals. Now, when the absorption spectrum is collected again against the blank, if the two chemicals do not interact, the spectrum obtained (called the 'difference absorption spectrum) is a flat line, which is indistinguishable from the blank. However, if the two chemicals physically interact, they affect each other's molecular orbitals sufficiently to give rise to differences in absorption in the same spectral ranges in which either one, or both, of them originally displayed some absorption. Therefore, the spectrum is no longer a flat line, but displays either negative or positive absorption over the blank spectrum; in particular, these positive/negative differences are seen in those regions of the spectrum in which either one of the two interacting components happens to display a pronounced absorption band [which undergoes an increase, or reduction, in absorbance due to the interaction, and the effects of effects of such interaction upon the electronic orbitals participating in the excitation transition(s)]. A difference absorption spectrum is thus a definitive indicator of a physical interaction occurring between two molecules, resulting in alterations in the absorptivity characteristics of either, or both. We took 300 μM arsenic trioxide (ATO) in water in one compartment and 30 μM 17-β-estradiol (E2) in water in the other compartment and the blank spectrum was collected between 200 and 600 nm. The cuvette was then inverted and the two solutions were allowed to mix. Then the difference absorption spectrum was collected.

B.3.5 Difference Circular Dichroism spectroscopy

The difference CD spectra were collected on a MOS-500 CD spectrometer in using 1cm path length difference absorption cuvette. Briefly, we took 300 μM arsenic trioxide (ATO) in water in one compartment and 30 μM 17-β-estradiol (E2) in water in the other compartment and the CD spectrum was collected between 190-400 nm. The cuvette was then inverted and the two solutions were allowed to mix. Then the difference CD spectrum was collected.

B.3.6 Voltammometery studies to estimate As (III) binding capacity of E2

Estimation of arsenic binding to E2 was done on Metrohm 797 VA Computrace voltammetry instrument DP voltammetry technique using Au RDE. E2 and ATO stocks were prepared in molecular biology grade ethanol and Milli-Q water (>18.2 MΩ cm) respectively. Working solutions of ATO, E2 and ATO/E2 mixtures were prepared by diluting the ATO and E2 stocks with ultrapure water in a 25 ml volumetric flask. The working solutions were passed through C18 sample preparation cartridges prior to voltammetry analysis. 5 ml ultrapure water and 5 ml HCl were added into measuring vessel and a blank voltammogram was recorded. 50 μl of C18 passed sample was added and voltammogram was recorded. The concentration of arsenic was determined by standard addition technique.

B.4 Results and Discussion

B.4.1. ATO Induces cell proliferation in MCF-7 at very low concentrations

Arsenic trioxide induced MCF-7 cell proliferation was assessed using MTT assay. Very briefly, MCF-7 cells were resuspended in minimum essential medium (MEM) supplemented with 5% fetal bovine serum (FBS), 1mM sodium pyruvate, 1mM L-glutamine, 2.2 g/l sodium bicarbonate, 0.01 mg/ml insulin, 1X antibiotic-antimycotic and plated at 5000 cells/well in a 96 well plate and incubated for 24 hours in humidified incubator at 37 °C in 5% CO_2. After 24 hours incubation the cells were washed with experimental medium (Phenol red free MEM supplemented with 1U/ml antibiotic-antimycotic) and incubated for 24 hours in experimental medium to purge the residual serum and phenol red mediated estrogenic activity. Spent media was removed and cells were treated with various concentrations of arsenic trioxide prepared in experimental media for 24 hours. 10 µl MTT reagent was added to each well using a multichannel pipette and further incubated the cells for 3 hours. Media was removed and 100 µl isopropanol containing 0.1N HCl was used to solubilize the MTT formazan crystals and absorbance was collected at 570 nm and 650 nm in plate reader. All the treatments were given in triplicate and experiment was repeated thrice. The serum in the media was completely avoided during treatment with arsenic as arsenic can bind serum proteins and the effective dosage of arsenic may not be achieved in the duration of the cell proliferation assay. Figure B.3, shows that ATO induces cell proliferation in MCF-7 cells in concentrations ranging from 100 pM to 1 µM with maximum cell proliferation at 10 nM, whereas at high concentrations of arsenic (10 µM and 20 µM), the cell proliferation decreased relative to the untreated control.

Wound healing assay was done to assess the effect of various concentrations of arsenic trioxide on scratch wound created in MCF-7 cell monolayer. For the assay MCF-7 cells were plated at high density in 24 well plates. Plates were incubated till a uniform monolayer of MCF-7 cells was formed in the well. A scratch wound was created in each well using 10-µl pipette tip. Subsequently each well was washed twice with phenol red free experimental medium without any serum.

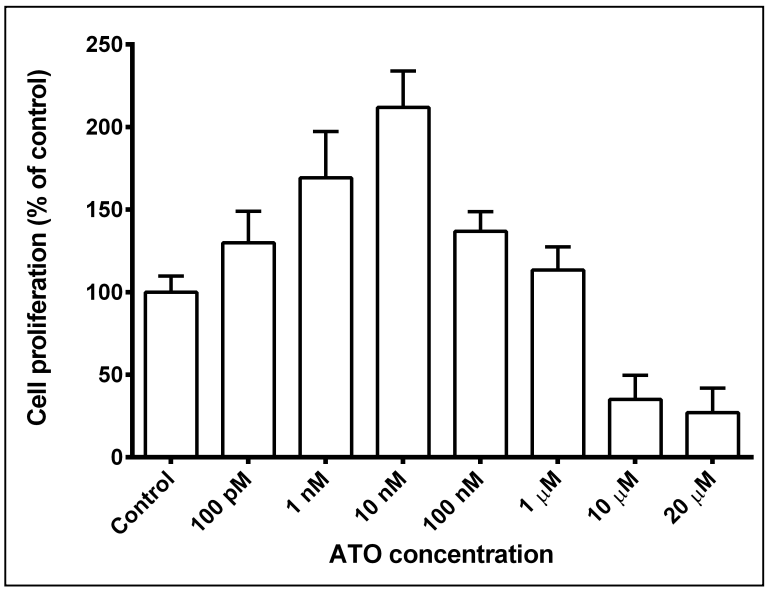

Figure B.3: Effect of ATO on MCF-7 cell proliferation: Control experiment. Effect of various concentrations of arsenic on cell proliferation achieved over 24 hours, using the MTT assay; Data presented here is representative of 5 independent experiments performed in identical conditions.

Freshly prepared arsenic trioxide solutions of various concentrations were applied to designated wells and photographed on Nikon-ti inverted microscope at 10x objective magnification and marked as T0 images. Cells were again imaged after 24 hours of incubation. The images were processed using ImageJ software from NCBI and % wound healing was calculated for control and arsenic trioxide treated cells. Figure B.4.A shows, ATO enhanced the scratch wound healing in MCF-7 monolayers at concentration ranging from 100 pM to 100 nm. Whereas arsenic trioxide showed decrease wound healing relative to control in concentration ranging from 1-10 μM. Also arsenic trioxide at 20 μM concentration induced cell death. Figure B.4.B, shows the histograms for measured of extent of wound closure estimated using scientific data processing software ImageJ, for three independent experiments under identical conditions.

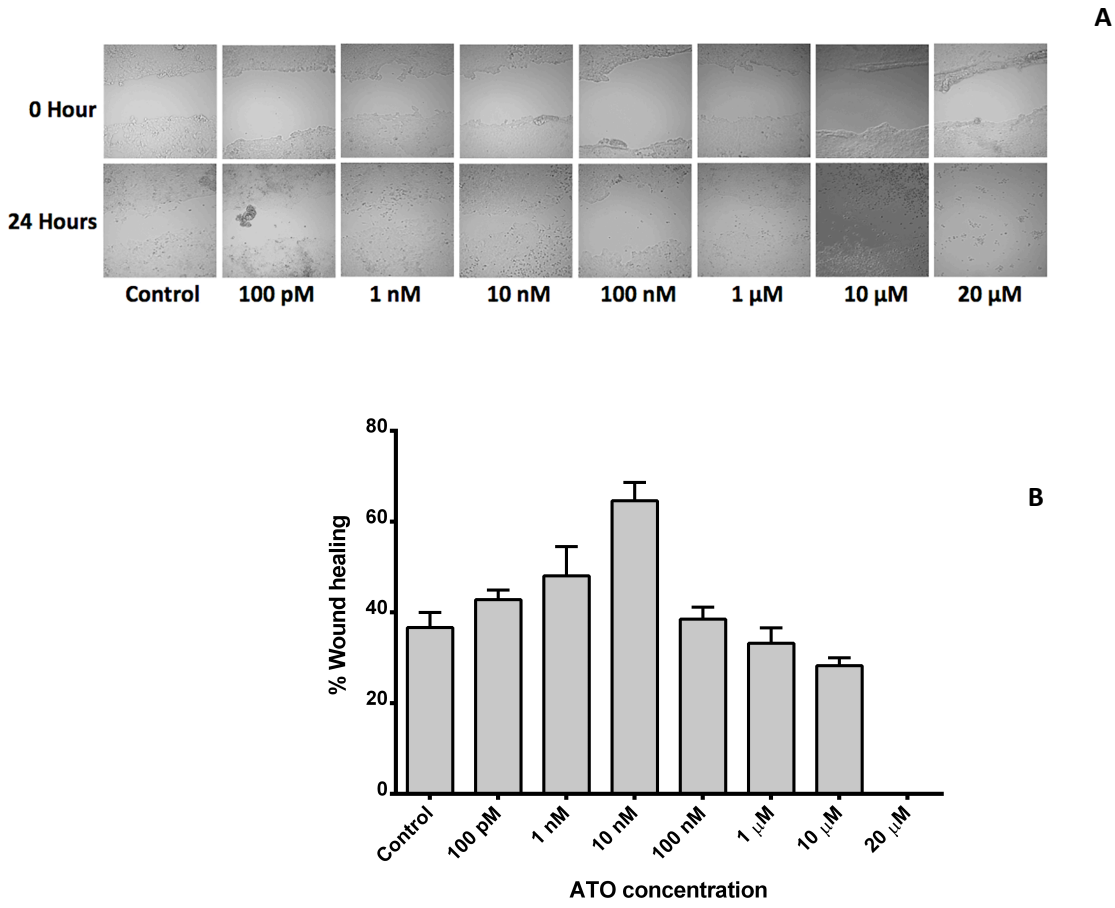

Figure B.4: Dose response of MCF-7 monolayer scratch wounds to various concentrations of ATO. B.4.A: Representative images of scratch wounds at 0 hour and 24 hours, treated with various concentrations of ATO. **B.4.B:** Histograms representing the extent of wound healing in MCF-7 monolayers after 24 hours of incubation, based on quantitation of the images from three independent experiments identical to that shown in panel A.

Earlier studies have demonstrated low concentration arsenic to be cell proliferation promoter in non-tumorigenic MCF10A breast epithelium cell line (30). Arsenic at low concentrations induces generation of ROS, which further activates AKT, p38 MAPK, and ERK1/2 leading to cell proliferation. Low dose arsenic induced ROS is susceptible to ROS inhibitor like NAC, which decreases the low dose arsenic dependent activation of p38 MAPK and AKT (30).

B.4.3 Effect of 17-β-estradiol on monolayer wound healing:

Wound healing assay was done to assess the effect of various concentrations of 17-β-estradiol (E2) on scratch wound created in MCF-7 cell monolayer. Figure B.5.A shows, E2 induced wound healing at concentrations ranging from 100 pM to 1 μM with maximum wound healing at 100 nM.

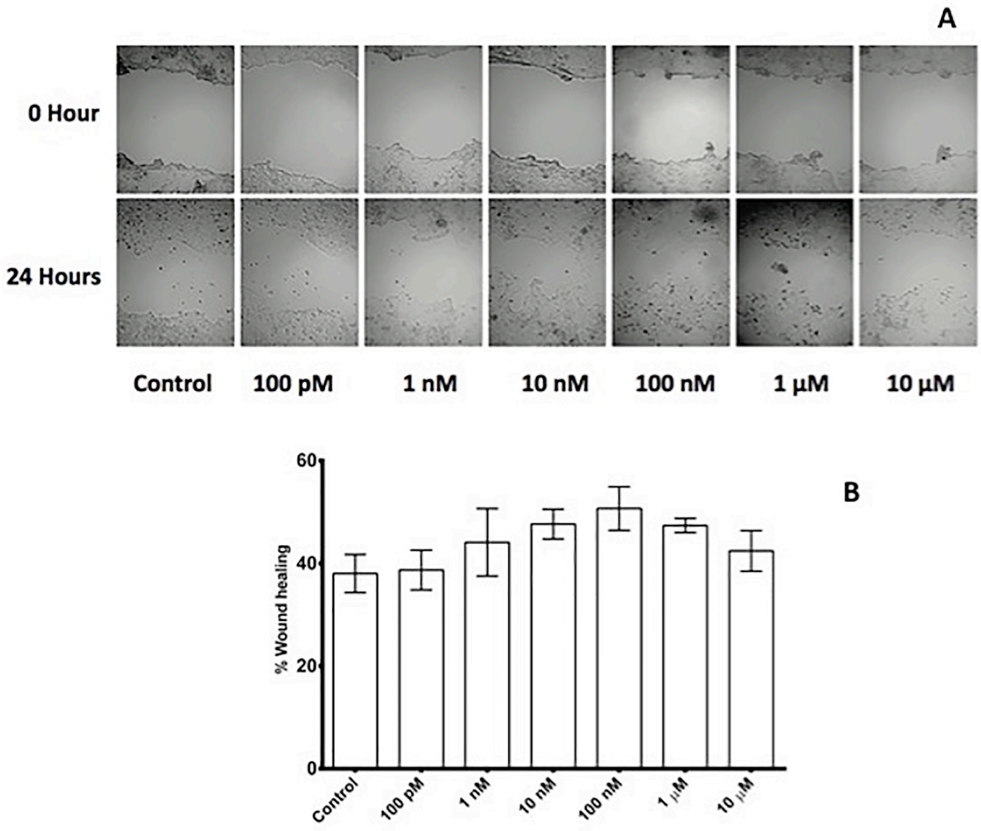

Figure B.5: Dose response of MCF-7 monolayer scratch wounds to various concentrations of E2. B.5.A: Representative images of scratch wounds at 0 hour and 24 hours, treated with various concentrations of E2. **B.5.B:** Histograms representing the extent of wound healing in MCF-7 monolayers after 24 hours of incubation, based on quantitation of the images from three independent experiments identical to that shown in panel A. As described in earlier chapter E2 can also increase cell proliferation in a genomic and non-genomic manner. We further wanted to investigate the cumulative effect of arsenic and E2 on MCF-7 monolayer wound healing. Figure B.5.B shows, the histograms for measured of extent of wound closure estimated with scientific data processing software ImageJ for three independent experiments under identical conditions.

B.4.4 Lack of synergism in ATO and E2 induced wound healing

Both ATO and E2 individually have ability to induce wound healing in MCF-7 monolayers. We wanted to know the possible synergism between ATO and E2 mediated scratch wound healing. When ATO and E2 at maximum wound healing concentrations of 10 nm and 100 nm respectively, were applied to MCF-7 monolayer scratch wound the extent of wound closure is equivalent to that of untreated control. Figure B.6.A represents the MCF-7 monolayer wounds treated with ethanol control, ATO, E2 and a combination of ATO and E2.

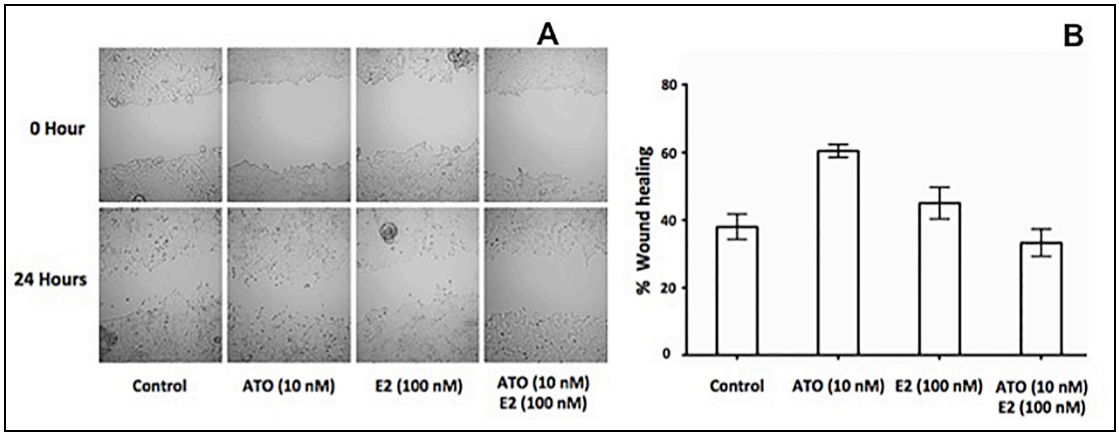

Figure B.6: Scratch wound healing of MCF-7 monolayers in presence of ATO, E2, and a mixture of ATO and E2. B.6.A: Scratch wounds were created in MCF-7 monolayers and imaged prior to treating with ethanol (control), ATO (10 nM), E2 (100 nM) and a combination of ATO (10 nM) and E2 (100 nM), and again after 24 hours. **B.6.B:** Histograms representing the extent of wound healing in MCF-7 monolayers after 24 hours of incubation, based on quantitation of the images from three independent experiments identical to that shown in panel A.

Figure B.6.B shows, the histograms representative for measured of extent of wound closure estimated with scientific data processing software ImageJ for three independent experiments under identical conditions.

ATO and E2 bind each other

ATO and E2 fail to produce scratch wound healing in MCF-7 monolayer in presence of each other. There are two probable mechanisms responsible for this observation. ATO and E2 might be activating cell proliferation pathways that might be antagonistic in nature, or second the might bind with each other in cell culture media, thereby mechanistically neutralizing the cellular effects of each other. So, we utilized a combination of spectroscopy and voltammetric methods to check the binding interaction between ATO and E2.

Spectroscopic evidences of ATO binding with E

Figure B.7.A shows the individual ultraviolet electronic excitation (absorbance) spectra of (i) ATO (ii) E2, in the range of 200-400 nm. Figure B.8.B shows the 'difference' absorbance (DA) spectrum for ATO and E2, obtained through mixing of components in a tandem quartz cuvette. Reagents which do not physically interact at the molecular level; upon mixing do not display DA spectra, i.e., the DA spectrum tends to be flat, and equivalent to the baseline ('zeroed') spectrum.

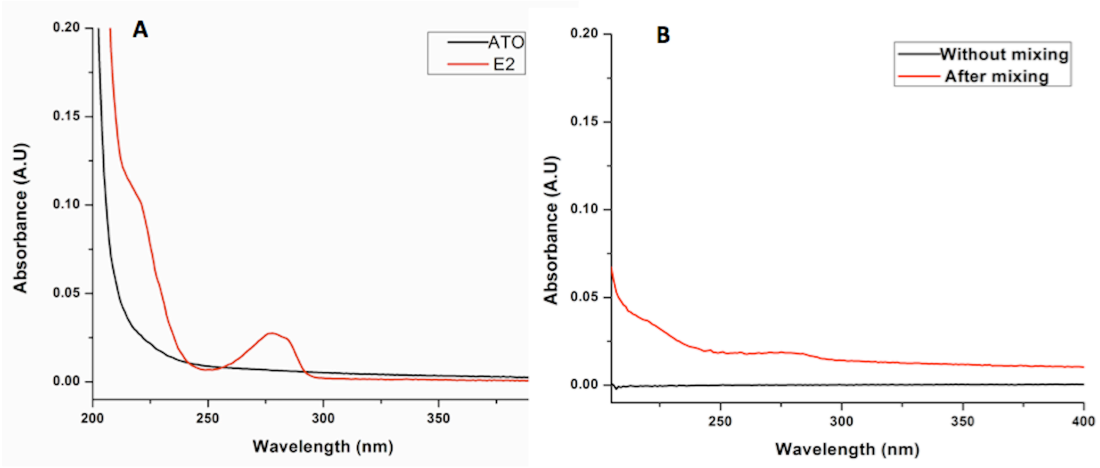

Figure B.7: Spectroscopic evidences of ATO binding with E2. B.7.A: Individual ultraviolet electronic excitation (absorbance) spectra of ATO (300 µM; in black) and E2 (30 µM; in red). **B.7.B:** The difference absorption spectrum (in red) of ATO (300 µM) and E2 (30 µM), shown with the 'zeroed' baseline (in black). spectrum collected with E2 (30 µM) and ATO (300 µM) in separate compartments of a tandem cuvette (in black) and upon mixing (in red).

In contrast, as Figure B.7.B clearly shows, ATO and E2 display a distinct DA spectrum upon being mixed, Displaying features clearly suggestive of alterations in E2's electronic excitation upon binding to ATO (in particular, the hyperchromic effects visible in the ~225 nm and ~280 nm absorption bands).

Separately, as shown in Figure B.8, it may be noted that E2 naturally displays differential absorption of left- and right-circularly polarized light, yielding a circular dichroic (CD) spectrum. The CD spectrum of E2 and the CD spectrum obtained upon mixing of E2 with ATO, also display differences in the two negative bands at ~225 nm and ~280 nm, in addition to a spectral cross-over at ~350 nm, indicating that binding of ATO affects the chirality of E2 and, therefore, its properties of differential absorption of left- and right- circularly polarized light.

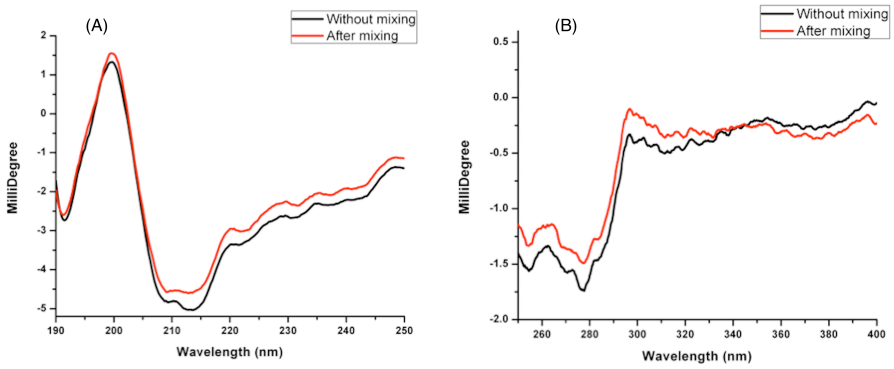

Figure B.8: Difference Circular Dichorism (DCD) Spectroscopic evidences of ATO binding with E2. B.8.A: Far-UV DCD spectra of ATO (300 µM) and E2 (30 µM. **B.8.B:** Near UV DCD spectra of ATO (300 µM) and E2 (30 µM); Black trace represents DCD spectra without mixing and red trace shows DCD spectra after mixing.

Voltammetry based evidences of ATO binding with E2

Figure B.9, shows results of voltammetric experiments performed to detect and quantitate the presence and level of arsenic [As (III)] in samples, following separate experiments involving the passing of E2, ATO and a mixture of E2 and ATO through a reverse-phase (C_{18}) cartridge. In each experiment, a baseline dataset (red curve) is shown along with a dataset monitoring the level of As (III) in the sample (blue curve), in addition to two calibration curves obtained through two successive super-additions of standard amounts of As (III) to the amount already present in each sample (black curve). The data shows monitoring of As (III) levels in 50 µl samples of 300 µM ATO (Figure B.9.A), 30 µM E2 (Figure B.9.B), and 300 µM ATO mixed with 30 µM E2 (Figure B.9.C), after passage of 25 ml volumes of each of these through a new C18 cartridge. The obtained data is presented in Table B.1

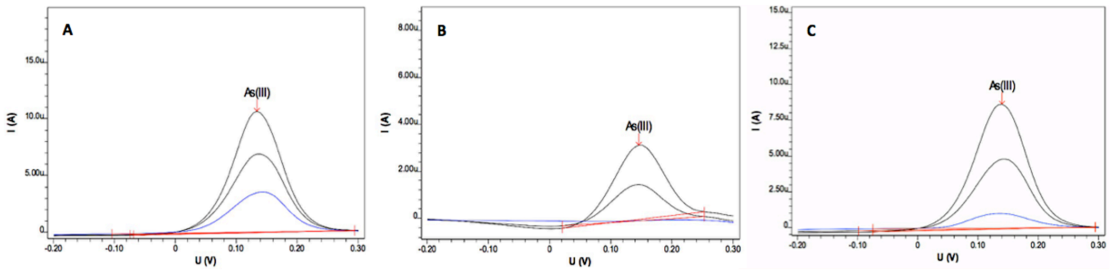

Figure B.9: Voltammetry experiments to validate and quantitate As(III) binding with E2: All panels show the baseline (in red), the sample (in blue), and two successive calibrating additions of ATO solution to quantitate the arsenic content of the sample (in black). **B.9.A:** The estimation of As (III) in ATO standard solution. **B.9.B:** Estimation of ATO in E2 (30 µM) solution after passage through the reverse-phase cartridge. **B.9.C:** Estimation of ATO in a mixture of 300 µM ATO and 30 µM E2 after passage through the reverse-phase cartridge, to examine whether the E2 bound to the cartridge retains ATO and reduces its level.

Table B.1: ATO binding to E2 quantified through voltammetry

Analyte	**As (III) (mg/l)**	**ATO (µM/l)**
300 µM/l ATO standard	44.81	299
30 µM/l E2 standard	ND	ND
30 µM/l E2 + 300 µM/l ATO	11.70	78

From the Table B1 and Figure B.9, it is clear that E2 (which binds to the C_{18} resin) is able to substantially retain ATO (which cannot bind to the C_{18} resin) on the C_{18} cartridge, resulting in a sharp drop in the detected As (III) level in the sample containing both E2 and ATO (Figure B.9.C; blue curve), in comparison with the ATO sample (Figure B.9.A; blue curve).

Interestingly, our data suggesting that arsenic (ATO) and estrogen (E2) bind to each other appears to explain a number of different reports that have appeared in the literature linking arsenic and reproductive health, providing interesting correlations. Briefly, it may be noted that each of the seven independent observations mentioned below is compatible with the hypothesis that arsenic binds to estrogen *in vivo*, with the semimetal and the hormone behaving as natural 'sequestrators' of each other which are capable of lowering each other's levels in circulation: **(1)** A report from Chile has shown that removal of arsenic from drinking water results in a significant increase in the incidence of breast cancer (43). It is well known

that breast cancer shows a positive correlation with levels of circulating and functional estrogen (44). It is conceivable that arsenic protects women with high levels of estrogen from breast cancer by reducing their functional and circulating levels of estrogen. **(2)** A report from Bangladesh has shown that men are far more susceptible to arsenic poisoning than women (45). It is well-known that women have higher circulating levels of estrogen than men (46), and it is conceivable, therefore, that estrogen plays a protective role against arsenic toxicity by binding to it, protecting women more than it protects men. **(3)** A study from India has shown that pre-pubertal exposure to arsenic significantly delays the age of menarche (47). It is well known that estrogen levels determine the age of sexual maturation in women (48). Thus pre-pubertal exposure to arsenic could potentially lower the circulating and functional levels of estrogen available to bring about menarche. **(4)** A study from the USA has shown that female rodents show delayed sexual maturation when they are chronically exposed to arsenic (51). Once again, this supports the contentions made in the previous case concerning the age of menarche. **(5)** A study from Bangladesh has shown that chronic exposure to arsenic results in women attaining menopause roughly two years before women in control populations (52). It is well known that estrogen levels correlate very strongly with the age of menopause, and the binding of arsenic could bring about early menopause by reducing the circulating functional levels of estrogen. **(6)** A study from Pakistan has shown that there is a dose-dependent lowering of plasma levels of estrogen in female rodents, with sustained exposure to arsenic (53). This could partially owe to the binding of estrogen to arsenic. However, a complete explanation would need to involve consideration of the complex feedback mechanisms involving all the other hormones running the female menstrual cycle in concert with estrogen (54). **(7)** A report from China shows that environmental exposure to arsenic results in poor sperm quality in men (55). Similarly, a Korean study shows that male rodents exposed to arsenic show significantly poorer fertility (56), as well as poorer sperm quality. Estrogen is well known to be essential for sperm maturation (57). Therefore, lowered estrogen levels in men (owing to direct sequestration of estrogen by arsenic) could conceivably affect fertility and sperm quality.

We would like to point to some interesting reports of the binding of arsenic to estrogen receptors, ostensibly at the same binding site on the receptor which involves estrogen binding (40). We suggest that these reports are based on data, which may be subject to alternative interpretation. A perusal of the references cited above shows that the conclusion that arsenic binds to the estrogen receptor was based on competitive inhibition data indicating a K_i of 5

nM, and the likely role of cysteine residues at the estrogen-binding site (which could potentially bind to arsenic), but not on actual structural data directly demonstrating arsenic bound to estrogen receptor. We aver that inhibition of E2's binding to its receptor in the presence of ATO could result from E2's sequestration by ATO, rather than by the competitive binding of ATO to the estrogen receptor.

The possibility of arsenic's binding to hormone estrogen has never before been reported or mentioned in the literature, although arsenic has been called a poison (58), as well as a medicine (59).

Conclusions and future prospects:

Arsenic can physically interact and bind with estradiol. We believe that the data presented (and correlations drawn) in this work require more studies of the consequences of such binding, given the obvious health implications. The key factors determining what happens upon chronic exposure of human beings to arsenic would appear to be: (i) the quantum, and duration, of exposure, and (ii) the natural estrogen levels of those living in arsenic-contaminated areas. Those with relatively high estrogen levels could probably benefit from some of the positive effects of low-grade arsenic exposure, such as efficacy in wound-healing and certain types of amelioration of cancer, without being subject to the negative effects. On the other hand, those with low levels of estrogen would be likely to suffer the most from the effects of high-grade arsenic exposure. The correlations between poor nutrition and poor estrogen levels become especially relevant for countries with poorer populations.

References:

1. Chaurasia N, Mishra A, Pandey SK (2012) Fingerprint of arsenic contaminated water in India-A Review. J Forensic Res 3:172.
2. Mazumder DNG, Ghosh A, Majumdar KK, Ghosh N, Saha C, et al. (2010) Arsenic contamination of ground water and its health impact on population of district of Nadia, West Bengal, India. Indian Journal of Community Medicine: Official Publication of Indian Association of Preventive & Social Medicine 35: 331-338.
3. Farias SS, Casa VA, Vazquer C, Ferpozzi L, Pucc GN, et al. (2003) Natural contamination with arsenic and other trace elements in ground waters of Argentine Pampean Plain. Science of Total Environment 309: 187-199.
4. Nickson R, McArthur J, Burgess W, Ahmed KM, Ravenscroft P, et al. (1998) Arsenic poisoning of Bangladesh groundwater. Nature 395: 338-338.
5. Marshall G, Ferreccio C, Yuan Y, Bates MN, Steinmaus C, et al. (2007) Fifty-Year Study of Lung and Bladder Cancer Mortality in Chile Related to Arsenic in Drinking Water. Journal of the National Cancer Institute 99: 920-928.
6. Armienta MA, Rodriguez R, Aguayo A, Ceniceros N, Villaseñor G, et al. (1997) Arsenic contamination of groundwater at Zimapán, Mexiko. Hydrogeology Journal 5: 39-46.
7. Rahman M, Naidu R, Bhattacharya P (2009) Arsenic contamination in groundwater in the Southeast Asia region. Environmental Geochemistry and Health 31: 9-21.
8. Berg M, Tran HC, Nguyen TC, Pham HV, Schertenleib R, et al. (2001) Arsenic contamination of groundwater and drinking water in Vietnam: A Human health threat. Environmental Science & Technology 35: 2621-2626.
9. Welch AH, Westjohn DB, Helsel DR, Wanty RB (2000) Arsenic in ground water of the United States: Occurrence and geochemistry. Ground Water 38: 589-604.
10. Straif K, et al. (2009) A Review of Human Carcinogens- Part C: Metals, arsenic, dusts, and fibers. The Lancet Oncology 10: 453-454.
11. Saxe, J. K., Bowers, T. S., and Reid, K. R. (2006). Arsenic in environmental forensics: Contaminant Specific Guide, pp. 279–292. Academic Press, Burlington, MA.
12. Lindberg A-L, Kumar R, Goessler W, Thirumaran R, Gurzau E, et al. (2007) Metabolism of low-dose inorganic arsenic in a central european population: Influence of sex and genetic polymorphisms. Environmental Health Perspectives 115: 1081-

1086.

13. Nickson R, McArthur J, Burgess W, Ahmed KM, Ravenscroft P, et al. (1998) Arsenic poisoning of Bangladesh groundwater. Nature 395: 338-338.
14. Huq SMI, Joardar JC, Parvin S, Correll R, Naidu R (2006) Arsenic contamination in food-chain: Transfer of arsenic into food materials through groundwater irrigation. Journal of Health, Population, and Nutrition 24: 305-316.
15. Järup L, Pershagen G, Wall S (1989) Cumulative arsenic exposure and lung cancer in smelter workers: A dose-response study. American Journal of Industrial Medicine 15: 31-41.
16. Walsh LM, Sumner ME, Keeney DR (1977) Occurrence and distribution of arsenic in soils and plants. Environmental Health Perspectives 19: 67-71.
17. Hossain MF (2006) Arsenic contamination in Bangladesh—An overview. Agriculture, Ecosystems & Environment 113: 1-16
18. Moghaddam AH, Mulligan CN (2008) Leaching of heavy metals from chromated copper arsenate (CCA) treated wood after disposal. Waste Management 28: 628-637.
19. Khan BI, Jambeck J, Solo-Gabriele HM, Townsend TG, Cai Y (2006) Release of arsenic to the environment from CCA-Treated Wood: Part II – Leaching and Speciation during Disposal. Environmental science & technology 40: 994-999.
20. Vahter M (2002) Mechanisms of arsenic biotransformation. Toxicology 181–182: 211-217.Loffredo CA, Aposhian HV, Cebrian ME, Yamauchi H, Silbergeld EK (2003) Variability in human metabolism of arsenic. Environmental Research 92: 85-91.
21. Calderon RL, Hudgens E, Le XC, Schreinemachers D, Thomas DJ (1999) Excretion of arsenic in urine as a function of exposure to arsenic in drinking water. Environmental Health Perspectives 107: 663-667.
22. Loffredo CA, Aposhian HV, Cebrian ME, Yamauchi H, Silbergeld EK (2003) Variability in human metabolism of arsenic. Environmental Research 92: 85-91.
23. Bissen M, Frimmel FH (2003) Arsenic — a Review. Part I: Occurrence, toxicity, speciation, mobility. Acta hydrochimica et hydrobiologica 31: 9-18.
24. Lewis AS (2007) Organic versus inorganic arsenic in herbal kelp supplements. Environmental Health Perspectives 115: A575-A575.
25. Shen S, Li X-F, Cullen WR, Weinfeld M, Le XC (2013) Arsenic binding to proteins. Chemical Reviews 113: 7769-7792.
26. Crane PK, Lippmann F (1953) The effect of arsenate on aerobic phosphorylation. J

Biol Chem 201: 235-43

27. Naujokas MF, Anderson B, Ahsan H, Aposhian HV, Graziano JH, Thompson C, Suk WA (2013) The broad scope of health effects from chronic arsenic exposure: Update on a worldwide public health problem. Environ Health Perspect 121:295–302
28. Martinez VD, Vucic EA, Becker-Santos DD, Gil L, Lam WL (2011) Arsenic exposure and the induction of human cancers. Journal of Toxicology 2011: 13.
29. Kitchin KT (2001) Recent advances in arsenic carcinogenesis: Modes of action, animal model systems, and methylated arsenic metabolites. Toxicology and Applied Pharmacology 172: 249-261.
30. Liu Y, Hock JM, Sullivan C, Fang G, Cox AJ, et al. (2010) Activation of the p38 MAPK/Akt/ERK1/2 signal pathways is required for the protein stabilization of CDC6 and cyclin D1 in low-dose arsenite-induced cell proliferation. Journal of Cellular Biochemistry 111: 1546-1555.
31. Paul S, Banerjee N, Chatterjee A, Sau TJ, Das JK, et al. (2014) Arsenic-induced promoter hypomethylation and over-expression of ERCC2 reduces DNA repair capacity in humans by non-disjunction of the ERCC2-Cdk7 complex. Metallomics 6: 864-873.
32. Singh RD, Tiwari R, Khan H, Kumar A, Srivastava V (2015) Arsenic exposure causes epigenetic dysregulation of IL-8 expression leading to proneoplastic changes in kidney cells. Toxicology Letters 237: 1-10.
33. Okui T, Fujiwara Y (1986) Inhibition of human excision DNA repair by inorganic arsenic and the co-mutagenic effect in V79 Chinese hamster cells. Mutation Research/Genetic Toxicology 172: 69-76.
34. Andrew AS, Burgess JL, Meza MM, Demidenko E, Waugh MG, et al. (2006) Arsenic exposure is associated with decreased DNA repair in vitro and in individuals exposed to drinking water arsenic. Environmental Health Perspectives 114: 1193-1198.
35. Sykora P, Snow ET (2008) Modulation of DNA polymerase beta-dependent base excision repair in cultured human cells after low dose exposure to arsenite. Toxicology and Applied Pharmacology 228: 385-394.
36. Fischer JM, Robbins SB, Al-Zoughool M, Kannamkumarath SS, Stringer SL, et al. (2005) Co-mutagenic activity of arsenic and benzo[a]pyrene in mouse skin. Mutation Research/Genetic Toxicology and Environmental Mutagenesis 588: 35-46.
37. Li JH, Rossman TG (1991) Comutagenesis of Sodium Arsenite with Ultraviolet Radiation in Chinese Hamster V79 cells. Biology of Metals 4:197-200

38. Liu, S.X., Athar, M., Lippai, I., Waldren, C., Hei, T.K. (2001). Induction of Oxygen Radicals by Arsenic: Implications for Mechanism of Genotoxicity. Proc. Natl. Acad. Sci. USA 98: 1643 – 1648
39. Ahmad, S., Kitchin, K.T., Cullen, W.R. (2000). Arsenic species that cause release of iron from ferritin and generation of activated oxygen. Arch. Biochem. Biophys. 382: 195 – 202.
40. Stoica A, Pentecost E, Martin MB (2000) Effects of arsenite on estrogen receptor-alpha expression and activity in MCF-7 breast cancer cells. Endocrinology 141: 3595-3602.
41. Chatterjee A., Chatterji U. (2010). Arsenic abrogates the estrogen-signaling pathway in the rat uterus. Reproductive Biology and Endocrinology. 8: 80.
42. Watson WH, Yager JD (2007) Arsenic: Extension of its Endocrine Disruption Potential to Interference with Estrogen Receptor-Mediated Signaling. Toxicological Sciences 98: 1-4.
43. Smith AH, Marshall G, Yuan Y, Steinmaus C, Liaw J, et al. (2014) Rapid reduction in breast cancer mortality with inorganic arsenic in drinking water. EBioMedicine 1: 58-63.
44. Russo J, Hasan Lareef M, Balogh G, Guo S, Russo IH (2003) Estrogen and its metabolites are carcinogenic agents in human breast epithelial cells. The Journal of Steroid Biochemistry and Molecular Biology 87: 1-25.
45. Watanabe C, Inaoka T, Kadono T, Nagano M, Nakamura S, et al. (2001) Males in rural Bangladeshi communities are more susceptible to chronic arsenic poisoning than females: analyses based on urinary arsenic. Environmental Health Perspectives 109: 1265-1270.
46. Hess RA (2003) Estrogen in the adult male reproductive tract: A review. Reproductive Biology and Endocrinology: RB&E 1, 52-52
47. Sen J, Chaudhuri ABD (2007) Effect of arsenic on the onset of menarcheal age. Bulletin of Environmental Contamination and Toxicology 79: 293-296.
48. Bernstein L, Pike M, Ross R & Henderson B (1991) Age at menarche and estrogen concentrations of adult women. Cancer Causes & Control 2: 221- 225.
49. Reilly MP et al. (2014) Prepubertal exposure to arsenic(III) suppresses circulating Insulin-like Growth Factor-1 (IGF-1) delaying sexual maturation in female rats. Reproductive toxicology (Elmsford, N.Y.) 44: 41-49.

50. Yunus FM, Rahman MJ, Alam MZ, Hore SK, Rahman M (2014) Relationship between arsenic skin lesions and the age of natural menopause. BMC Public Health 14: 419-419.
51. Akram Z et al. (2010) Adverse effects of arsenic exposure on uterine function and structure in female rat. Experimental and Toxicologic Pathology 62: 451-459
52. Messinis IE (2006) Ovarian feedback, mechanism of action and possible clinical implications. Hum. Reprod. Update 12:557-571
53. Xu W et al. (2012) Environmental exposure to arsenic may reduce human semen quality: associations derived from a Chinese cross-sectional study. Environmental Health 11: 46
54. Chang SI, Jin B, Youn P, Park C, Park J-D, et al. (2007) Arsenic-induced toxicity and the protective role of ascorbic acid in mouse testis. Toxicology and Applied Pharmacology 218: 196-203.
55. Carreau S, Bouraima-Lelong H, Delalande C (2011) Estrogens in male germ cells. Spermatogenesis 1: 90-94.
56. Watson WH, Yager JD (2007) Arsenic: Extension of its endocrine-disruption potential to interference with estrogen receptor-mediated signaling. Toxicol. Sci. 98, 1-4 (2007).
57. Saha JC, Dikshit AK, Bandyopadhyay M, Saha KC (1999) A review of arsenic poisoning and its effects on human health. Critical Reviews in Environmental Science and Technology 29: 281-313.
58. Efferth T, Li PCH, Konkimalla VSB, Kaina B (2007) From traditional Chinese medicine to rational cancer therapy. Trends in Molecular Medicine 13, 353-361.
59. Deb D et al. (2013) Nutritional deficiency and arsenical manifestations: a perspective study in an arsenic-endemic region of West Bengal, India. Public Health Nutrition 16: 1644-1655.

Section C

Role of CHIP1 in 17-α-ethinyl estradiol induced MCF-7 cell proliferation and survival

C.1 Introduction

Cancer originating in breast tissue is termed as breast cancer. Breast cancer is one of leading cause of cancer deaths in women (1,2). Breast cancer is of two types: ductal carcinoma and lobular carcinoma. In ductal carcinoma, cancer develops in the lining of milk ducts. Lobular carcinoma develops in lobules of breast. Various risk factors are associated with higher incidence of breast cancer such as aging, alcohol abuse, breast tissue density, exposure to environmental carcinogens, race, genetics, height, hormone replacement therapy, obesity and occupation. It may be noted that some parts of this introduction have also been published in review form.

C.1.2 Risk factors associated with breast cancer

C.1.2.1 Aging

Age is a key risk factor in developing in malignancies. Risk of developing breast cancer increases with age. Approximately 80% percent of new breast cancer cases constitute by women older than age 50 (3). Cancer being a multifactor disease requires mutations in different regulatory factors. These mutations take years to accumulate and develop into full-blown cancer. Epigenetic changes at transcriptional level also contribute to breast cancer risk and prognosis (4).

C.1.2.2 Alcohol abuse

Heavy alcohol consumption has been linked to increased instances of breast cancer whereas in case of lower alcohol consumption the risk of developing breast cancer is dependent on the circulating plasma hormone levels. A study on low dose alcohol intake in postmenopausal women has demonstrated an increase in plasma levels of estrone sulphate and DHEAS after consuming 15-30 g alcohol every day (5). Folate supplementation is helpful in decreasing alcohol consumption associated breast cancer in postmenopausal women (6).

C.1.2.3 Breast tissue density

Breast tissue density is also a risk factor in developing breast cancer. The risk of developing breast cancer increases 4 to 6 fold in women having high breast tissue density. High breast density is also found to be associated with aggressive tumor characteristics (7). Breast tissue density is influenced by estrogen. Treatment with estrogen antagonist tamoxifen resulted in

decrease in breast tissue density in women earlier treated for unilateral breast cancer and reduced risk of relapse (8).

C.1.2.4 Exposure to environmental carcinogens

Exposure to environmental carcinogens is also an important risk factor in developing breast cancer. Agricultural pesticides and Industrial effluents such as DDT, organochlorine, polychlorinated biphenyls, polycyclic aromatic hydrocarbons have been implicated in increasing the breast cancer risk in women exposed to these pollutants (9). Chlorine is also implicated in increasing risk of breast cancer. A Greenpeace study report suggests chlorine and other industrial waste chemical to be the culprit behind the increasing breast cancer risk (10).

C.1.2.5 Race

There exists a complex and poorly defined relation between propensity of developing breast cancer and race. Different racial and ethnic groups have different propensity of developing breast cancer. Women belonging to white ethnicity are at greater risk of developing breast cancer than women of Asian decent (11). Similarly women of African decent have greater chances of developing triple negative breast cancers, where the tumors lack estrogen receptors, progesterone receptors and HER2 receptors (12). These triple negative cancers do not respond to drug regimes that block estrogen synthesis or estrogen receptors, like aromatase inhibitors or tamoxifen, or to HER-2 inhibitors lapantinib and trastuzumab. Jewish women of Eastern European decent carry mutations in BRCA genes and greater risk of developing breast cancer (13).

C.1.2.6 Genetics

Genetic also play a role in developing cancer. Genetic mutations are responsible in 5-10% of all breast cancer cases. Women carrying mutations of BRCA1 and BRCA2 have a 35-80% greater chance of developing breast cancer (14); also men carrying these mutations have higher risk of developing breast cancer (15). Mutations of PTEN and p53 are frequently found associated with increased risk of developing breast cancer (15).

C.1.2.7 Height

Several studies have shown that the risk of developing breast cancer has a positive correlation with person height. The hormones responsible for regulation of height may also stimulate breast and other tissue cells to grow abnormally and turn cancerous (16).

C.1.2.8 Hormone replacement therapy

Hormone replacement therapy (HRT) involves administration of a combination of synthetic estrogens, estrogen conjugates and progestins to reduce the symptoms of menopause (17). Along with the benefits of long term HRT has been associated increased risk of developing breast cancer. Epidemiological studies indicate a positive correlation between breast cancer risk and HRT with conjugated estrogens (18). Also many studies have reported that Progestins used in HRT induce breast epithelium proliferation, which may further add to the risk of developing breast cancer in patients undergoing long term HRT (19,20).

C.1.2.9 Obesity

Many studies have shown that obese postmenopausal women have a greater risk of developing breast cancer (21,22,23). The risk of breast cancer further increases in obese postmenopausal women with a family history of breast cancer (24).

C.1.2.10 Occupation

Women employed in occupations with high-level exposure to chemical carcinogens have a higher risk of developing breast cancer. A study involving postmenopausal women engaged in occupational category of craft, repair and precision production showed a threefold increase in breast cancer risk (25,26).

C.1.3 Role of estrogens in breast cancer

C.1.3.1 Estrogens:

Estrogens are steroid hormones secreted primarily from the ovaries and testes of females and males respectively. Estrogens are also synthesized from adrenal glands, adipose tissue, brain, liver and mammary glands of both the sexes (27). Estrogens play crucial role in normal physiology of both human genders.

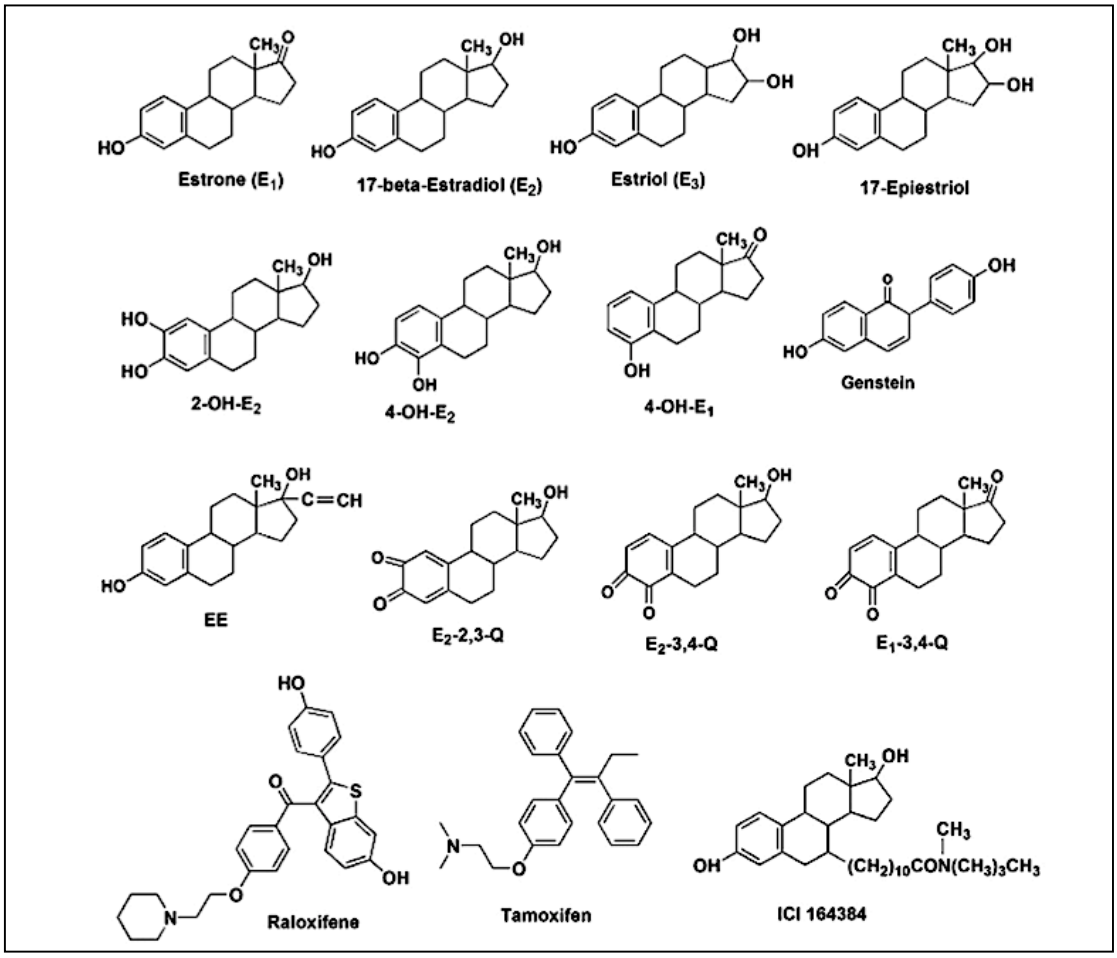

Figure C.1: The roles of estrogens, estrogen metabolites and selective estrogen receptor modulators (SERMs) in redox cycling of estrogens: 17-β Estradiol (17-β-E2) or (E2), estrone (E1) and estriol (E3) are natural female steriod hormones collectively called as estrogens and also present in male at low concentration. Genestein is a phytoestrogen, present in high amount in soybeans and in low amount in other legumes and act through ERα. Ethinylestradiol (EE) and 17-epiestriol are synthetic estrogens act via ERα and ERβ respectively. 2-OH-estradiol (2-OH- E2), 4-OH-estradiol (4-OH-E2) are hydroxylated products of 17-β-E2. Enzymes involve in hydroxylation reaction are CYP1A1 (mainly responsible for hydoxylation at C_2 position) and CYP1B1 (responsible for hydoxylation at both C_2 and C_4 position). 4-OH-estrone (4-OH-E1) is hydroxylated product of estrone (E1), enzyme involve in hydroxylation reaction is CYP1B1. 2,3-Estradiol quinone (2,3-E2-Q) and 3,4-estradiol quinone (3,4-E2-Q) are oxidative metabolites of 17-β-E2 and 3,4-estrone quinone (3,4-E1-Q) are oxidative metabolites of E1 produced by oxidizing enzyme via an intermediate semiquinone form. Raloxifene, tamoxifene and ICI 164384 are selective estrogen receptor modulators (SERMs) and antagonist to estrogen.

However, physiological levels of estrogens are significantly higher in females of reproductive age because of high-level generation of aromatase, the enzyme responsible for conversion of testosterone to estrogens (28).

There is increasing body of evidences indicating role of estrogen in carcinogenesis. Estrogens are positively correlated with human breast cancer (29). The exact mode of estrogen-induced carcinogenesis is unclear. Three possible modes of estrogen induced carcinogenesis have been proposed: promotion of growth and proliferation by receptor mediated hormonal activity, free radical mediated genotoxic stress resulting from estrogen metabolism by cytochrome P450 complex and estrogens induced aneuploidy by inhibiting tubulin polymerization to microtubules (mitotic inhibition and aneuploidy induction by naturally occurring and synthetic estrogens in Chinese hamster ovary (CHO) cells *in vitro*). Figure C.1 depicts various naturally occurring and synthetic estrogens.

C.1.3.2 Estrogen signaling pathways

C.1.3.2.1 Estrogen Receptor: Estrogen signaling is effected by estrogen receptors (ERs) (30). Estrogen receptor-α (ERα) and estrogen receptor-β (ERβ) transduce estrogen mediated cellular signaling. ERs are members of nuclear receptor super family of transcription factors. ERs contain three distinct domains N-terminal domain containing activation function (AF) domains 1 and 2 called AF1 and AF2, central DNA-binding domain (CBD) and C-terminal ligand-binding domain (LBD). The N-terminal domain is most variable domain with variable sequence and length in ERs. It also contains constitutively activated AF1 domain. The central DBD is most conserved domain and is involved in DNA recognition and binding. The –C terminal LBD is multifunctional ligand binding domain. The LBD domain also contains ligand dependent AF2. AF domains engage co-regulatory protein complexes to DNA bound ERs (31).

C.1.3.2 Modes of estrogen signaling

Estrogen binding to ERs starts a ligand dependent signaling. The cellular response to estrogen signaling depends on cell type more particularly the kind of estrogen response elements (ERE) in the promoters of estrogen responsive genes and composition of co-regulatory proteins in a given cell. Estrogens can demonstrate genomic (involvement of gene activation) and non-genomic (without involvement of gene activation) signaling (32,33).

C.1.3.3 Genomic actions of estrogens The genomic pathways of estrogen signaling involve diffusion of estrogen across cell membrane and binding to cytosolic ERs. ERs are present in differential quantity in cell membrane, cytosol, nucleus and mitochondria of various cell types and thereby exert their cell type specific biological functions. ERs present in cytosol and nucleus are termed as class I nuclear steroid receptors (32). Estrogens bind to specific ERs present in cytoplasm. In absence of estrogens, cytosolic ERs are kept in inactive state by heat shock proteins (HSP-90, HSP-56). Binding of estrogen activates the ER by releasing the bound HSPs and exposing the nucleus localization sequence (NLS). Resulting ER-estrogen complex translocates to nucleus and can interact with estrogen target genes in two distinct methods: Firstly, ER-estrogen complex directly interacts with DNA sequences within the ERE in the promoter region of the estrogen responsive genes and consequently activate or inhibit the transcription of these genes (33,34). Secondly, estrogens alter the expression of target genes devoid of any ERE with the aid of transcription factors such as nuclear factor kappa-B (NF-κB) (35), AP-1 (36), SP-1 (37) and GATA (38), that binds with their specific respective sequence elements (e.g. NF-kB binds with NF-kB site) in the promoter region of the responsible genes giving rise to diversity and versatility of estrogen signaling. Collectively both of these signaling are termed as genomic mode of action of estrogens depicted in figure C.2. Genomic mode of action of estrogen takes from a few minutes to hours to show its effects.

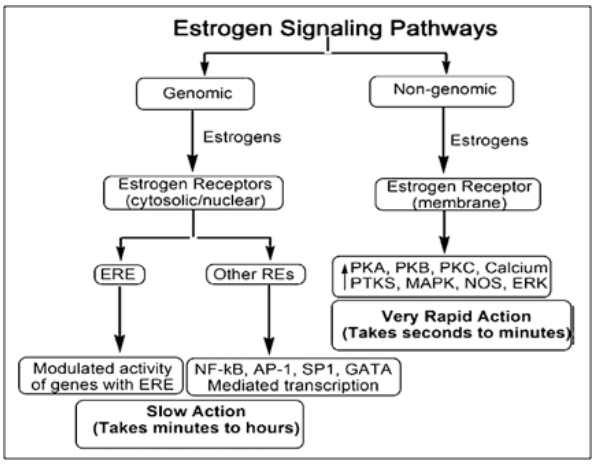

Figure C.2: Genomic and non-genomic actions of estrogens. The genomic action involve cytosolic estrogen receptors and non genomic action involves membrane associated estrogen receptors

C.1.3.4 Non-genomic actions of estrogens

Membrane ERs are involved in non-genomic estrogen signaling. The non-genomic actions only take a couple of minutes without the involvement of any gene activation. The Membrane ERs (mER) were first discovered in hepatocyte plasma membrane and endometrial cells by Pietras *et al* (39,40). mER have also been reported in the breast cancer cell lines MCF-7 and MDAMB-231 (41) T47D cells (42), Chinese hamster ovary (CHO) cells (43), pituitary tumor cells (44), endothelial cells (45) and other cell lines. There are sufficient evidences that ERs can associate with plasma membrane in various types of cells. ERs associate with caveolae and large protein complexes of the membrane in various cell types (46). Of the two types of ERs, ERα activation of metabotropic glutamate receptor (mGluR) is dependent on caveolin 1 (CAV 1) whereas caveolin 3 (CAV 3) is necessary for ERα and ERβ activation of mGluR2/ 3 (47). While S-palmitoylation of ERs accelerates their association with plasma membrane and CAV 1 (40), preferential palmitoylation of ERα variant (46 kDa) has also been reported in plasma membrane (48). Of note, palmitylation helps in anchoring a protein into the plasma membrane. Another membrane protein striatin serves as a scaffold for ERα–G protein complex and mediates the ERα translocation (49). Of note, G-proteins are small GTP binding proteins. An adapter protein (MNAR) is also found to be required for these membrane estrogen actions (50). The ERs thus found localized in the plasma membrane, also respond to the non-genomic actions of estrogens (51) as depicted in figure C.2.

C.1.4 Role of ubiquitin proteasome system (UPS) in estrogen signaling

The ubiquitin-proteasome system (UPS) maintains the normal cell homeostasis by targeting nearly 90% of the proteins found in the cell for degradation at various points of time depending upon cellular physiology (52). UPS is essential for estrogen signaling. Inhibition of proteasome with proteasome inhibitor MG132 also inhibits the estrogen signaling (53).

C.1.4.1 Components of UPS

Ubiquitin is a highly conserved protein consisting of 76 amino acid residues. Covalent attachment of poly-ubiquitin chains to a protein marks the protein for proteasomal degradation (54). E1, E2, E3 ligases and 26S proteasome are the functional components of UPS described in Figure C.3. E1 ubiquitin ligase acts as ubiquitin activating enzyme utilizing ATP. Activated ubiquitin is transferred to ubiquitin conjugating enzyme or E2. E3 complete the substrate protein ubiquitination by transferring ubiquitin from E2 to substrate. The gating

proteins in 26S proteasome detect the polyubiqutinated proteins and subject them to proteasomal degradation (54).

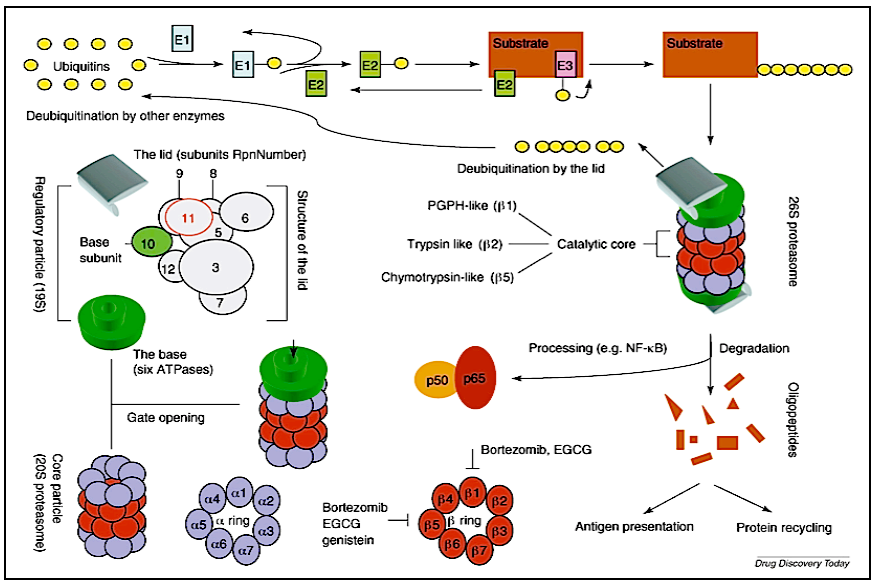

Figure C.3: Components of the ubiquitin-proteasome system (53). Ubiquitin-proteasome system consists of E1, E2, E3 ligases and 26S proteasome are the functional components of UPS. E1 ubiquitin ligase acts as ubiquitin activating enzyme utilizing ATP.

C.1.4.2 Role of UPS in cancer cell survival

UPS plays a very important role in regulatory mechanisms for stability and function of the proteome including ERs and other steroid receptors. Estrogen binding to ER not only induces cystoplasmic ERs to translocate to nucleus and modulates the activity of genes containing ERE in their promoter but also shortly followed by UPS mediated degradation (53). ERs while initiation of transcription gets ubiquitinated which target them to nuclear proteasomal degradation. Active proteasomal machinery is essential in not only for degradation of ERs but also for ERs mediated transcription which is inhibited when cells are treated with proteasome inhibiter MG132 (55). UPS also plays important role unfolded protein response by degradation of unfolded proteins accumulated in endoplasmic reticulum resulting in cell survival. In unfolded protein response; accumulation of unfolded proteins in endoplasmic reticulum elicits the endoplasmic reticulum associated degradation of the unfolded proteins. The unfolded proteins are ubiquitnated and subjected to proteasome-mediated degradation (56).

C.1.5.1 Role of CHIP in breast cancer:

CHIP is a chaperone dependent E3 ubiquitin ligase belonging to tertracopeptide repeats family (TPR) of proteins. Ballinger *et al* discovered CHIP in the year 1998 (57). CHIP gene is located on chromosome 16p13.3 encoding a 35 kDa protein. The primary structure consists of three distinct domains: N-terminal TPR domain, an internal charged domain and a C-terminal U-box domain as depicted in figure C.4. High levels of CHIP1 expression are observed in tissues such as brain, skeletal muscles and cardiac muscles with high metabolic activity and proteasome mediated protein turnover (57). CHIP1 acts as a prosurvival protein by activating Heat shock transcription factor1 (HSF1) under stress conditions (59).

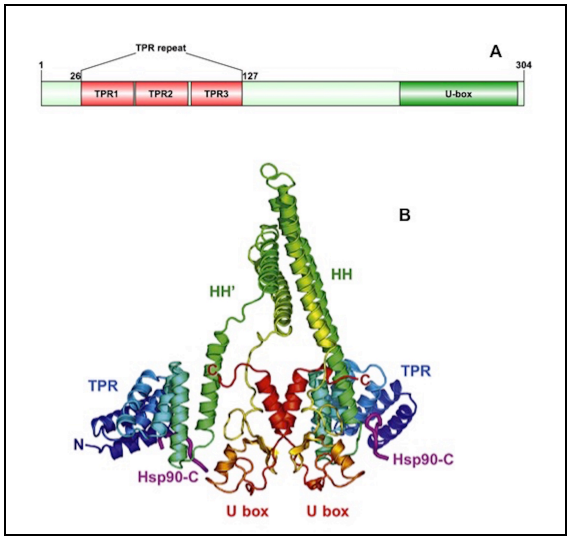

Figure C.4: Domain structure of CHIP1: C.4.A: Linear representation of functional domains across the polypeptide length. **C.4.B:** Functional dimer of CHIP1 (58)

CHIP1 can act as tumor suppressor or tumor promoter depending upon the cell type and physiological state of cells. CHIP1 functions as upstream regulator of proteins likes ERα, HIF1α and p53. These genes are involved in cancer cell survival (60-62). On the contrary CHIP has been implicated in tumorigenesis of glioma (63).

C.1.5.2 Functions of CHIP1

CHIP1 functions mainly as a tumor suppressor protein (64), although it is implicated as a oncogene in gliomas in mice and human (65,66). Research in field of CHIP1 has discovered a large no of proteins that are targeted to turnover by CHIP1 further signifying its role in cellular physiology and pathophysiology. CHIP1 is known to act as E3 ubiquitin ligase for ErbB2/Neu (64), ER-α (60), GR (65), tau (66,67), MEKK2 (68) and several other key proteins involved in carcinogenesis. CHIP1 is also demonstrated to degrade mutant keratins

(69) and stabilize malin which is an aggregation prone E3 ubiquitin ligase associated with Lafora disease (65,66).

C.1.5.3 Regulation of CHIP1

Regulation of CHIP1 has not been studied exhaustively. There are some studies that confirm that CHIP1 is regulated at transcriptional as well post-transcriptional level. CHIP1 is induced under various cell stress conditions (59). Elevated levels of CHIP1 mRNA are observed in cells exposed to endoplasmic, oxidative and proteasomal stress. The subsequent CHIP1 protein expression confers a protection against the stress induced cell death (59). Induction of CHIP1 protein expression helps the cells to adept to the stress conditions. CHIP1 mRNA synthesis is also induced in the cells expressing expanded polyQ (73). However levels of CHIP1 mRNA and protein are considerably lowered in breast, colorectal and gastric cancer Similar to transcriptional regulation there are fewer studies on post-transcriptional regulation of CHIP1 (74). Post-transcriptional regulation of CHIP1 was first observed in studies pertaining to osteoblast differentiation in which miR-764-5P represses the translation of CHIP1 by targeting the 3′ UTR region of CHIP1 transcript, that suggests that miRNA might regulate CHIP1 in response to external and internal stimuli (75).

C.1.6 Role of Poly (ADP-Ribose) Polymerase 1 in breast cancer

Poly (ADP-Ribose) Polymerase 1 (PARP1) is nuclear tumor suppressor protein involved in the repair of the DNA single strand breaks by base excision repair (BER). PARP1 is a member of PARP family consisting of 18 members. PARP1 is the most prominent and well-studied member of the family. PARP1 is 113 kDa protein consisting of six domains: Two amino terminal Zn finger domain for DNA binding followed by domain B required for nuclear localization followed by domain D consisting of BRCT required for auto modification activity and a carboxyl terminal domain F which has active site (AS) domain. However, functions of domains C and E are unknown. PARP1 has additional role of promotion of tumor through NF-κB activation. Inhibition of PARP1 results in inhibition of sporadic tumors with functional DNA repair machinery. Various studies indicate the potential benefit of PARP1 inhibition in HER2 positive breast cancer, Ewing's sarcoma, neuroblastoma, and pancreatic cancer (76-79). Results from all these studies point towards the functions of PARP1 other DNA repair activity. Figure C.5 describes the schematic representation of PARP1 domains.

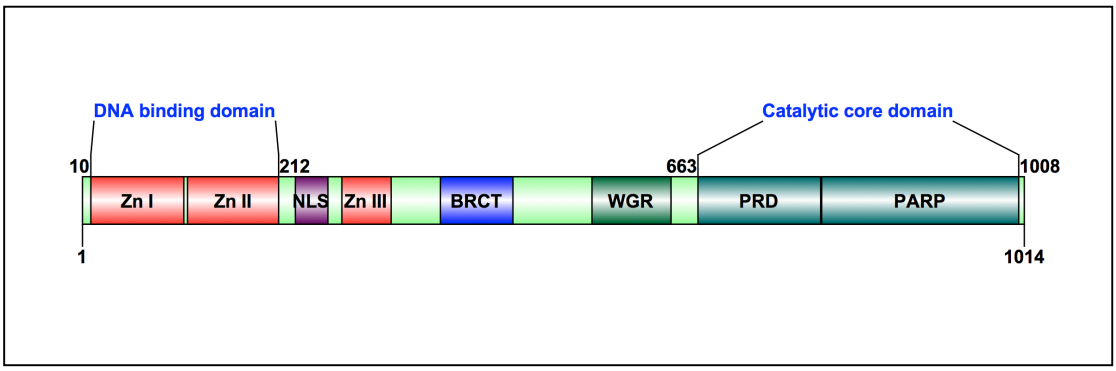

Figure C.5: Schematic representation of PARP1 domains: Domain A or DNA binding domain consisting of two zinc finger domains which assist in DNA binding, Domain B is consist of a nuclear localization sequence, Domain D consist of a auto modification domain BRCT which act as a site for covalent auto-poly (ADP-ribosyl)ation and a domain F or catalytic core domain is catalytic domain consisting of active site for PARP1.

C.1.6.1 PARP1 promotes NF-κB dependent inflammation

The NF-κB signaling is frequently found to be constitutively active in breast cancers. PARP1 regulates the NF-κB activation with multiple mechanisms. PARP1 upregulates the expression of NF-κB by interacting with histone acetyltransferase and CREB-binding protein (80,81). The activation of PARP1 has a variable effect on NF-κB activation depending upon cell type (82).

C.1.6.2 Functions of Poly (ADP-Ribose) Polymerase

PARP1 is activated by single strand DNA breaks. PARP1 forms homodimers or heterodimers with PARP2 at the site of nicks in DNA and synthesize polymers of ADP-ribose on itself and other DNA associated proteins. PARP-1 and PARP-2 form homo dimers and hetero dimers at DNA breaks catalyzing the formation of long PAR chains covalently attached to PARP-1 itself (auto modification) or other nuclear proteins like histone H1 hetero modification adjacent to the DNA breaks. These negatively charged polymers form a scaffold for base excision repair proteins when PARP1 is inhibited the replication fork stalls at the DNA breaks (83).

In addition to the function of single strand nick repair; PARP1 serves a variety of functions in cellular physiology. Several studies indicate the role of PARP1 in inflammation, immunity and cancer. PARP1 also displays an up regulation of its target genes by enhancing RNA polymerase activity in a sequence specific manner (84). PARP1 modulates the expression of genes involved in tumourigenesis, angiogenesis and metastasis by activating ERK signaling. Also ERK2 can interact with PARP1 and activate it. The resulting ERK2-PARP1 complex

shows enhanced pERK2 mediated phosphorylation of target transcription factors. Inhibition of PARP1 leads to decreased phosphorylation of ERK2 target proteins (86). PARP1 has an important role in cell division. PARP1 synthesizes PAR; which is involved in spindle assembly (87). PARP1 PARylates centromere and centrosome proteins (88). Activity of PARP1 also plays a role in early mitotic checkpoint by interacting with CHFR. CHFR is an E3 ubiquitin ligase regulating early mitotic checkpoint (89).

C.1.7 Rationale of present study

CHIP1 has been demonstrated to regulate broad spectrum of biological processes. CHIP1 predominantly acts as a tumor suppressor protein and it regulates the cellular levels of a large number of target proteins. But regulation of cellular levels of CHIP1 is poorly understood. Present study addresses the modulation of CHIP1 expression and overall levels under physiologically relevant conditions and overall effects on cell survival. In the present study we describe the turnover of CHIP1 induced by physiological levels of 17α-ethinylestradiol (17αEE) in a time dependent manner. Off note, 17αEE is a synthetic estrogen and used as a major component of contraceptive pills. Use of high level of 17αEE is related to breast and endometrial cancers. As an E3 ubiquitin ligase CHIP1 is very important molecule because these ligases are limiting factors in UPS (107).

We have used western blotting to study the cellular localization and nuclear translocation of CHIP1 after treating MCF-7 cells with 17αEE. We have discovered that CHIP1 translocates to nucleus following 17αEE treatment. Coimmunoprecipitation studies confirm binding interaction between CHIP1 and PARP1. In the present study we also examined the effects of 17αEE on the expression of PARP1.

C.2.1 Cell line

MCF-7 breast cancer cell line was procured from ATCC. As indicated by ATCC, the MCF-7 breast cancer cell line isolated from a pleural effusion of a 69-years-old Caucasian women with breast adenocarcinoma. MCF-7 cell line is one of the most widely used cell line, because it has retained some of the characteristics of differentiated mammary epithelial cells as these express cytosolic ERs and can be stimulated to form domes. These cells have a population doubling time of 29 hours (108).

C.2.2 Materials

Minimum essential medium, charcol-dextran treated fetal bovine serum (FBS), L- glutamine, sodium pyruvate, NP-40, 17α-ethinylestradiol (17αEE), Anti CHIP1 antibody, anti HSP90 antibody, anti β-actin antibody, CHIP1 siRNA, control siRNA and NTER nanopeptide based transfection kit were purchased from Sigma Chemical (St. Louis, USA). Anti PARP-1 and

Anti Phospho-AKT1-S476 antibodies were purchased from Abcam. MG132 was purchased from Calbiochem. Sterile cell culture flasks and plates were obtained from Corning. Antibiotic-antimycotic, FBS and insulin were purchased from HiMedia. RNA isolation kit was purchase from Zymo research, iScript cDNA synthesis kit was purchased from Bio-Rad laboratories, and QT-PCR strips were purchased from Axygen.

C.2.3 Methods

C.2.3.1 *In-vitro* culture of MCF-7 breast cancer cell

MCF-7 cells were grown in minimum essential medium (MEM) supplemented with 5% FBS, 2 mM L glutamine, 0.01 mg/ml insulin, 1 mM sodium pyruvate, 1U/ml antibiotic-antimycotic and 1.5g/L sodium bicarbonate. For experimentation the culture medium was replaced by phenol red free MEM supplemented with 2% serum (charcoal-dextran treated), 1U/ml antibiotic-antimycotic and 1.5g/L sodium bicarbonate.

C.2.3.2 Small inhibitory RNA based transient knockdown assay

Small inhibitory RNA (siRNA) based transient knockdown was done using siRNA against CHIP1.

(i) Preparation of nanoparticle formation solution

N-TER peptide and 5µM siRNA working stock were thawed at room temperature for nearly 10 minutes. Vortex and spin down the contents. Nanoparticle formation solution (NFS) was prepared by adding the contents listed in table:

Reagent	siRNA	N-TER peptide
5uM siRNA	5.99 µL	----
N-TER peptide	-----	3.69µL
SiRNA dilution Buffer	17.07µL	----
Water	-----	19.38µL
Total	23.08µL	23.08µL

1. MCF-7 breast cancer cells were seeded at a seeding density of $2.4x10^5$ in 35 mm plates. Cells were washed with experimental media upon reaching 60-70% confluence.
2. Incubated the cells for 12 hours at 37 °C in experimental medium to acclimatized cells to serum deprivation during transfection.

3. Prepared serum free transfection medium as by diluting 46.15 µl of target siRNA nanoparticle forming solution into 1453.85 µl of serum free medium.
4. Cells were incubated for 4-6 hours at 37 °C with transfection medium.
5. siRNA containing media was replaced with normal experimental media and incubated for 12 hours at 37 °C prior to treating with 17αEE.
6. Transfected cells were incubated with 17αEE for 24 hours at 37 °C and subjected to MTT assay as described earlier.

C.2.3.3 QT-PCR

QT-PCR was done to assess the levels of CHIP1 mRNA at various time points after treatment of MCF-7 breast cancer cells with 17αEE on Eppendorf Reaplex Mastercycler. Procedure for QT-PCR is described below.

(i) Isolation of Total RNA

Total RNA was isolated from the MCF-7 breast cancer cells following treatment with 17αEE using Zymo Research's Mini RNA isolation II kit. Detailed procedure for total RNA is described below.

1. Experimental media was removed and cells were washed with ice cold PBS followed by addition of 600 µl of ZR RNA Buffer and scrapped with a cell scrapper to enhance cell detachment and homogenization.
2. Transferred the sample in ZR RNA Buffer from step 1 into a Zymo-Spin Column.
3. Spun in a micro centrifuge at 10,000 rpm to facilitate binding of RNA to membrane.
4. Added 350 µl RNA Wash Buffer to the column and centrifuged at 10,000 rpm for 1 minute. Discarded the flow-through.
5. Repeated step 4.
6. Transferred the column to an RNase-free 1.5 ml microcentrifuge tube.
7. Added 50 µl DNase/RNase-Free water directly to the membrane of the column, and, after 2 minutes, centrifuged at 10,000 rpm for 1 minute to elute the RNA.
8. Eluted RNA was quantified and stored at -80 °C till further use.

(ii) cDNA synthesis

cDNA was prepared from 1µg of RNA isolated from MCF-7 breast cancer cells using Bio-Rad's iScript cDNA synthesis kit (170-8897). The following procedure was followed:

Component	Volume
Nuclease free water	Variable
5X iScript Select Reaction Mix	4 µl
Oligo dT	2 µl
RNA template	1µg
Reverse Transcriptase	1µl
Total Volume	**20 µl**

The above components were mixed in 1.5 ml eppendorf tube and incubated at 42 °C for 60 minutes. The reaction was terminated by incubating at 85 °C for 5 minutes. The cDNA formed was stored at -80 °C.

(iii) QT-PCR

cDNA obtained from cDNA synthesis reaction was diluted 100 fold with molecular biology grade water. Qt-PCR was done using 5x HOT FIREPol EvaGreen® qPCR Mix Plus (ROX) from Solis Biodyne according to manufacturer's protocol.

Composition of Master mix:

Component	Initial concentration	Volume Taken	Final Concentration
5x HOT FIREPol EvaGreen® qPCR Mix Plus (ROX)	5X	2µl	1X
FW Primer	1 µM	2.5 µl	250 nM
RW Primer	1 µM	2.5 µl	250 nM
Template		2.5 µl	1-50 ng/µl
H_2O		0.5 µl	
Total		**10 µl**	

QT-PCR Program:

Initial denaturation : 95 °C for 5 minutes

Denaturation: 95 °C for 15 seconds

Annealing: For CHIP1 and β-actin: 56.7 °C for 20 seconds

Extension: 72 °C for 20 seconds.

Number of cycles: 40.

C.2.3.4 Western Blotting to detect time dependent modulation of proteins of interest:

(i) Preparation of cell lysate:

1. MCF-7 breast cancer cells were harvested by trypsanization and cells were pelleted at 3000 RPM for five minutes.
2. Resuspended the cell pellet in 1 ml of ice cold PBS with help of pipette.
3. Cell suspension was transferred to 1.5 ml microcentrifuge tube and centrifuged at 3000 RPM for five minutes in a centrifuge pre-cooled at 4 °C.
4. Supernatant was discarded and step 3 was repeated twice.
5. Discarded the supernatant and added 100 µl of chilled lysis buffer (50 mM HEPES (pH 7.5), 1 mM DTT, 150 mM NaCl, 1 mM EDTA, 0.1% Tween 20, 10% glycerol, 10 mM β-glycerophosphate, 1 mM NaF, 0.1 mM sodium orthovanadate, 10 µg/ml leupeptin, 10 µg/ml aprotinin, and 0.1 mM PMSF) to the cell pellet.
6. Cell pellet was vortexed vigorously for 10 seconds and placed in ice. This process was repeated every five minutes for total duration of 30 minutes. Followed by centrifugation at 13,000 RPM for 15 minutes at 4 °C.
7. Supernatant was collected and used for protein measurements and western blotting.
8. Supernatant was stored -80 °C till further use.

(ii) SDS PAGE and protein transfer

Depending upon the experiment 30-100 µg of total protein subjected to SDS polyacrylamide gel electrophoresis and transferred to PVDF membrane using a semi-dry transfer apparatus. Following blocking with 3-5% nonfat dry milk/BSA for 1h at room temperature (RT), the membranes incubated with 1st antibody at RT for 3 hours or overnight (O/N) at 4 °C (the incubation time depends upon the expression level of the protein of interest). The following antibodies were used: Following washing with the Tween20-Tris buffer saline (TTBS) buffer the membranes then will be incubated in diluted (1:5000 to 1: 10000) HRP linked (conjugated) 2nd antibody for 60 min at RT. The protein bands detected using ECL Western blotting detection kit and exposing the membrane to X-Ray film.

Following molecules were detected by Western blotting technique:

Molecule	% of gel used	Amount of protein loaded	Blocking conditions	1st antibody treatment	2nd antibody treatment	ECL developing
CHIP1	10	50 µg	5% non fat dry milk in TTBS for 1 hr	1:3000 in TTBS O/N treatment	anti-rabbit HRP-conjugated 1:5000 in TTBS, for 1 hr	30 sec exposure with film
PARP1	8	50 µg	3% BSA in TTBS for 1 hr.	1:3000 in TTBS O/N treatment	anti-rabbit HRP-conjugated 1:5000 in TTBS, for 1 hr	10 min exposure with film
AKT-S473	10	50 µg	5% non fat dry milk in TTBS for 1 hr	1:3000 in TTBS O/N treatment	anti-mouse HRP-conjugated, 1:5000 in TTBS, for 1 hr	10 min exposure with film
β-actin	10	50 µg	5% non fat dry milk in TTBS for 1 hr	1:5000 in TTBS 3 hours treatment	anti-mouse HRP-conjugated, 1:5000 in TTBS, for 1 hr	20 seconds exposure with film
HSP90	8	50 µg	5% non fat dry milk in TTBS for 1 hr	1:3000 in TTBS O/N treatment	anti-mouse HRP-conjugated, 1:5000 in TTBS, for 1 hr	2 min exposure with film

C.2.3.5 Co-immunoprecipitation

MCF-7 breast cancer cells were treated with 10 nM 17αEE for 0, 1 hours, 3 hours, 10 hours and 30 hours before extraction. Whole cell extracts were prepared using modified RIPA buffer (50 mM Tris, pH 7.4, 1% NP-40, 150 mM NaCl, and 1.0 mM EDTA) for 60 min on

ice. Insoluble material was removed by centrifugation at 21,000 *g* for 10 min. The supernatant was used as the extract for the immunoprecipitation experiments. In brief, 10 µg anti–STUB1 antibody were added to pre cleared, whole cell extracts (300 µg diluted 10-fold in 10 mM Tris-HCl (pH 7.9), 20 mM HEPES (pH 7.9), 8% glycerol, 45 mM KCl, 8 mM $MgCl_2$, 5 mM $(NH_4)_2SO_4$, 2% polyethylene glycol, 4.5 mM β-mercaptoethanol, 0.05 mM EDTA, and 0.025% sodium lauryl sarcrosine) and incubated for 2 h at 4 °C. Protein G–Sepharose (150 µl of a 50% solution; GE Healthcare) was added, and the mixture was incubated for an additional 2 h at 4 °C. The beads were washed five times with five volumes of IP dilution buffer. Bound proteins were recovered by boiling the washed beads in SDS sample buffer. The eluted proteins were separated by 10% SDS-PAGE and probed for PARP1 by using anti-PARP1 antibody.

C.2.3.6 Nuclear localization Analysis

MCF-7 breast cancer cells were seeded into 90 mm cell culture plates in MEM supplemented with 10% FBS, 2 mM L-glutamine, 0.01 mg/ml insulin, 1 mM sodium pyruvate, 1U/ml antibiotic-antimycotic and 1.5 g/L sodium bicarbonate and incubated for 24 hours in humidified incubator with 5% CO_2. Cells were washed with 1X PBS to remove serum and phenol red. Cells were further incubated for 24 hours in experimental media to acclimatize the cells to low serum concentration and dissipate any residual estrogenic activity of phenol red/serum. Cells were treated with 17αEE (10 nM) for different time points and were further processed to prepare cytosolic and nuclear extracts. To prepare cytosolic extracts post 17αEE treatment; the cells were washed twice with ice cold PBS to remove traces of cell culture media components and kept on ice. Added 500 µl of cytosolic extraction buffer (10 mM HEPES, 1.5 mM $MgCl_2$, 10 mM KCl, 0.5 mM DTT, 0.05% NP40 pH 7.9) and cells were scrapped with a cell scrapper and kept on ice for 10 minutes. Resulting mixture was collected and centrifuged for 10 minutes at 4 °C at 3000 rpm. Supernatant or cytosolic extract was collected in a sterile tube, quantified and stored at -80 °C till further use. Remaining pellet was washed twice with ice cold PBS. Resuspend pellet in 374 µl of nuclear extraction buffer (5 mM HEPES, 1.5 mM $MgCl_2$, 0.2 mM EDTA, 0.5 mM DTT, 26% glycerol (v/v), pH 7.9) and added 26 µl of 4.6 M NaCl. Homogenize the resuspended pellet with 20 full strokes in Dounce homogenizer on ice and incubated on ice for 30 minutes. Centrifuge at 24,000 g for 20 minutes at 4 °C. Supernatant containing the nuclear proteins was collected, quantified and stored at -80 °C till further use.

C.3 Results and discussion

C.3.1 CHIP1 protein but not mRNA levels are modulated by 17-α-ethinylestradiol

The serum starved MCF-7 breast cancer cells were treated with 17αEE and were harvested at time points of 0, 1, 3, 10, 30 hours respectively; for total cellular protein and total cell RNA respectively. CHIP1 was found to be regulated at protein levels by 17αEE. CHIP1 levels decrease in a time dependent manner following treatment with. CHIP1 is induced by cell stress. The experimental media contained only 2% charcol-dextran treated serum, creating a condition of serum and growth factor deprivation for MCF-7 breast cancer cells. These MCF-7 breast cancer cells upon treatment with 17αEE showed time dependent decrease in CHIP1 levels as shown in figure C.6.

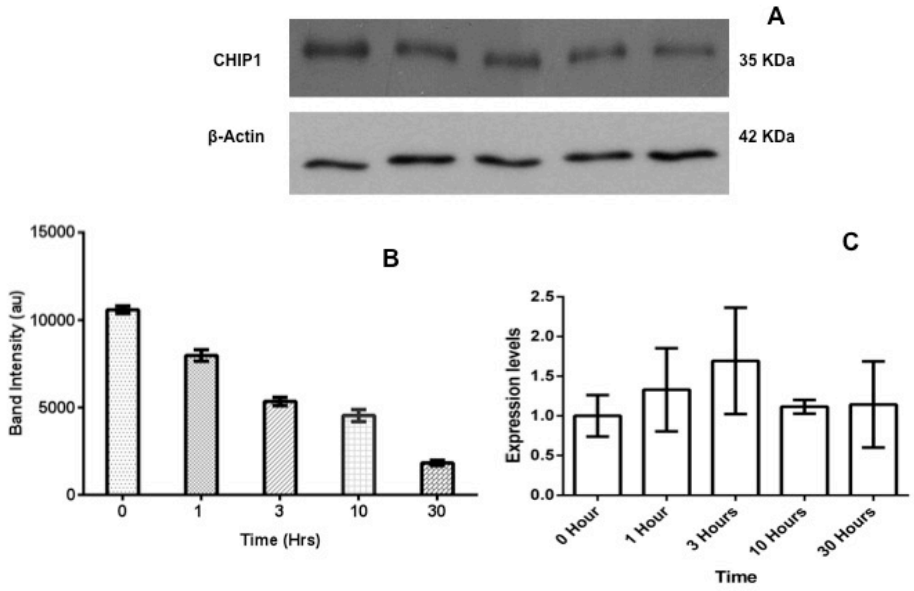

Figure C.6 CHIP1 modulation by 17-α-ethinylestradiol. **C.6.A:** CHIP1 expression levels detection: 50 μg of total cellular protein was loaded onto 10% denaturing SDS-PAGE. The resolved proteins were transferred onto PVDF membrane and probed with anti-CHIP1 antibody. **C.6.B:** ImageJ quantification of CHIP1 at different time points.**C.6.C:** Relative quantification of CHIP1 mRNA expression in MCF-7 cells treated with 17-α-ethinylestradiol. Data are presented as mean ± s.d. of triplicate samples and are representative of three independent experiments

Modulation of CHIP1 may have manifold effects on cell physiology. E3 ubiquitin ligases are the scarce resource in the cells and are key controller to proteasome mediated protein degradation (105). 17αEE targets CHIP1 to degradation. In experimental settings when cell culture media is changed from the one containing 5% FBS to 2% charcol-dextran treated serum the cells get stressed and expression of CHIP1 increases to assist the cells to cope up with the change in cellular environment. The adeptogenic and stress induced expression of CHIP1 is occurs during cell stress conditions. The cytoprotective effects of estrogens are also thoroughly studied. Estrogens can decrease the cell stress in many ways. Estrogens enhance the cell membrane integrity and act as cytoprotective agent at nanomolar concentrations by enhancing the redox environment of the cytoplasm (110). Estrogens also modulate the expression of genes that lead to cell proliferation and migration.

Here treating MCF-7 cells with 17αEE results in decrease in the cellular levels of CHIP1 in a time dependent manner suggesting that 17αEE stabilizes the cell environment leads to decrease in cell stress as a result of which CHIP1 levels start to decrease with time. However there is another possibility that 17αEE might mechanistically increase the auto ubiqutination of CHIP1 resulting in its proteasome mediated degradation or 17αEE may enhance the bulk autophagy of stress induced proteins resulting in their rapid degradation in the cells.

C.3.2 Effect of 17α-ethinylestradiol on AKT-S476 phosphorylation

Effect of 17αEE on phosphorylation of AKT-s476 studied using Western blotting as shown in figure C.7. 17αEE modulates the levels of phosphorylated AKT-S476 and in a time dependent manner. AKT1-S476 phosphorylation levels were found to decrease in a time dependent manner. AKT is an important prosurvival protein involved in anchorage independent growth and proliferation. AKT is very rapidly phosphorylated in response to estrogens in HepG2 cells (111). Here we demonstrate for time dependent decrease in AKT phosphorylation by upon treatment with 17αEE. Perhaps the high levels of AKT-S473 at zero time point are due to 17αEE stimulation of AKT-S476 phosphorylation during the washing and harvesting the cells for lysate preparation. Serum starvation may also change the phosphorylation levels of AKT-S476 (112).

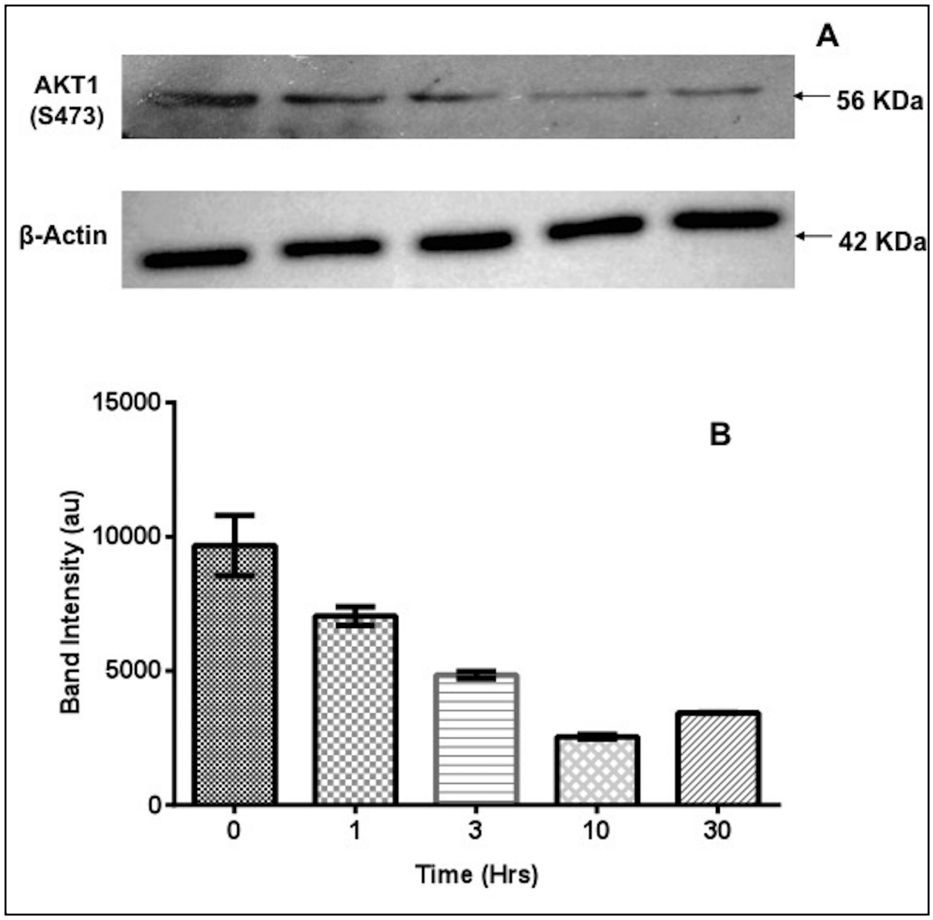

Figure C.7: Modulation of AKT1 (S473) phosphorylation by 17-α-ethinylestradiol treatments. C.7.A: AKT1 (S473) expression levels detection: 50 μg of total cellular protein was loaded onto 10% denaturing SDS-PAGE. The resolved proteins were transferred onto PVDF membrane and probed with anti-CHIP1 antibody. **C.7.B:** ImageJ quantification of phosphorylated AKT1 at different time points. Data are presented as mean±s.d. of triplicate samples and are representative of three independent experiments.

C.3.3 Effect of 17α-ethinylestradiol on HSP 90 expression

HSP 90 protein levels are modulated by 17αEE in MCF-7 breast cancer cells. HSP 90 is a chaperone protein involved in protein folding and protein quality control. Its steady levels are crucial for cell function and survival. Figure C.8 shows, HSP 90 protein levels decrease upon treatment with 17αEE after 1 hour post treatment and again matches to 0 hour control after 3 hours. After 10 and 30 hours post treatment with 17αEE the HSP 90 levels are slightly less than 0 hour control. Hsp90 stabilizes the unligated cytosolic androgen receptors including ERs. It also stabilizes the ERs conformation favorable to estrogen binding. So conditions modulating the cellular levels of HSP 90 protein can affect the ERs mediated estrogen signaling. The interaction between heat shock protein and steroid receptors have been described in detail in (110). A decrease in levels of HSP 90 compromises steroid receptor action in vivo.

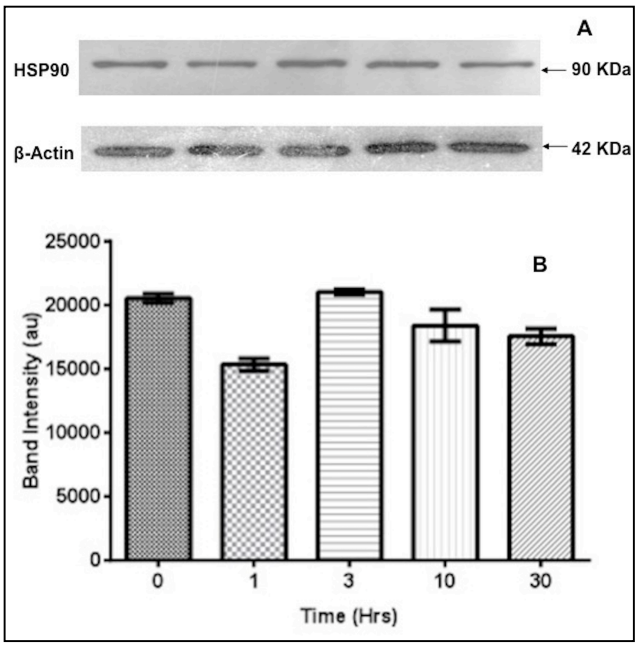

Figure C.8: Modulation of HSP 90 levels by 17-α-ethinylestradiol treatments. **C.8.A:** HSP 90 expression levels detection: 50 μg of total cellular protein was loaded onto 10% denaturing SDS-PAGE. The resolved proteins were transferred onto PVDF membrane and probed with anti-CHIP1 antibody. **C.8.B:** Image J quantification of HSP 90 at different time points. Data are presented as mean±s.d. of triplicate samples and are representative of three independent experiments.

C.3.4 Effect of 17α-ethinylestradiol on PARP1 expression

PARP1 level showed biphasic modal response to 17αEE treatment. Figure C.9 shows, The PARP1 levels increased after 1 hour incubation with 17αEE followed by a sharp decrease after 3 Hours of incubation with 17αEE. After 30 hours treatment PARP1 levels again rise near to the initial time point.

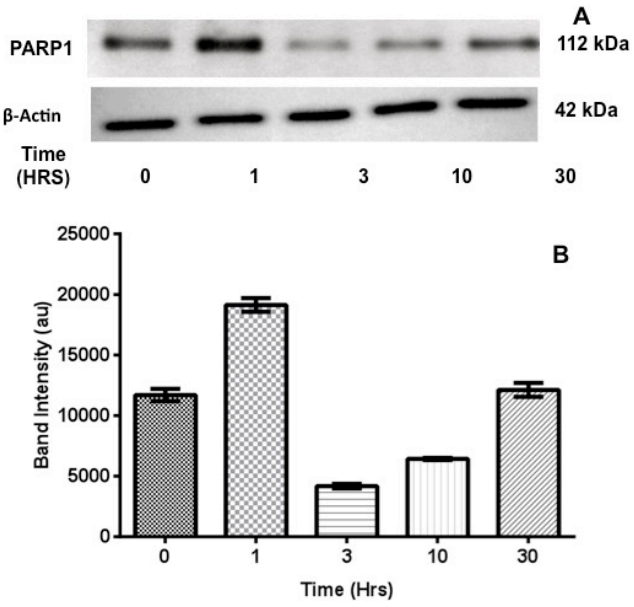

Figure C.9: Modulation of PARP1 levels by 17-α-ethinylestradiol treatments. C.9.A: PARP1 expression levels detection: 50 μg of total cellular protein was loaded onto 10% denaturing SDS-PAGE. The resolved proteins were transferred onto PVDF membrane and probed with anti-PARP1 antibody. **C.9.B:** ImageJ quantification of PARP1 at different time points. Data are presented as mean±s.d. of triplicate samples and are representative of three independent experiments.

C.3.5 Effect of ICI 164384 on 17αEE dependent modulation of CHIP1:

17αEE decreased the cellular levels of CHIP1 in a time dependent manner. To understand the mechanism of 17αEE dependent CHIP1 down-regulation, MCF-7 cells were pretreated with 3 μM ICI 164384 for 6 hours prior to treatment with 10 nM 17αEE. ICI 164384 is a competitive inhibitor that binds both ERα and ERβ and prevents estrogen dependent ER signaling. It was observed that ICI 164384 inhibited the 17αEE dependent down-regulation of CHIP1 as depicted in Figure C10.

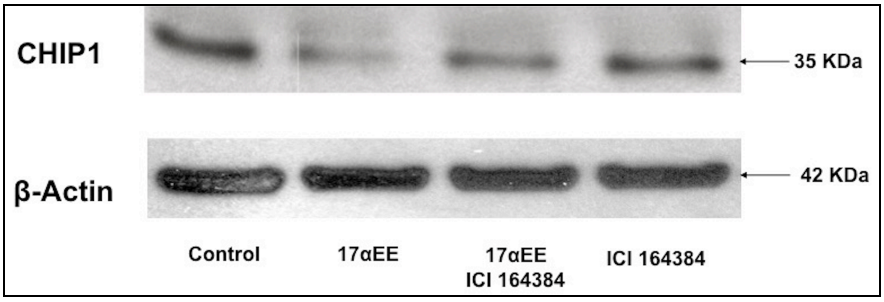

Figure C.10 Effect of ERs inhibition with ICI 164384 on CHIP1 expression: MCF-7 cells were pretreated with 3 μM ICI 164384 for 6 hours prior to treatment with 10 nM 17αEE. After 24 hours treatment with 17αEE, cells were harvested to prepare total cell lysate. 50 μg of total lysate from each treatment was subjected to western blotting and probed for CHIP1 expression.

The inhibition of 17αEE dependent down-regulation of CHIP1 indicates the role of estrogen signaling in the regulation of CHIP1 levels in MCF-7 breast cancer cells. The levels of CHIP1 decrease in the MCF-7 cells with 17αEE treatment. The pre-treatment of MCF-7 cells with ICI 164384 prior to 17αEE treatment, results in increased levels of CHIP1. This indicates that ER signaling is involved in 17αEE dependent CHIP1 degradation. Previous studies have shown transcription associated degradation of ERs. While other E3 ubiquitin ligases are involved in transcription associated and ligand dependent degradation of ERs, CHIP1 interacts with misfolded ERs and subject them to UPS mediated degradation. The above results indicate that CHIP1 itself might be regulated by the ERs signaling.

C.3.6 CHIP 1 levels are modulated in nucleus

The effect of 17αEE on nuclear CHIP1 levels was also studied by treating MCF-7 cells with 17αEE and harvested to prepare nuclear extract. The nuclear extracts were subjected to western blotting and probed for CHIP1 and PARP1 respectively. Figure C.11 shows, time dependent modulation of CHIP1 and PARP1 in nucleus.

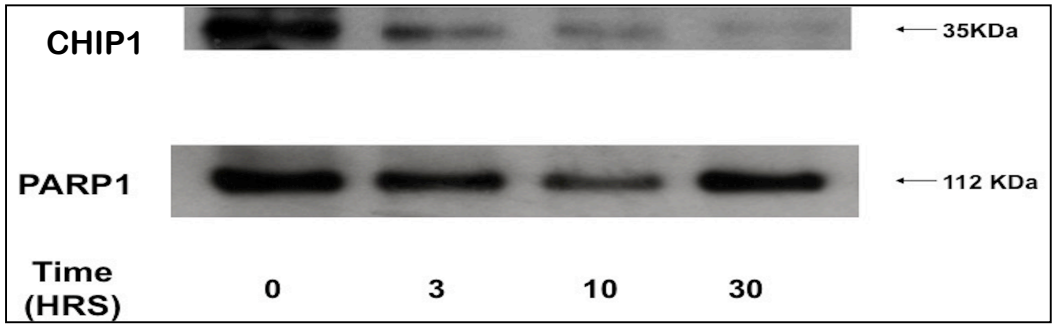

Figure C.11: Effects of 17αEE on nuclear levels of CHIP1 and PARP1. The nuclear levels of CHIP1 and PARP1 are modulated in a time dependent manner. CHIP1 levels decreased in a time dependent manner after treatment of MCF-7 cells with 17αEE. PARP1 levels are also modulated by 17αEE as in total cell lysate.

C.3.7 Coimmunoprecipitation assay to check CHIP1 binding interactions with PARP1

MCF-7 cells were treated with 10 nM 17αEE and harvested at various time points to prepare lysates that were subjected to coimmunoprecipitation.

These results indicate that CHIP and PARP1 are interacting partners. But PARP1 is a nuclear protein whereas CHIP1 is chiefly a cytosolic protein. There is some piece of work that demonstrates that CHIP1 is able to translocate to nucleus. These results demonstrate that CHIP1 might be stimulated to enter nucleus by 17αEE. The nuclear CHIP1 then interacts with PARP1.The coimmunoprecipitation study used the whole cell lysate that mixes the nuclear and cellular proteins so overall PARP1 captured by anti-CHIP1-CHIP complex might be influenced by total CHIP1 content of the treated lysate as well as the total content of PARP1 in the total cell lysate. Western blotting of total cell lysate in Figure C.12 shows, high levels of PARP1 expression in 0 hour, 1 hour and 30 hours; whereas equivalent treatment group shows lesser expression in coimmunoprecipitation experiment.

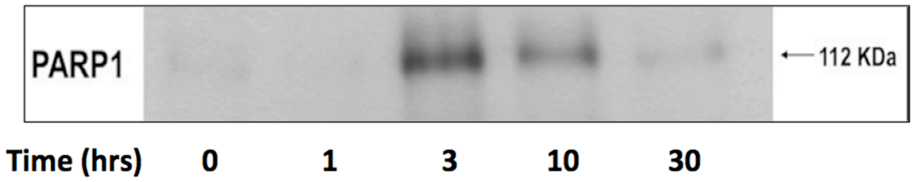

Figure C.12: CHIP1-PARP1 interaction visualized through coimmunoprecipitation: MCF-7 cells were treated with 10 nM 17αEE and harvested at various time points to prepare lysates that were subjected to coimmunoprecipitation.

Effect of CHIP1 knockdown on cell survival:

Figure C.13 shows, effect of CHIP1 knockdown on 17α-EE induced cell proliferation was studied using transient knockdown of CHIP1 using siRNA against CHIP1. Prior to 17α-EE treatment cells were transfected with CHIP1 siRNA. 17α-EE treatments were given as described in material and methods section. After 24 hours incubation the media was removed and MEM containing MTT was added to wells.

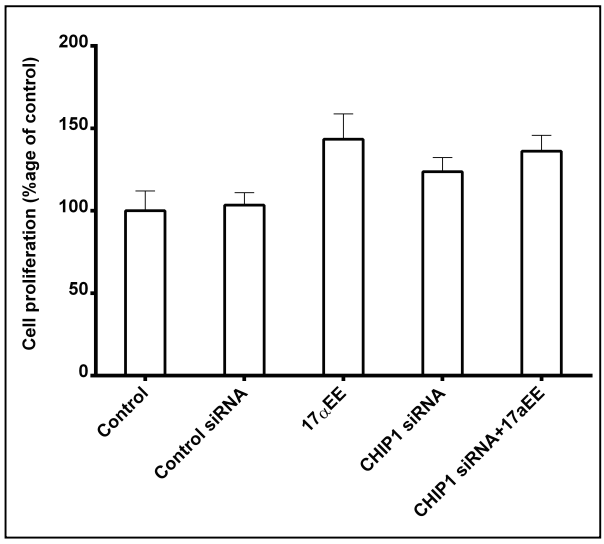

Figure C.13: Effect of CHIP1 knockdown on MCF-7 cell proliferation. MCF-7 cells were transfected with CHIP1 siRNA 8 hours prior to 17α-EE treatments. Post 17α-EE treatment cells were washed with PBS and incubated with cells were incubated for 3 h with 1 ml of 5mg/ml of MTT, dissolved in serum free medium (MEM) Washing with PBS (1 ml) was followed by the addition of 1 ml MTT solvent (0.1N HCl propanol) and cell plates were covered with aluminum foil and placed on rotary shaker for 10 minutes to completely dissolve the MTT product. Absorbance was taken with Cary 50 spectrophotometer at 570 nm with background subtraction at 650 nm. All treatments were given in triplicates and experiments were repeated thrice.

Conclusions and future prospects:

CHIP1 is an important mediator of cellular stress response in cellular physiology. 17α-EE regulates cytosolic and nuclear levels of CHIP1 in a time dependent manner. 17α-EE also regulates the cellular levels of AKT1 (S473) and PARP1 in a time dependent manner. We also discovered that CHIP1 is a binding partner of PARP1. PARP1 is very important molecule in breast cancer and cancer drug resistance. Further work is required to discover the physiological and pathophysiological relevance of CHIP1 binding with PARP1

References:

1. DeSantis C, Ma J, Bryan L, Jemal A (2014) Breast cancer statistics, 2013. CA Cancer J Clin. 64: 52-62.
2. Youlden DR, Cramb SM, Dunn NA, Muller JM, Pyke CM, Baade PD (2012) The descriptive epidemiology of female breast cancer: an international comparison of screening, incidence, survival and mortality. Cancer Epidemiol. 36: 237-248.
3. Smigal C, Jemal A, Ward E, Cokkinides Z, Smith R, Howe HL, Thun M (2006) Trends in breast cancer by race and ethnicity: update 2006. CA Cancer J Clin. 56: 168-83.
4. Yau C, Fedele V, Roydasgupta R, Fridlyand J, Hubbard A, et al. (2007) Aging impacts transcriptomes but not genomes of hormone-dependent breast cancers. Breast cancer research. BCR 9: R59-R59.
5. Dorgan JF, Baer DJ, Albert PS, Judd JT, Brown ED, et al. (2001) Serum Hormones and the Alcohol–Breast Cancer Association in Postmenopausal Women. Journal of the National Cancer Institute 93: 710-715.
6. Tjonneland A, Christensen J, Olsen A, Stripp C, Nissen SB, et al. (2005) Folate intake, alcohol and risk of breast cancer among postmenopausal women in Denmark. Eur J Clin Nutr 60: 280-286.
7. Yaghjyan L, Colditz GA, Collins LC, Schnitt SJ, Rosner B, et al. (2011) Mammographic Breast Density and Subsequent Risk of Breast Cancer in Postmenopausal Women According to Tumor Characteristics. Journal of the National Cancer Institute 103: 1179-1189.
8. White J (2000) Breast Density and Cancer Risk: What Is the Relationship? Journal of the National Cancer Institute 92: 443-443.
9. Fernandez SV, Russo J (2010) Estrogen and Xenoestrogens in Breast Cancer. Toxicologic pathology 38: 110-122.
10. Driedger SM, Eyles J (2001) Organochlorines and breast cancer: The Uses of Scientific Evidence in Claimsmaking. Social Science & Medicine 52: 1589-1605.
11. Gomez SL, Quach T, Horn-Ross PL, Pham JT, Cockburn M, et al. (2010) Hidden Breast Cancer Disparities in Asian Women: Disaggregating Incidence Rates by Ethnicity and Migrant Status. American journal of public health 100: S125-S131.
12. Dietze EC, Sistrunk C, Miranda-Carboni G, O'Regan R, Seewaldt VL (2015) Triple-negative breast cancer in African-American women: disparities versus biology. Nat Rev Cancer 15: 248-254.

13. Brandt-Rauf SI, Raveis VH, Drummond NF, Conte JA, Rothman SM (2006) Ashkenazi Jews and Breast Cancer: The Consequences of Linking Ethnic Identity to Genetic Disease. American Journal of Public Health 96: 1979-1988.
14. Kwei KA, Kung Y, Salari K, Holcomb IN, Pollack JR (2010) Genomic instability in breast cancer: pathogenesis and clinical implications. Molecular oncology 4: 255-266.
15. Tai YC, Domchek S, Parmigiani G, Chen S (2007) Breast cancer risk among male BRCA1 and BRCA2 mutation carriers. Journal of the National Cancer Institute 99: 1811-1814.
16. Baer HJ, Rich-Edwards JW, Colditz GA, Hunter DJ, Willett WC, et al. (2006) Adult height, age at attained height, and incidence of breast cancer in premenopausal women. International Journal of Cancer 119: 2231-2235.
17. Hou N, Hong S, Wang W, Olopade OI, Dignam JJ, et al. (2013) Hormone Replacement Therapy and Breast Cancer: Heterogeneous Risks by Race, Weight, and Breast Density. JNCI Journal of the National Cancer Institute 105: 1365-1372.
18. Ross RK, Paganini-Hill A, Wan PC, Pike MC (2000) Effect of hormone replacement therapy on breast cancer risk: estrogen versus estrogen plus progestin. Journal of the National Cancer Institute 92: 328-332.
19. Colditz GA, Hankinson SE, Hunter DJ, Willett WC, Manson JE, et al. (1995) The use of estrogens and progestins and the risk of breast cancer in postmenopausal women. New England Journal of Medicine 332: 1589-1593.
20. Pike MC, Spicer DV, Dahmoush L, Press MF (1993) Estrogens progestogens normal breast cell proliferation and breast cancer risk. Epidemiologic reviews 15: 17-35.
21. Stoll BA (1996) Obesity and breast cancer. International journal of obesity and related metabolic disorders: journal of the International Association for the Study of Obesity 20: 389-392.
22. Lorincz AM, Sukumar S (2006) Molecular links between obesity and breast cancer. Endocrine-related cancer 13: 279-292.
23. Harvie M, Hooper L, Howell AH (2003) Central obesity and breast cancer risk: a systematic review. Obesity reviews 4: 157-173.
24. Sellers TA, Kushi LH, Potter JD, Kaye SA, Nelson CL, et al. (1992) Effect of family history, body-fat distribution, and reproductive factors on the risk of postmenopausal breast cancer. New England Journal of Medicine 326: 1323-1329.
25. Brophy JT, Keith MM, Gorey KM, Luginaah I, Laukkanen E, et al. (2006) Occupation and Breast Cancer. Annals of the New York Academy of Sciences 1076: 765-777.

26. Band PR, Le ND, Fang R, Deschamps M, Gallagher RP, et al. (2000) Identification of occupational cancer risks in British Columbia: a population-based case-control study of 995 incident breast cancer cases by menopausal status, controlling for confounding factors. Journal of Occupational and Environmental Medicine 42: 284-310.
27. Simpson E, Rubin G, Clyne C, Robertson K, O'Donnell L, et al. (2000) The role of local estrogen biosynthesis in males and females. Trends in Endocrinology & Metabolism 11: 184-188.
28. Simpson ER, Davis SR (2001) Minireview: aromatase and the regulation of estrogen biosynthesis—some new perspectives. Endocrinology 142: 4589-4594.
29. Russo J, Hasan Lareef M, Balogh G, Guo S, Russo IH (2003) Estrogen and its metabolites are carcinogenic agents in human breast epithelial cells. The Journal of Steroid Biochemistry and Molecular Biology 87: 1-25.
30. Kumar V, Green S, Stack G, Berry M, Jin J-R, et al. (1987) Functional domains of the human estrogen receptor. Cell 51: 941-951.
31. Schwabe JW, Chapman L, Finch JT, Rhodes D (1993) The crystal structure of the estrogen receptor DNA-binding domain bound to DNA: how receptors discriminate between their response elements. Cell 75: 567-578.
32. Rollerova E, Urbancikova M (2000) Intracellular estrogen receptors, their characterization and function. Endocr. Regul. 34: 203–218.
33. O'Lone R, Frith MC, Karlsson EK, Hansen U. (2004) Genomic targets of nuclear estrogen receptors. Mol. Endocrinol. 18: 1859–1875.
34. Cheskis BJ, Greger JG, Nagpal S, Freedman LP (2007) Signaling by estrogens, J. Cell. Physiol. 321: 610–617.
35. Stice JP, Knowlton AA (2008) Estrogen, NFκB, and the heat shock response. Mol. Med. 14: 517–527.
36. Kushner PJ, Agard DA, Greene GL, Scanlan TS, Shiau AK, Uht RM, Webb P (2000) Estrogen receptor pathways to AP-1, J. Steroid Biochem. Mol. Biol. 74: 311–317.
37. Saville B, Wormke M,Wang F, Nguyen T, Enmark E, Kuiper G, Gustafsson JA, Safe S (2000) Ligand-, cell-, and estrogen receptor subtype (alpha/beta)-dependent activation at GC-rich (SP1) promoter elements. J. Biol. Chem. 275: 5379–5387.
38. Briegel K, Lim KC, Plank C, Beng CH, Engel JD, Zenke M (1993) Ectopic expression of a conditional GATA 2/estrogen receptor chimera arrests erythroid differentiation in a hormone dependent manner. Genes Dev. 7: 1097–1109.
39. Pietras RJ, Szego CM (1977) Specific binding sites for oestrogen at the outer surfaces of

isolated endometrial cells. Nature 265: 69–72.

40. Levin ER (2001) Cell localization, physiology and nongenomic actions of estrogen receptors, J. Appl. Physiol. 91: 1860–1867.
41. Berthois Y, Pourreau-Schneider N, Gandilhon P, Mittre H, Tubiana N, Martin PM (1986) Estradiol membrane binding sites on human breast cancer cell lines. Use of fluorescent estradiol conjugate to demonstrate plasma membrane binding systems, J. Steroid Biochem. 25: 963–972.
42. Kampa M, Nifli AP, Charalampopoulos I, Alexaki VI, Theodoropoulos PA, E.N. Stathopoulos EN (2005) Opposing effects of estradiol and testosterone membrane binding sites on T47D breast cancer cell apoptosis, Exp. Cell Res. 307: 41–51.
43. Razandi M, Pedram A, Green GL, Levin ER (1999) Cell membrane and nuclear estrogen receptors (ERs) originate from a single transcript: studies of ERalpha and ERbeta expressed in Chinese hamster ovary cells, Mol. Cell. Endocrinol. 13: 307–319.
44. Pappas TC, Gametchu B, Watson CS (1995) Membrane estrogen receptors identified by multiple antibody labeling and impeded-ligand binding, FASEB J. 9: 404–410.
45. Kim KH, Moriarty K, Bender JR (2008) Vascular cell signaling by membrane estrogen receptors, Steroids 73: 864–869.
46. M. Razandi M, Oh P, Pedram A, Schnitzer J, Levin ER (2002) ERs associate with and regulate the production of cavealin: implication for signaling and cellular actions. Mol. Endocrinol. 16: 100–115.
47. Boulware MI, Kordasiewicz H, Mermelstein PG (2007) Caveolin proteins are essential for distinct effects of membrane estrogen receptors in neurons. J. Neurosci. 27: 9941–9950.
48. Acconcia F, Ascenzi P, Bocedi A, Spisni E, Tomasi V, Tretalance A (2005) Palmitoylation-dependent estrogen receptor alpha membrane localization: regulation by 17-beta-estradiol. Mol. Biol. Cell 16: 231–237.
49. Lu Q, Pallas DC, Surks HK, Baur WE, Mendelsohn ME, Karas RH (2004) Striatin assembles a membrane signaling complex necessary for rapid, nongenomic activation of endothelial NO synthases by estrogen receptor alpha. PNAS (USA) 101: 17126–17131.
50. Barletta F, Wong CW, McNally C, Komm BS, Katzenellenbogen B, Cheskis BJ (2004) Characterization of the interactions of estrogen receptor and MNAR in the activation of cork, Mol. Endocrinol. 18: 1096–1108.
51. Vasudevan N, Pfaff DW (2008) Non-genomic actions of estrogens and their interaction with genomic actions in the brain. Front. Neuroendocrinol. 29: 238–257.

52. Jung T , Catalgol B, Grune T (2009) The proteasomal system. Molecular Aspects of Medicine 30: 191–296.
53. Laıos I, Journe´F, Nonclercq D, Vidal DS, Toillon RA, Laurent G, Leclercq G (2005) Role of the proteasome in the regulation of estrogen receptor α turnover and function in MCF-7 breast carcinoma cells. Journal of Steroid Biochemistry & Molecular Biology. 94: 347–359.
54. Nalepa G, Rolfe M, Harper W (2006) Drug discovery in the ubiquitin-proteasome system. Nature Reviews Drug Discovery. 5: 596-613.
55. Zafar N, Lonard DM, Dennis AP, Smith CL, O' Malley BW (1999) Proteasome-dependent degradation of the human estrogen receptor. PNAS (USA) 96: 1858-1862.
56. Martin S, Kaufman RJ (2005) The mammalian unfolded protein response. Annu. Rev. Biochem. 74: 739-789.
57. Ballinger CA, Connell P, Wu Y, Hu Z, Thompson LJ, et al. (1999) Identification of CHIP, a Novel Tetratricopeptide Repeat-Containing Protein That Interacts with Heat Shock Proteins and Negatively Regulates Chaperone Functions. Molecular and Cellular Biology 19: 4535-4545.
58. Zhang M, Windheim M , Roe SM, Peggie M, Cohen P, Prodromou C, Pearl LH (2005) Chaperoned Ubiquitylation—Crystal Structures of the CHIP U Box E3 Ubiquitin Ligaseand a CHIP-Ubc13-Uev1a Complex. Molecular Cell. 20: 525–538.
59. Zhang Q-g, Han D, Wang R-m, Dong Y, Yang F, et al. (2011) C terminus of Hsc70-interacting protein (CHIP)-mediated degradation of hippocampal estrogen receptor-α and the critical period hypothesis of estrogen neuroprotection. Proceedings of the National Academy of Sciences of the United States of America 108: E617-E624.
60. Sun C, Li H-l, Chen H-r, Shi M-l, Liu Q-h, et al. (2015) Decreased expression of CHIP leads to increased angiogenesis via VEGF-VEGFR2 pathway and poor prognosis in human renal cell carcinoma. Sci Rep 5.
61. Esser C, Scheffner M, Höhfeld J (2005) The chaperone-associated ubiquitin ligase CHIP is able to target p53 for proteasomal degradation. Journal of Biological Chemistry 280: 27443-27448.
62. Naito AT, Okada S, Minamino T, Iwanaga K, Liu M-L, et al. (2010) Promotion of CHIP-mediated p53 degradation protects the heart from ischemic injury. Circulation research 106: 1692-1702.

63. Xu T, Zhou Q, Zhou J, Huang Y, Yan Y, et al. (2011) Carboxyl terminus of Hsp70‐interacting protein (CHIP) contributes to human glioma oncogenesis. Cancer science 102: 959-966.
64. Wang Y, Ren F, Wang Y, Feng Y, Wang D, et al. (2013) CHIP/Stub1 functions as a tumor suppressor and represses NF-κB-mediated signaling in colorectal cancer. Carcinogenesis: bgt393.
65. Sengupta S, Badhwar I, Upadhyay M, Singh S, Ganesh S (2011) Malin and laforin are essential components of a protein complex that protects cells from thermal stress. Journal of cell science 124: 2277-2286.
66. Rao SNR, Sharma J, Maity R, Jana NR (2010) Co-chaperone CHIP stabilizes aggregate-prone malin, a ubiquitin ligase mutated in Lafora disease. Journal of Biological Chemistry 285: 1404-1413.
67. Xu W, Marcu M, Yuan X, Mimnaugh E, Patterson C, et al. (2002) Chaperone-dependent E3 ubiquitin ligase CHIP mediates a degradative pathway for c-ErbB2/Neu. Proceedings of the National Academy of Sciences 99: 12847-12852.
68. Cardozo CP, Michaud C, Ost MC, Fliss AE, Yang E, et al. (2003) C-terminal Hsp-interacting protein slows androgen receptor synthesis and reduces its rate of degradation. Archives of Biochemistry and Biophysics 410: 134-140.
69. Lee JH, Shin SK, Jiang Y, Choi WH, Hong C, et al. (2015) Facilitated Tau Degradation by USP14 Aptamers via Enhanced Proteasome Activity. Scientific reports 5.
70. Petrucelli L, Dickson D, Kehoe K, Taylor J, Snyder H, et al. (2004) CHIP and Hsp70 regulate tau ubiquitination, degradation and aggregation. Human molecular genetics 13: 703-714.
71. Maruyama T, Kadowaki H, Okamoto N, Nagai A, Naguro I, et al. (2010) CHIP‐dependent termination of MEKK2 regulates temporal ERK activation required for proper hyperosmotic response. The EMBO journal 29: 2501-2514.
72. Löffek S, Wöll S, Höhfeld J, Leube RE, Has C, et al. (2010) The ubiquitin ligase CHIP/STUB1 targets mutant keratins for degradation. Human Mutation 31: 466-476.
73. Jana NR, Dikshit P, Goswami A, Kotliarova S, Murata S, et al. (2005) Co-chaperone CHIP associates with expanded polyglutamine protein and promotes their degradation by proteasomes. Journal of Biological Chemistry 280: 11635-11640.
74. Chen C, Seth AK, Aplin AE (2006) Genetic and expression aberrations of E3 ubiquitin ligases in human breast cancer. Molecular Cancer Research 4: 695-707.

75. Guo J, Ren F, Wang Y, Li S, Gao Z, et al. (2012) miR-764-5p promotes osteoblast differentiation through inhibition of CHIP/STUB1 expression. Journal of Bone and Mineral Research 27: 1607-1618.
76. O'Shaughnessy J, Osborne C, Pippen J, Yoffe M, Patt D, et al. (2009) Efficacy of BSI-201, a poly (ADP-ribose) polymerase-1 (PARP1) inhibitor, in combination with gemcitabine/carboplatin (G/C) in patients with metastatic triple-negative breast cancer (TNBC): results of a randomized phase II trial pp. 3.
77. Brenner JC, Feng FY, Han S, Patel S, Goyal SV, et al. (2012) PARP-1 inhibition as a targeted strategy to treat Ewing's sarcoma. Cancer research 72: 1608-1613.
78. Daniel RA, Rozanska AL, Thomas HD, Mulligan EA, Drew Y, et al. (2009) Inhibition of poly (ADP-ribose) polymerase-1 enhances temozolomide and topotecan activity against childhood neuroblastoma. Clinical Cancer Research 15: 1241-1249.
79. Fogelman DR, Wolff RA, Kopetz S, Javle M, Bradley C, et al. (2011) Evidence for the Efficacy of Iniparib, a PARP-1 Inhibitor, in BRCA2-associated Pancreatic Cancer. Anticancer research 31: 1417-1420.
80. Cohen-Armon M, Visochek L, Rozensal D, Kalal A, Geistrikh I, et al. (2007) DNA-independent PARP-1 activation by phosphorylated ERK2 increases Elk1 activity: a link to histone acetylation. Molecular cell 25: 297-308.
81. Hassa PO, Haenni SS, Buerki C, Meier NI, Lane WS, et al. (2005) Acetylation of poly (ADP-ribose) polymerase-1 by p300/CREB-binding protein regulates coactivation of NF-κB-dependent transcription. Journal of biological chemistry 280: 40450-40464.
82. Hassa PO, Covic M, Hasan S, Imhof R, Hottiger MO (2001) The enzymatic and DNA binding activity of PARP-1 are not required for NF-κB coactivator function. Journal of Biological Chemistry 276: 45588-45597.
83. Schreiber V, Amé J-C, Dollé P, Schultz I, Rinaldi B, et al. (2002) Poly (ADP-ribose) polymerase-2 (PARP-2) is required for efficient base excision DNA repair in association with PARP-1 and XRCC1. Journal of Biological Chemistry 277: 23028-23036.
84. Krishnakumar R, Gamble MJ, Frizzell KM, Berrocal JG, Kininis M, et al. (2008) Reciprocal binding of PARP-1 and histone H1 at promoters specifies transcriptional outcomes. Science 319: 819-821.
85. Cohen-Armon M, Visochek L, Rozensal D, Kalal A, Geistrikh I, et al. (2007) DNA-independent PARP-1 activation by phosphorylated ERK2 increases Elk1 activity: a link to histone acetylation. Molecular cell 25: 297-308.

86. Hassa PO, Haenni SS, Buerki C, Meier NI, Lane WS, et al. (2005) Acetylation of poly (ADP-ribose) polymerase-1 by p300/CREB-binding protein regulates coactivation of NF-κB-dependent transcription. Journal of biological chemistry 280: 40450-40464.
87. Saxena A, Wong LH, Kalitsis P, Earle E, Shaffer LG, et al. (2002) Poly (ADP-ribose) polymerase 2 localizes to mammalian active centromeres and interacts with PARP-1, Cenpa, Cenpb and Bub3, but not Cenpc. Human molecular genetics 11: 2319-2329.
88. Kraus WL (2008) Transcriptional control by PARP-1: chromatin modulation, enhancer-binding, coregulation, and insulation. Current opinion in cell biology 20: 294-302.
89. Kashima L, Idogawa M, Mita H, Shitashige M, Yamada T, et al. (2012) CHFR protein regulates mitotic checkpoint by targeting PARP-1 protein for ubiquitination and degradation. Journal of Biological Chemistry 287: 12975-12984.